



LAWRENCE
LIVERMORE
NATIONAL
LABORATORY

UCRL-TR-203991

Flash X-Ray Injector Study

A. C. Paul

March 26, 2004

This document was prepared as an account of work sponsored by an agency of the United States Government. Neither the United States Government nor the University of California nor any of their employees, makes any warranty, express or implied, or assumes any legal liability or responsibility for the accuracy, completeness, or usefulness of any information, apparatus, product, or process disclosed, or represents that its use would not infringe privately owned rights. Reference herein to any specific commercial product, process, or service by trade name, trademark, manufacturer, or otherwise, does not necessarily constitute or imply its endorsement, recommendation, or favoring by the United States Government or the University of California. The views and opinions of authors expressed herein do not necessarily state or reflect those of the United States Government or the University of California, and shall not be used for advertising or product endorsement purposes.

This work was performed under the auspices of the U.S. Department of Energy by University of California, Lawrence Livermore National Laboratory under Contract W-7405-Eng-48.

FXR INJECTOR STUDY

Arthur C. Paul

January 31, 2003

Motivation

The study described in this report¹ models the FXR injector from the cathode to the exit of the injector. The calculations are compared to actual experimental measurements², table 1. In these measurements the anode voltage was varied by changing the Marks-Bank charging voltage. The anode-cathode spacing was varied by adjusting the location of the cathode in hopes of finding an island of minimum emittance (none found). The bucking coil current was set for zero field on the cathode. In these measurements, a pepper-pot mask was inserted into FXR at beam bug I35 and viewed downstream via a wiggle probe³ diagnostic at cell gap J21, figure 1. The observed expansion of the beamlets passing through the mask of known geometric layout and hole size allow a calculation of the phase space beam properties.^{4 5}

Table 1.
Edge emittance (cm-mr) at exit of injector

A-K gap (cm)	Charge Voltage (kV)										
	20.0	20.5	21.0	21.5	22.0	22.3	23.0	23.5	24.0	24.5	25.0
10.5	-	-	-	-	-	-	-	-	-	-	-
11.0	-	84	69	76	76	-	-	-	-	-	-
11.5	83	78	69	-	78	74	-	-	-	-	-
12.0	85	63	75	72	83	-	78	-	80	-	-
12.6	94	-	78	-	77	-	69	-	77	-	76
13.0	-	-	-	-	-	-	-	-	-	-	-
Normalized edge emittance (cm-mr)											
10.5	-	-	-	-	-	-	-	-	-	-	-
11.0	-	332	279	314	321	-	-	-	-	-	-
11.5	320	308	279	-	330	320	-	-	-	-	-
12.0	328	249	303	298	351	-	344	-	367	-	-
12.6	363	-	315	-	325	-	304	-	354	-	363
13.0	-	-	-	-	-	-	-	-	-	-	-

The average value of these measurements tabulated in table 1 is

$$\varepsilon = 77.0 \pm 1.3 \text{ cm} - \text{mr}$$

I will use a anode potential of 2.1 MV for a charge voltage⁶ of 2x23 kV. Assuming linearity of charge

¹ LapT:WRK/fxr/inj/inow/case/xx text

² Glen Westinskow, Frank W. Chambers

³ FXR uses a special probe, affectionately called a wiggle probe, that can be "threaded" down a port into the accelerator bore at the location of the first cell of each four cell block unit. A viewing foil on the end of this probe can be monitored via a gated TV image system using smoke and mirrors in the control room.

⁴ "ETA-II Beam Brightness Measurement", A.C.Paul, S.L.Allen, Y-J.Chen, F.W.Chambers, F.J.Deadrick, W.C.Turner, Submitted to the 1991 IEEE Particle Accelerator Conference, San Francisco, CA., May 1991, UCRL-JC-105556.

⁵ "Emittance Measurements on Field Emitter Diodes", B.Kulke, R.Kihara, Submitted to the Pulse Power Conference, Texas Tech University, June 12-14, 1979. April 1979, UCRL-82533.

⁶ According to Ray Scarpetti the anode potential is 2.0 MV for a charge voltage of 2x23 kV. Jan Zentler gives a value of 2.2 MV for a charge voltage of 2x23 kV (07/30/02). The Lin33 tune uses a charge voltage of 2x23 kV. The Zentler scans were done with a charge voltage of 2x23 kV and are best fit with a beam energy unfolded giving an anode potential of 2.1 MV, section 11 of this report.

voltage and anode potential, the average normalized edge emittance of the 22 measurements in table 1 is

$$\varepsilon_n = 321.3 \pm 5.9 \text{ cm-mr}$$

In a conference paper⁷ the emittance at the exit of the injector and accelerator was reported as given in table 2. The measurement was done with the dia-magnetic loop diagnostic at bugs I35 and DR2B. This diagnostic measures the RMS values which must be multiplied by two to convert to the edge values used throughout this report⁸. The injector normalized edge emittance extracted from table 2 is

$$\varepsilon_n = 450 \text{ cm-mr}$$

Dividing this by $\beta\gamma = 36$ (17.9 MeV) gives an emittance at the exit of the FXR accelerator of $\varepsilon = 12.5 \text{ cm-mr}$, compared with the measured value of 22.2 cm-mr edge showing a degradation in emittance of a factor of two in the accelerator.

Table 2.
Dia-magnetic Loop (DML) Measured RMS Emittance

Location	gamma	R(cm)	R'(mr)	ε (cm-mr)
Injector	4.7	2.5 ± 0.2	-64.9 ± 8.5	47.9 ± 8.6
Accelerator	36	0.90 ± 0.03	-7.1 ± 0.3	11.1 ± 0.5

For the ETA⁹ injector current of 1500 Amperes and 1.2 MV, a measurement of the beam emittance was made after the first two accelerator cells at an energy 2.5 MeV¹⁰ ($\beta\gamma = 5.807$) giving $\varepsilon = 19.1 \text{ cm-mr}$ or a normalized emittance of ε_n of 1109 mm-mrad. Scaling this to the FXR parameters of 3300 Amperes and 1.8 MV ($\beta\gamma = 4.41$) would give an expected FXR edge emittance of $\varepsilon = 37.3 \text{ cm-mr}$ at the injector exit, and an edge emittance of

$$\varepsilon = 4.5 \text{ cm-mr} \quad [0.1]$$

at the accelerator exit, 18.0 MeV $\beta\gamma = 36.2$. These values are a factor of 3-4 smaller than the experimentally measured FXR emittance values (we will discuss latter the relation between the RMS emittance and the edge emittance) . This raises the question as to if the FXR injectors brightness can be improved and this is the subject of this report.

Other accelerators operating in the multi-kilo-ampere and multi-mega-volt range report beam emittance's smaller than those observed at FXR, table 3.

⁷ "Reconstruction of FXR Beam Conditions", W.E.Nexsen, R.D.Scarpetti, J.Zentler, WPAH127.

⁸ See section 6 for the conversion factors between the different definitions of emittance.

⁹ (LLNL Building 431) J.C.Clark et al., "Design and Initial Operation of the ETA-II Induction Accelerator", Proceedings of the 14th International LINAC Conference, Williamsburg, VA, Oct 3-7,1988, CEBAF-Report-89-001, June, 1989, pp.19-23.

¹⁰ "ETA-II Beam Brightness Measurement", A.C.Paul, S.L.Allen, F.W.Chambers, Y-J.Chen, F.J.Deadrick, W.C.Turner, IEEE Particle Accelerator Conference, 1991. UCRL-JC-105556.

Table 3.
High Current Linear Induction Machines

Machine	Ref	Energy MeV	Current Amperes	$\beta\gamma$	Measured ϵ_{RMS} cm-mr	Measured ϵ_{Edge} cm-mr	Edge Values ϵ_n cm-mr	Scaled cm-mr
ETA	1)	2.5	1500	5.807	-	19.1	110.9	4.5
ATA	2)	2.5	10000	5.807	-	68.	400.	6.35
	3)	45.0	8500	89.06	-	10.0	890.6	15.3
	4)	8.7	2500	18.0	-	9.4	169.2	5.4
DARHT-1	5)	19.7	4000	39.64	-	3.03	120.0	3.0
DARHT-2	6)	18.0	2000	36.2	-	3.0	108.6	3.8
AIRIX	7)	3.8	1920	8.377	-	25.0	209.4	7.6
FXR	8)	1.94	3300	4.7	47.9	(95.8)	450.0	12.5
	9)	17.9	3300	36.0	11.1	(22.2)	799.2	22.1
	10)	16.5	2800	33.3	-	13.0	432.9	12.5
	11)	-	-	-	-	-	-	-
	12)	17.5	3000	35.2	9.47	(18.9)	666.7	18.9

The "Scaled" column is the normalized edge emittance ϵ_n scaled to the FXR beam current and accelerator exit energy.

$$\epsilon_{\text{Scaled}} = \epsilon_n \sqrt{\frac{I_{\text{FXR}}}{I_{\text{mach}}}} \frac{1}{\beta\gamma(\text{FXR})} \quad [0.2]$$

Table 4 - References

1)	Reference 2XX - Velvet cathode -
2)	ATA Injector - Hot cathode + extraction grid UCID-19862, "First Studies of ATA Injector", D.S.Prono, et.al., 8/01/83. UCRL-88265, "The Advanced Test Accelerator Injector", 1983 Particle Accelerator Conference, Santa Fe, New Mexico, March 9, 1983
3)	
4)	Arthur C. Paul, Jeffrey S. Kallman, Ping Lee, "Unfolding ATA Beam Parameters from TV image vs Cell Block Excitation", April 1989, RM88-62.
5)	
6)	Design values - "DARHT-II Final Beamline Report", Arthur C. Paul, January 25, 2002, UCRL-ID-147135. Machine not currently operational.
7)	"Comparison of FXR/DARHT/AIRIX", unpublished note, 11/10/2000, Ray Scarpelli, presented at FXR Performance Meeting, April 26, 2001, Rattlesnake room, B801.
8)	DML measurement at injector exit. Reference ibid.
9)	DML measurement at accelerator exit. Reference ibid.
10)	Beam reconstruction from single Gaussian fits to foil light scan of FF4 Cherenkov light shots 129 583-751 - FXR meeting 07/16/01
11)	Beam reconstructed from final focus FF4 scans using film - time integrated Shots 129 149-192
12)	"Time-Resolved Emittance Characterization of an Induction Linac Beam Using Optical Transition Radiation", G.P.Le Sage. PACS Codes: 29.27.-a Three values were measured at 20 nsec intervals 10.7 ± 1.3 , 8.6 ± 1.0 , and 9.1 ± 2.1 with average value of 9.47 ± 1.47 cm-mr.

The "scaled" column of table 3 for machines other-than FXR give an expected FXR emittance in the range of 3 - 8 cm-mr. The 45 MeV ATA value of 15 cm-mr should be ignored as this value includes the beam breakup associated with the full 180 accelerator cells of ATA. The measured FXR values are two to four times higher than these scaled values. This type of scaling assumes no emittance growth in the accelerator and ignores the difference in the number of accelerator cells of the machine, the larger the number of cells the potentially larger contribution to emittance growth from beam breakup.

Contents

Motivation	1
Contents	4
Index of Tables	4
Index of Figures	5
1) Estimate of Expected FXR Beam Emittance	6
2) Injector Geometry	7
3) Injector Magnets	11
4) Off Axis Fields	13
5) Off Axis Field Expansions	18
6) Beam Emittance	23
7) Injector Modeling	26
8) Cathode Temperature	27
9) Matching the Beam to the Magnetic Field	28
10) Magnetic Field Tunes	30
11) Zentler Scans	35
12) Transport To End of Accelerator	36

Index of Tables

Table 1) Measured FXR Edge emittance	1
Table 2) Measured FXR RMS DML emittance	2
Table 3) Comparison High Current Linear Induction Machines	3
Table 4) References	3
Table 5) FXR Emittance at injector exit and accelerator exit	7
Table 6) FXR inner pipe wall radius	9
Table 7) EGUN data Lin33 tune	10
Table 8) EGUN data to end of gun	11
Table 9) Injector Magnets	12
Table 10) Ferrite data	13
Table 11) Magnetic field fitting coefficients	14
Table 12) Forth, Sixth, Eighth order coefficients	19
Table 13) Maximum field values for Poisson code, 1st, 3rd, and 6th order	22
Table 14) Off axis field errors	22
Table 15) Comparison between the different phase space distributions	25
Table 16) Cathode temperature and transverse energy	27
Table 17) Matched beam radius 2.0 MeV, 75 cm-mm	28
Table 18) Matched beam radius 2.1 MeV, 25 cm-mm	29
Table 19) Summary of Tunes: Lin33, SPU28, and DP	30
Table 20) Performance of tunes Lin33, SPU28, and DP	30
Table 21) EGUN data for the SPU28 tune	32
Table 22) EGUN data for the DP tune	34
Table 23)	
Table 24)	
Table 25) Zentler scans, series 1, 2, 3, injector magnet current values	35
Table 26) Zentler scans, beam current measured at bug I35	35
Table 27) Ideal Stair Step field approximation Lin33, SPU28 and DP	37
Table 28) Transport Data	39

Index of Figures

Figure 1)	* FXR - layout injector, accelerator, external beam	40
Figure 2)	* Injector + first cell block layout, coils, Fe Cores.	41
Figure 3)	* FXR layout, coils, Fe Cores, beam envelope, pipe wall, etc.	42
Figure 4)	cathode shroud	43
Figure 5)	anode shroud	44
Figure 6)	0-30 cm egun mesh and electrodes	45
Figure 7)	Measured field - fitted field J25	46
Figure 8)	poisson field, analytic fit A)I20, B)I21, C)I22	47
Figure 9)	Poisson field, analytic fit A)I22, B)I24, C)I25	48
Figure 10)	Poisson field, analytic fit A)I31, B)I32, C)I33, D)I34	49
Figure 11)	Poisson field, analytic fit I35	50
Figure 12)	synthysized field Lin33	51
Figure 13)	I25 fitted function r=0 (r=5 Bz and Br)	52
Figure 14)	4th order	53
Figure 15)	6th order	54
Figure 16)	8th order	55
Figure 17)	off axis field r=1, 2, 3, 4 cm	56
Figure 18)	off axis field r=5, 6, 7, 8 cm	57
Figure 19)	synthsized field SPU28	58
Figure 20)	synthsized field double pulse	59
Figure 21)	egun 0-30 cm zone	60
Figure 22)	egun 20-355 cm zone	61
Figure 23)	egun plot 0-30	62
Figure 24)	egun phase 20 cm	63
Figure 25)	egun plot 20-355 cm	64
Figure 26)	beam 0-355 cm	65
Figure 27)	emittance 0-355 cm	66
Figure 28)	current profile	67
Figure 29)	magnetic field	68
Figure 30)	beam envelope	99
Figure 31)	effect of cathode temerature on beam emittance	70
Figure 32)	egun envelope 0-30 cm with Tc=2e4 K	71
Figure 33)	phase space, 20cm Tc=2e4 K	72
Figure 34)	beam envelope 0-355 cm Tc=2e4 K	73
Figure 35)	emittance 0-355 cm Tc=2e4 K	74
Figure 36)	phase space z=200cm, Tc=0 and Tc=2e4 K	75
Figure 37)	SPU28 Egun 0-30 cm	76
Figure 38)	SPU28 0-355 trajectories	77
Figure 39)	SPU28 emit vs z	78
Figure 40)	SPU28 current vs z	79
Figure 41)	SPU28 Bz(z)	80
Figure 42)	SPU28 phase space at 20 cm	81
Figure 43)	DP Egun 0-30 cm	82
Figure 44)	DP 0-355 trajectories	83
Figure 45)	DP emit vs z	84
Figure 46)	DP current vs z	85
Figure 47)	DP Bz(z)	86
Figure 48)	DP phase space at 20 cm	87
Figure 49)	Overplot Bz(z) fields for Lin33, SPU28, and DP tunes.	88
Figure 50)	Zentler scans Bz(z)	89
Figure 51)	Measured beam current series 1, 2, 3	90
Figure 52)	Envelopes series 1	91
Figure 53)	Envelopes series 1	92
Figure 54)	Envelopes series 1	93
Figure 55)	Current 1.9 MV	94
Figure 56)	Current 2.0 MV	95
Figure 57)	Current 2.1 MV	96
Figure 58)	Current 2.2 MV	97
Figure 59)	Phase space for start of Transport Calculations	98
Figure 60)	Stair step approximation to field	99
Figure 61)	Transport beam envelope in injector 20-355 cm	104
Figure 62)	Transport beam envelope in accelerator	100
Figure 63)	Transport Solenoid Accelerator Field Tune	101
Figure 64)	Starting phase space 355 cm	102
Figure 65)	Target Phase Space	103

1. Estimate of Expected FXR Beam Emittance

Neil¹¹ in an unpublished report estimates that

$$\varepsilon_n = 32.0 \sqrt{I_b} \quad [1.1]$$

where ε_n is the normalized edge emittance in mm-mrad, I_b is the beam current in Amperes. This equation is based on empirical scaling of data from various linear accelerators. Other authors have used different empirical constants¹². Dattoli et.al.¹³ give the following two equations as "best fit" of high current machines using Lawson-Penner scaling, I in Amperes, emittance in cm-radians.

$$\bar{I} = 1.1 \times 10^4 \beta^2 \gamma^2 \varepsilon_x \varepsilon_y \quad [1.2]$$

$$\bar{I} = 4.9 \times 10^4 \beta^2 \gamma^2 \varepsilon_x \varepsilon_y \quad [1.3]$$

These reduce to

$$\varepsilon_n = \beta \gamma \varepsilon \text{ (mm - mrad)} = \begin{cases} 95 \\ 45 \end{cases} \sqrt{I \text{ (Amperes)}} \quad [1.4]$$

That the upper coefficient gives the FXR emittance value should be of no surprise as FXR was included in the accelerators for which these equations were derived. Neils coefficient eq[1.1] does not include FXR. For FXR and equations [1.1], [1.2], and [1.3] we have

Table 5
Projected Emittance at exit of Injector and Accelerator

Edge Emittance	FXR EQ[1.1]	FXR EQ[1.2]	FXR EQ[1.3]	
Current ε_n (normalized)	3300 1838	3300 2585	3300 5457	Amperes mm-mr
Injector exit				
Energy $\beta \gamma$ emittance	1.8 4.410 41.7	1.8 4.410 58.6	1.8 4.410 124	MeV cm-mr
Accelerator exit				
Energy $\beta \gamma$ emittance	18.0 36.21 5.07	18.0 36.21 7.14	18.0 36.21 15.1	MeV cm-mr

¹¹ SRI Tech. Rep. JSR-79-10, V.K.Neil

¹² J.D.Lawson, S.Penner, IEEE Journal of Quantum Electronics, QE-21, page 174, February 1985.

¹³ "Lawson-Penner Limit and Single Passage Free Electron Lasers Performances", G.Dattoli, T.Letardi, J.M.Madey, and A.Renieri, IEEE Journal of Quantum Electronics Vol QE-20, page 637, June 1984.

2. Injector Geometry

The FXR injector consists of a pulsed flash cathode diode some six and a half meters in length. The re-entrant cathode stalk threads six ferrite cores. The re-entrant anode stalk threads four ferrite cores. The nominal anode cathode potential is 2.0 Mega-Volts. The cathode emission surface is 5.4 cm in radius with an anode cathode gap adjustable between 11 and 14 cm. The nominal AK gap is 12.0 cm. As the cathode axial position is adjustable, we use the anode tip position of 6.9665 meters from the alignment monument as the fixed reference in these calculations, with zero being 14 cm toward the cathode.

$$J(A/cm^2) = 2.335 \times 10^{-6} \frac{V^{3/2}}{d^2} \quad [2.1]$$

$$I(Amperes) = J \pi r^2 \quad [2.2]$$

Taking the nominal injector design parameters of $d = 12$ cm, $V = 2.0 \times 10^6$ Volts, and $r = 5.4$ cm, we have $J = 45.86 A/cm^2$ and $I = 4201.5$ Amperes. Note the electric fringing field extending into the anode bore would actually give an effective value of d larger than the nominal 12 cm AK gap. The 3300 Ampere beam current observed from the FXR injector operated at 2.0 MV implies a current density $J = 36.02 A/cm^2$ and an effective d of 13.4 cm.

An external axial focusing magnetic field is established by five solenoid magnets exterior to the injector vacuum vessel in the region of the re-entrant anode between the last cathode ferrite and the first anode ferrite core. Four solenoids inside the anode ferrite cores extend this focusing field to the end of the injector, figure 2. An external bucking coil at the nominal axial position of the cathode is used to zero out the magnetic field on the cathode. We will use the EGUN¹⁴ code to model the starting conditions of the FXR injector. The methodology used is described in many previous reports and references¹⁵ and so will not be covered here (this reference explicitly shows an early version of the FXR injector).

¹⁴ "Electron Trajectory Program", William B. Herrmannsfeldt, Stanford Linear Accelerator Center, SLAC-166, September 1973.

¹⁵ "High-Current Relativistic Electron Guns", Arthur C. Paul, V. Kelvin Neil, pages 141-170 in "Applied Charged Particle Optics", supplement 13c, edited by A. Septier, 1983, Academic Press.

Table 6
FXR inner pipe wall radius

z(m)	z(cm)	r(mm)	comment
0.	-	-	Alignment Monument
6.8221	0.	-	EGUN data origin
6.8465	3.0	-	Cathode Lin33 tune
6.9665	14.80	-	Anode tip
		r(z)	Figure 4
7.1019	16.10	66.6	Anode minimum radius
7.3289	19.27	78.3	
7.7539	28.69	78.3	
		r(z)	Linear tapper
8.1189	53.19	41.8	
9.6569	84.46	41.8	
		r(z)	Linear tapper
9.7019	152.8	48.5	
10.3869	272.3	48.5	
10.3871	276.8	73.0	
10.4552	348.4	73.0	"Official" end of injector
44.4780	-	73.0	Location of beam bug I35

The EGUN code will model the electric field in the anode cathode gap using the actual shape of the cathode and anode shrouds, figures 4 and 5. This data is shown in table 7.

Table 7
EGUN data 0-30 cm

FXR Injector study 2 mm grid Lin33 12cm AK gap	0 41 75 0. 2.
bscale 1.0	0 41 76 0. 2.
jinput1	2 40 76 2. 0.7
fudge = -1.0	2 39 76 -0.1 0.05
converge 1.0e-6 400	2 38 75 2. 0.7
rlim=41 zlim=151	2 37 75 2. 0.4
mi=4	2 36 75 2. 0.2
mpot=1.0e5	2 35 75 2. 0.05
potn=5	2 34 75 2. 0.01
pot=0. 2.0e6 0. 0. 0.	2 33 75 2. 0.05
zphase=100.0	2 32 75 2. 0.15
magsig = -1	2 31 75 2. 0.5
jend1	2 30 76 0.01 0.01
-22.368 -21.645 -20.89 -20.107 -19.29 -18.438 -17.55 -16.628	2 29 76 2. 0.8
-15.668 -14.67 -13.634 -12.558 -11.44 -10.284 -9.086 -7.846	2 28 77 0.8 2.
-6.564 -5.240 -3.875 -2.468 -1.019 0.471 2.001 3.572	2 28 78 0.01 0.01
5.183 6.832 8.520 10.245 12.006 13.803 15.635 17.500	2 27 79 0.5 2.
19.399 21.330 23.292 25.286 27.309 29.362 31.443 33.553	2 27 80 0.2 2.
35.691 37.858 40.051 42.273 44.522 46.798 49.103 51.435	2 27 81 0.01 2.
53.796 56.186 58.606 61.055 63.534 66.045 68.588 71.163	2 27 82 0.01 2.
73.772 76.414 79.092 81.805 84.555 87.342 90.168 93.033	2 27 83 0.2 2.
95.938 98.883 101.87 104.9 107.973 111.089 114.25 117.456	2 27 84 0.6 2.
120.708 124.0 127.35 130.74 134.18 137.667 141.2 144.786	2 27 85 0.99 2.
148.417 152.097 155.825 159.6 163.427 167.299 171.22 175.186	2 28 86 0.6 2.
179.2 183.26 187.365 191.514 195.708 199.944 204.22 208.539	2 31 91 0 0.
212.897 217.292 221.724 226.19 230.69 235.223 239.785 244.375	2 33 96 0.5 2.
248.99 253.63 258.29 262.97 267.669 272.38 277.105 281.839	2 34 97 0.1 -0.2
286.58 291.324 296.07 300.815 305.554 310.287 315. 319.717	2 34 98 0.3 2.
324.409 329.08 333.73 338.354 342.949 347.51 352.038 356.526	2 34 122 0.3 2.
360.973 365.376 369.73 374.036 378.287 382.48 386.618 390.693	2 34 150 0.3 2
394.704 398.648 402.524 406.329 410.06 413.716 417.296 420.797	2 34 151 0.3 0
424.217 427.556 430.81 433.985 437.07 440.074 442.989 445.817	0 15 151 2. 0
448.559 451.21 453.779 456.259 458.65 460.957 463.177 465.312	0 0 151 0. 0
467.363 469.330	0 0 110 0. 0.
s	0 0 16 0. 0.
1 0 15 0. -0.99	888
1 10 15 2. -0.99	noinital
1 27 15 2. -0.99	jinput5
1 28 15 2. -0.99	av=15
5 29 15 2. -0.6	avr=0.5
5 30 15 0.5 -0.1	hold=5
5 31 16 2. -0.8	pervo=1.0
5 32 16 0.8 -0.4	ns=20
5 34 17 0. 0.	cl=27.0
5 35 18 0.5 -0.4	spc=0.5
5 36 19 2. -0.7	zc=16.7
5 37 19 0.2 -0.15	rmag=5
5 38 20 2. -0.7	maxray=84
5 39 20 0.5 -0.2	bscale=1.000
5 40 21 2. -0.8	magord=6
5 41 21 0. -0.4	punch=100
0 41 22 0. 2.	unit=0.002
0 41 30 0. 2.	jend5
0 41 74 0. 2.	end

Table 8
EGUN data continuation to end of gun

Data line	comments
continue FXR orbits through gun transfer point at 100 MU (20.0 cm)	\$ title line
Jinput1	\$ start input1 data
ledge 10 26 2 60	
rlim 17 zlim=201	\$ mesh 0.5 cm
zmax=201. 25.	
magseg=-1	
mi=3	
potn=26 pot=0. 2.50e6 0 0 0 0 0 0 0 2.5e6r17	
save=0	\$ read next boundary
]end1	\$ end input1 data
0r168 s	\$ zero magnetic field
10 0 1 0 -0.99	\$ Input boundary data: ipt ir iz dr dz
11 1 1 2. -0.99	\$ boundary data in mesh units
12 2 1 2. -0.99	
13 3 1 2. -0.99	
14 4 1 2. -0.99	
15 5 1 2. -0.99	
16 6 1 2. -0.99	
17 7 1 2. -0.99	
18 8 1 2. -0.99	
19 9 1 2. -0.99	
20 10 1 2. -0.99	
21 11 1 2. -0.99	
22 12 1 2. -0.99	
23 13 1 2. -0.99	
24 14 1 2. -0.99	
25 15 1 2. -0.99	
26 16 1 0. -0.99	
2 16 2 0.99 2.	\$ anode stalk
2 16 100 0.99 2.	
2 16 200 0.99 2.	
2 16 201 0.99 2.	\$ right boundary
0 8 201 2. 0.	
0 0 201 0. 0.	
0 0 200 0. 2.	\$ return along the axis
0 0 80 0. 2.	
0 0 2 0. 2.	
888	
noinital	\$ end bound data
Jinput5	\$ no initialization of U() array
save=2	\$ start input5 data
zo=-20.	
skal=0.4	\$ orbit transfer from 20 cm 0.002 meter/mesh unit data
unit=0.005	\$ 0.002/0.005 = 0.4 = old/new unit
ns=1	\$ meters/mesh unit
spc=1.0	\$ number of poisson - trajectory cycles
rmag=10.	\$ apply full space charge on this one cycle
start=cards	\$ output magnetic field at this radius
bscale = 1.0	\$ for continue from childa start, save=2
]end5	\$ end input5 data
coilgen 1.0 30.0	\$ mu/cm and zorg
-1900 332.0 50 150	
end	\$ end data

In running EGUN, a UNIX script is used to replace any "zero" magnetic field data with the real field data list generated by synthesis of the magnetic field for the tune that is being used. This script uses as its "key word" the egun data line "]end1". The number of field points to be read is specified by the repeat operator

on the next line, e.g., for the data in table 8 the repeat operator indicates 168 data points. The "s" indicates stop data input to the field free input routine.

3. Injector Magnets

The injector magnets are modeled with the Poisson code¹⁶ including the effect of the nearby ferrite cores. The data for these calculations are taken from the values shown in tables 9 and 10 for the magnets and ferrite. The field calculated on axis by Poisson is fit to a reciprocal polynomial by the simplex method¹⁷.

Table 9
Injector Magnets

Magnet Name	Generic type	Center Line Position(m)	Physical Length(mm)	radius(mm) Inner	Outer	Turns	Maximum Current(A)	Power Supply Max(Amps)
I20	Buck	Z	19.05	471.0	534.0	16	350	306
I21	SHTTRN	7.1302	138.1	154.0	169.6	33	850	588
I22	HALFCO	7.2809	138.1	154.0	169.6	33/2	850	800
I23	SHTTRN	7.4319	138.1	154.0	169.6	33	850	294
I24	LNGTRN	7.6146	200.2	154.0	169.6	49	650	104
I25	LNGTRN	7.8276	200.2	154.0	169.6	49	650	104
I31	FOC2	8.3685	400.0	102.0	117.2	105.5	500	286
I32	FOC2	8.8740	400.0	102.0	117.2	105.5	500	375
I33	FOC2	9.3795	400.0	102.0	117.2	105.5	500	375
I34	FOC4	9.8850	400.0	86.3	117.9	211	500	154
I35	BRG2	10.2755	52.0	160.0	303.0	44	1750	667
Accelerator Magnets - First Cell Block								
J21	FOC4	10.6950	400.0	86.3	117.9	211	500	-
J22	FOC4	11.2010	400.0	86.3	117.9	211	500	-
J23	FOC4	11.7065	400.0	86.3	117.9	211	500	-
J24	FOC4	12.2120	400.0	86.3	117.9	211	500	-
J25	BRG5	12.6390	130.0	160.0	303.0	110	1750	-

Magnets I21 - I35 are fit to a symmetric three parameter (c_1 , c_2 , and c_3) function

$$B_z(z) = \frac{B_o}{1 + c_1 z^2 + c_2 z^4 + c_3 z^6} \quad [3.1]$$

B_o being the magnet center field value. Poisson calculates the field on axis $B_z(z, 0)$ including the effect of adjacent ferrite cores. This is fit with a least squares algorithm giving the coefficients shown in table 11.

The asymmetric bucking coil requires a ten parameter fit, equation XX. This function is really the difference between two functions of the form of equation 3.2 with axial displacements from the magnet centerline given by c_5 and c_{10} with relative amplitude weightings of c_4 and c_9 . Define $u \equiv z - c_5$ and $w \equiv z - c_{10}$, then

¹⁶ Poisson/Superfish, Los Alamos Accelerator Code Group, LA-UR-87-126.

¹⁷ "Fitting Curves to Data", Marco Caceci, William Cacheris, Byte May 1984, page 340.

$$B_z(z) = B_o \left[\frac{c_4}{1 + c_1 u^2 + c_2 u^4 + c_3 u^6} + \frac{c_9}{1 + c_6 w^2 + c_7 w^4 + c_8 w^6} \right] \quad [3.2]$$

This function provides an excellent fit to the field from the cathode onward toward the anode. The field behind the cathode is not used in the calculations and so the quality of fit is of no importance, figure 8A.

Field measurements were made in 1995 by Rod Kerr of the J25 bridging coil (five pancakes) when it was mounted to the J20 cell block. The J20 cell block was not on the accelerator at the time so that the ferrite of cell J31 was not present. The measured central field value was 3.02 Gauss per Ampere with the coil excited at 300 Amperes. Figure 7 shows the fitted equation and the measured data. The field leakage between the gap in the ferrite cores J23-J24 is visible. The Poisson calculations were done at 10,000 Ampere turns or 90.9 Amperes in the 110 turn coil. The peak field was 271.9 Gauss giving a central field value of 2.991 Gauss per Ampere. This is 0.96% less than the measured value.

Table 10
Ferrite Data

Cell Name	Focus Coil		Ferrite Stack			
	z1(mm)	z2(mm)	z1(mm)	z2(mm)	r1(mm)	r2(mm)
I11	-	-	3558.6	3934.0	12.7	25.4
I12	-	-	4064.1	4439.5	12.7	25.4
I13	-	-	4569.6	4945.0	12.7	25.4
I14	-	-	5075.1	5450.5	12.7	25.4
I15	-	-	5814.1	6189.5	13.97	25.4
I16	-	-	6319.6	6695.0	13.97	25.4
I20a	6799.9	6818.9	-	-	-	-
I20b	6825.3	6844.3	-	-	-	-
Cathode	6836.0	-	-	-	-	-
Anode tip	6966.0	-	-	-	-	-
I21	7061.4	7199.1	-	-	-	-
-	7101.0	-	-	-	-	-
I22	7211.8	7349.9	-	-	-	-
-	7328.9	-	-	-	-	-
I23	7362.6	7501.1	-	-	-	-
I24	7513.8	7715.5	-	-	-	-
I25	7728.2	7927.0	-	-	-	-
-	7753.9	-	-	-	-	-
-	8118.9	-	-	-	-	-
I31	8168.5	8568.5	8205.1	8580.5	12.7	25.4
I32	8674.0	9074.0	8710.6	9086.0	12.7	25.4
I33	9179.5	9579.5	9216.1	9591.5	12.7	25.4
I34	9685.0	10085.0	9721.6	10097.0	12.7	25.4
-	9656.9	-	-	-	-	-
-	9701.9	-	-	-	-	-
I35	10248.5	10302.4	-	-	-	-

The normal axial extent of a solenoid field is several coil diameters. The bucking coil diameter of a meter requires that we include the first anode ferrite and the two or three cathode ferrite cores in the calculation. For all other coils, only the nearest ferrite coils adjacent to the winding needs to be included in the simulations. Figure 8A show the bucking coil field with two cathode and two anode ferrite cores. The effect of the ferrite is seen by the overlay of the the coils field without the ferrite (lower amplitude symmetric curve). The small asymmetry in coils I21, I25, I31, and I34 is barely perceptible in figures 8B, 9C, 10A, and 10D. The symmetric fitting functions eliminates this small effect except for the bucking coil.

Table 11
Magnet Field Fitting Coefficients

Magnet name	Length cm	B ₀ Gauss	z(CL) meters	c ₁ c ₆	c ₂ c ₇	c ₃ c ₈	c ₄ c ₉	c ₅ c ₁₀
I20	39.7691	68.91	682.20	7.2272e-04 2.6102e-03	3.9450e-08 1.2530e-06	2.4346e-12 9.3325e-08	1.0206 -0.6341	-2.2491 -25.629
I21	21.0337	351.57	713.00	4.3815e-03	4.6034e-06	4.6122e-10		
I22	21.0113	351.35	728.10	4.3379e-03	5.0122e-06	1.0866e-10		
I23	21.0391	350.94	743.20	4.3087e-03	5.0920e-06	5.3037e-11		
I24	23.4813	323.38	761.50	3.1334e-03	4.7381e-06	5.6616e-11		
I25	23.3923	325.36	782.80	3.2520e-03	4.1017e-06	7.2716e-10		
I31	31.6844	301.47	836.80	7.6863e-04	1.7006e-06	7.1508e-09		
I32	31.8256	301.66	887.40	8.1476e-04	1.2614e-06	7.6065e-09		
I33	31.8346	301.62	938.00	8.2509e-04	1.1379e-06	7.7810e-09		
I34	31.9792	302.52	988.50	7.8165e-04	7.7172e-07	9.1144e-09		
I35	24.7086	292.62	1027.55	3.1523e-03	-7.5555e-07	8.7111e-09		
J21	31.7641	302.28	1069.50	7.8577e-04	8.3206e-07	9.4112e-09		
J22	31.8791	302.37	1120.10	8.0327e-04	7.2659e-07	9.3196e-09		
J23	31.8718	302.40	1170.60	8.0831e-04	5.8959e-07	9.5881e-09		
J24	31.8437	302.36	1221.20	8.0229e-04	7.0671e-07	9.4651e-09		
J25	23.5413	202.26	1263.90	3.4308e-03	-1.3871e-06	1.3079e-08		

Figures 8 through 11 show the Poisson field over-plotted on a cartoon of the location of the coil and any adjacent ferrite cores used in the Poisson code data. These figures show the field generated by the fitting function in the right most frame. Every fifth point of the Poisson calculated field is plotted on the fitted curve for comparison. The field for each coil can be summed over the axial length of the injector to obtain the total field from all coils for a given tune. Figure 12 shows such a synthesized axial field profile for the Lin33 tune. Note that the field at the cathode is zero. Over-plotted on this figure is a stair-step approximation to the real field profile that will be used latter in a beam envelope treatment of the injector with the transport code.

4. Off Axis Fields

The axial fitting functions, EQ[3.1] and [3.2] provide the fields off axis by Taylor series expansion and Maxwell's equations. We show now, that sixth order expansion is sufficient to represent the fields out to 7 cm off axis for the FXR magnets. These sixth order expansions are used in the EGUN code. Analytic values can be derived for the derivatives of EQ[3.1], but these expressions become progressively more unwieldy the higher the order of expansion. To avoid this, we will use numerical interpolation of field values generated by these equations on a regular grid. The interpolating functions return the values of the derivatives up to the order of the interpolation, e.g., fourth order interpolation returns the 1st, 2nd, 3rd derivatives, and the fourth derivative is zero, etc.

Interpolations

The fundamental equation for Lagrangian interpolation is:

$$\begin{aligned}
 y(x) = & \frac{(x - x_2)(x - x_3)(x - x_4) \cdots (x - x_N)}{(x_1 - x_2)(x_1 - x_3)(x_1 - x_4) \cdots (x_1 - x_N)} y_1 + \\
 & \frac{(x - x_1)(x - x_3)(x - x_4) \cdots (x - x_N)}{(x_2 - x_1)(x_2 - x_3)(x_2 - x_4) \cdots (x_2 - x_N)} y_2 + \cdots \cdots +
 \end{aligned} \quad [4.1]$$

$$\frac{(x - x_1)(x - x_2)(x - x_4) \cdots (x - x_N)}{(x_N - x_1)(x_N - x_2)(x_N - x_3) \cdots (x_N - x_{N-1})} y_N$$

where N is the order of the interpolation. We will now derive the fourth, sixth, and eighth order formulas. Here the value of y is y_1 at x_1 etc. and the desired interpolated value of y is $y(x)$ at abscissa x. Take the N points to be equally spaced with spacing h. Let a be the distance from the expansion point to the location at which we are interpolating. Then

$$\begin{aligned} x_2 &= x_1 + h \\ x_3 &= x_1 + 2h \\ x_4 &= x_1 + 3h \\ &\dots \\ x_{N-1} &= x_1 + (N-2)h \\ x_N &= x_1 + (N-1)h \end{aligned} \quad [4.2]$$

and

$$x = x_1 + \left(\frac{N}{2} - 1 \right) h + a \quad [4.3]$$

Define the normalized displacement of the point in question from the expansion point to be

$$\delta \equiv \frac{a}{h} \quad [4.4]$$

δ has numerical value in the range of 0 - 1. In the special case where all points are evenly spaced, the denominator will take the form of $(N-1)!$ or its ratio with some other factorial, $(N-1)!/m!$ with $m < N-1$. The numerator when expanded out will generate numerical coefficients in a power series in the displacement δ . The point about which the expansion is hinged ($0 \leq \delta \leq 1$) is y_2 , at x_2 for fourth order, and y_3 , at x_3 for sixth order, and y_4 , at x_4 for eighth order.

Consider first the case of fourth order interpolation. The expansion will be from the second point, $x = x_1 + h + a$ with $x_2 \leq x \leq x_3$.

$$\begin{aligned} y(x) &= \frac{(x - x_2)(x - x_3)(x - x_4)}{(x_1 - x_2)(x_1 - x_3)(x_1 - x_4)} y_1 + \\ &\quad \frac{(x - x_1)(x - x_3)(x - x_4)}{(x_2 - x_1)(x_2 - x_3)(x_2 - x_4)} y_2 + \\ &\quad \frac{(x - x_1)(x - x_2)(x - x_4)}{(x_3 - x_1)(x_3 - x_2)(x_3 - x_4)} y_3 \\ &\quad \frac{(x - x_1)(x - x_2)(x - x_3)}{(x_4 - x_1)(x_4 - x_2)(x_4 - x_3)} y_4 \end{aligned}$$

Substituting equations [4.2] and [4.3] we have

$$\begin{aligned}
y(x) = & \frac{a(a-h)(a-2h)}{(-h)(-2h)(-3h)} y_1 + \\
& \frac{(a+h)(a-h)(a-2h)}{(h)(-h)(-2h)} y_2 + \\
& \frac{(a+h)(a)(a-2h)}{(2h)(h)(-h)} y_3 + \\
& \frac{(a+h)(a)(a-h)}{(3h)(2h)(h)} y_4
\end{aligned}$$

Expanding and re-arranging

$$\begin{aligned}
y(x) = & y_2 + \delta (-2y_1 - 3y_2 + 6y_3 - y_4) \\
& + \delta (3y_1 - 6y_2 + 3y_3) \\
& + \delta (-y_1 + 3y_2 - 3y_3 + y_4) / 6
\end{aligned} \quad [4.5]$$

The normalized derivatives are

$$\begin{aligned}
dy/d\delta = & (-2y_1 - 3y_2 + 6y_3 - y_4 + \delta (6y_1 - 12y_2 + 6y_3 + \delta (-3y_1 + 9y_2 - 9y_3 + 3y_4))) / 6 \\
d^2y/d\delta^2 = & y_1 - 2y_2 + y_3 + \delta (-y_1 + 3y_2 - 3y_3 + y_4) \\
d^3y/d\delta^3 = & -y_1 + 3y_2 - 3y_3 + y_4 \\
d^4y/d\delta^4 = & 0
\end{aligned} \quad [4.6]$$

The range of δ is 0-1 so the real field derivatives of the function with respect to the independent variable, x, are

$$dB/dx = \frac{1}{h} dy/d\delta, \quad d^2B/dx^2 = \frac{1}{h^2} d^2y/d\delta^2, \quad d^3B/dx^3 = \frac{1}{h^3} d^3y/d\delta^3, \quad d^4B/dx^4 = 0 \quad [4.7]$$

For sixth order interpolation, the expansion will be from the third point with $x_3 \leq x \leq x_4$. From the expansion of equation [4.1] through sixth order, we find the coefficients

$$t_1 \equiv 6y_1 - 60y_2 - 40y_3 + 120y_4 - 30y_5 + 4y_6$$

$$t_2 \equiv -5y_1 + 80y_2 - 150y_3 + 80y_4 - 5y_5$$

$$t_3 \equiv -5y_1 - 5y_2 + 50y_3 - 70y_4 + 35y_5 - 5y_6$$

$$t_4 \equiv 5y_1 - 20y_2 + 30y_3 - 20y_4 + 5y_5$$

$$t_5 \equiv -y_1 + 5y_2 - 10y_3 + 10y_4 - 5y_5 + y_6$$

The interpolating polynomial is

$$y(x) = y_3 + \delta (t_1 + \delta (t_2 + \delta (t_3 + \delta (t_4 + \delta t_5)))) / 120 \quad [4.8]$$

with normalized derivatives of

$$\frac{dy}{d\delta} = (t_1 + \delta (2 t_2 + \delta (3 t_3 + \delta (4 t_4 + 5 \delta t_5)))) / 120 \quad [4.9]$$

$$\frac{d^2y}{d\delta^2} = (t_2 + \delta (3 t_3 + \delta (6 t_4 + 10 \delta t_5))) / 60$$

$$\frac{d^3y}{d\delta^3} = (t_3 + 2 \delta (2 t_4 + 5 \delta t_5)) / 20$$

$$\frac{d^4y}{d\delta^4} = (t_4 + 5 \delta t_5) / 5$$

$$\frac{d^5y}{d\delta^5} = t_5$$

$$\frac{d^6y}{d\delta^6} = 0$$

The range of δ is 0-1 so the real field derivatives of the function with respect to the independent variable, x, are

$$\frac{dB}{dx} = \frac{1}{h} \frac{dy}{d\delta}, \quad \frac{d^2B}{dx^2} = \frac{1}{h^2} \frac{d^2y}{d\delta^2}, \quad \frac{d^3B}{dx^3} = \frac{1}{h^3} \frac{d^3y}{d\delta^3}, \quad [4.10]$$

$$\frac{d^4B}{dx^4} = \frac{1}{h^4} \frac{d^4y}{d\delta^4}, \quad \frac{d^5B}{dx^5} = \frac{1}{h^5} \frac{d^5y}{d\delta^5}, \quad \frac{d^6B}{dx^6} = 0$$

For eighth order interpolation, the expansion will now be from the fourth point, with $x_4 \leq x \leq x_5$. From the expansion of equation [4.1] through eighth order we find the coefficients

$$t_1 \equiv -48 y_1 + 504 y_2 - 3024 y_3 - 1260 y_4 + 5040 y_5 - 1512 y_6 + 336 y_7 - 36 y_8$$

$$t_2 \equiv 28 y_1 - 378 y_2 + 3780 y_3 - 6860 y_4 + 3780 y_5 - 378 y_6 + 28 y_7$$

$$t_3 \equiv 56 y_1 - 497 y_2 + 336 y_3 + 1715 y_4 - 3080 y_5 + 1869 y_6 - 448 y_7 + 49 y_8$$

$$t_4 \equiv -35 y_1 + 420 y_2 - 1365 y_3 + 1960 y_4 - 1365 y_5 + 420 y_6 - 35 y_7$$

$$t_5 \equiv -7 y_1 - 14 y_2 + 189 y_3 - 490 y_4 + 595 y_5 - 378 y_6 + 119 y_7 - 14 y_8$$

$$t_6 \equiv 7 y_1 - 42 y_2 + 105 y_3 - 140 y_4 + 105 y_5 - 42 y_6 + 7 y_7$$

$$t_7 \equiv -y_1 + 7 y_2 - 21 y_3 + 35 y_4 - 35 y_5 + 21 y_6 - 7 y_7 + y_8$$

The interpolating polynomial is

$$y(x) = y_4 + \delta (t_1 + \delta (t_2 + \delta (t_3 + \delta (t_4 + \delta (t_5 + \delta (t_6 + \delta t_7)))))) / 5040 \quad [4.11]$$

with normalized derivatives of

$$\frac{dy}{d\delta} = t_1 + \delta (2 t_2 + \delta (3 t_3 + \delta (4 t_4 + \delta (5 t_5 + \delta (6 t_6 + 7 \delta t_7))))) / 5040 \quad [4.12]$$

$$\frac{d^2y}{d\delta^2} = t_2 + \delta (3 t_3 + \delta (6 t_4 + \delta (10 t_5 + \delta (15 t_6 + 21 \delta t_7)))) / 2520$$

$$\frac{d^3y}{d\delta^3} = t_3 + \delta (4 t_4 + 5 \delta (2 t_5 + \delta (4 t_6 + 7 \delta t_7))) / 840$$

$$\frac{d^4y}{d\delta^4} = t_4 + 5 \delta (t_5 + \delta (3 t_6 + 7 \delta t_7)) / 210$$

$$\frac{d^5y}{d\delta^5} = t_5 + \delta (6 t_6 + 21 \delta t_7) / 42$$

$$\frac{d^6y}{d\delta^6} = (t_6 + 7 \delta t_7) / 7$$

$$\frac{d^7y}{d\delta^7} = t_7$$

$$\frac{d^8y}{d\delta^8} = 0$$

Remember, the actual magnetic field derivatives are

$$\begin{aligned} dB/dx &= \frac{1}{h} dy/d\delta, & d^2B/dx^2 &= \frac{1}{h^2} d^2y/d\delta^2, & d^3B/dx^3 &= \frac{1}{h^3} d^3y/d\delta^3, & d^4B/dx^4 &= \frac{1}{h^4} d^4y/d\delta^4 \\ d^5B/dx^5 &= \frac{1}{h^5} d^5y/d\delta^5, & d^6B/dx^6 &= \frac{1}{h^6} d^6y/d\delta^6, & d^7B/dx^7 &= \frac{1}{h^7} d^7y/d\delta^7, & d^8B/dx^8 &= 0 \end{aligned} \quad [4.13]$$

It should be noted that for any order of interpolation, fourth, sixth, etc. that if $\delta = 0$ the interpolated value is the value of the data point from which the expansion is hinged, namely y_2 for fourth order, y_3 for sixth order, and y_4 for eighth order.

$$y(x) \mid \delta = 0 = \begin{cases} y_2, & 4 \text{ th order} \\ y_3, & 6 \text{ th order} \\ y_4, & 8 \text{ th order} \end{cases}$$

If $\delta = 1$ then the sum of the numerical coefficients of any of the y values is zero with the exception of the $(N/2)$ and $(N/2)+1$ values. These are equal to $-y_{(N/2)}$ and $y_{(N/2)+1}$ respectively. Specifically in the case of eighth order, $\delta = 1$

$$\sum_{j=1}^{N-1} a_j y_1 = 0, \quad \sum_{j=1}^{N-1} a_j y_2 = 0, \quad \sum_{j=1}^{N-1} a_j y_3 = 0,$$

$$\sum_{j=1}^{N-1} a_j y_4 = -y_4, \quad \sum_{j=1}^{N-1} a_j y_5 = y_5$$

$$\sum_{j=1}^{N-1} a_j y_6 = 0, \quad \sum_{j=1}^{N-1} a_j y_7 = 0, \quad 7 \sum_{j=1}^{N-1} a_j y_8 = 0,$$

These are a good test to make for checks on numerical typo errors. Four the three cases considered here, the numerical coefficients are summarized in table 12 along with their row and column sums

Fourth Order $(N-1)! = 3 * 2 * 1 = 6$, sixth Order $(N-1)! = 5 * 4 * 3 * 2 * 1 = 120$, and eighth Order $(N-1)! = 7 * 6 * 5 * 4 * 3 * 2 * 1 = 5040$.

Table 12
Coefficients, equation row and column sums, $\delta = 1$.

row Σ	1	2	3	4	5	6	7	8
Fourth Order								
0	-2	-3	6	-1				
0	3	-6	3					
0	-1	3	-3	1				
0 column->	0	-6	6	0				
Sixth Order								
0	6	-60	-40	120	-30	4		
0	-5	80	-150	80	-5			
0	-5	-5	50	-70	35	-5		
0	5	-20	30	-20	5			
0	-1	5	-10	10	-5	1		
0 column->	0	0	-120	120	0	0		
Eighth Order								
0	-48	504	-3024	-1260	5040	-1512	336	-36
0	28	-378	3780	-6860	3780	-378	28	
0	56	-497	336	1715	-3080	1869	-448	49
0	-35	420	-1365	1960	-1365	420	-35	
0	-7	-14	189	-490	595	-378	119	-14
0	7	-42	105	-140	105	-42	7	
0	-1	7	-21	35	-35	21	-7	1
0 column->	0	0	0	-5040	5040	0	0	0

5. Off Axis Field Expansions

EGUN uses sixth order expansions of the axial magnetic field to find the values of $B_z(z, r)$ and $B_r(z, r)$ at the trajectory coordinates during integration. We now show that for the radial range of interest in the FXR injector, these expansions are sufficient and the fitting equations EQ[3.1] and EQ[3.2] are adequate for modeling the FXR injector magnets.

The axial field component from a solenoid magnet is given from an assumed power series expansion of $B_z(0, z)$ along the axis of cylindrical symmetry ($r=0$)

$$B_z(r, z) = b_0(z) + b_2(z)r^2 + b_4(z)r^4 + b_6(z)r^6 + \dots \quad [5.1]$$

Odd powers of r do not occur from the condition of axial symmetry and the b 's are functions only of z .

$$\vec{B} = \nabla \times \vec{A} = \hat{r} \left[\frac{1}{r} \frac{\partial A_z}{\partial \theta} - \frac{\partial A_\theta}{\partial z} \right] + \hat{\theta} \left[\frac{\partial A_r}{\partial z} - \frac{\partial A_z}{\partial r} \right] + \hat{z} \left[\frac{1}{r} \frac{\partial}{\partial r} (r A_\theta) - \frac{1}{r} \frac{\partial A_r}{\partial \theta} \right] \quad [5.2]$$

Only A_θ components exist since current loops are concentric with the z axis in cylindrically symmetry.

$$\vec{B} = -\hat{r} \frac{\partial A_\theta}{\partial z} + \hat{z} \frac{1}{r} \frac{\partial}{\partial r} (r A_\theta)$$

$$B_r = -\frac{\partial A_\theta}{\partial z} \quad B_z = \frac{1}{r} \frac{\partial}{\partial r} (r A_\theta)$$

Integration of the B_z equation gives the value of A_θ in terms of the expansion coefficients b_n .

$$r A_\theta = \int r B_z(r) dr = \int \left(b_0 r + b_2 r^3 + b_4 r^5 + b_6 r^7 + b_8 r^9 + \dots \right) dr$$

$$= \frac{1}{2} b_0 r^2 + \frac{1}{4} b_2 r^4 + \frac{1}{6} b_4 r^6 + \frac{1}{8} b_6 r^8 + \dots$$

$$A_\theta = \frac{1}{2} b_0 r + \frac{1}{4} b_2 r^3 + \frac{1}{6} b_4 r^5 + \frac{1}{8} b_6 r^7 + \dots$$

$$B_r = -\frac{\partial A_\theta}{\partial z} = -\frac{1}{2} b_0' r - \frac{1}{4} b_2' r^3 - \frac{1}{6} b_4' r^5 - \frac{1}{8} b_6' r^7 + \dots$$

with $b_n' \equiv db_n/dr$. Since we have no current conductors inside the region of consideration, $\nabla \times B = 0$

$$\frac{\partial B_r}{\partial z} - \frac{\partial B_z}{\partial r} = 0$$

$$\frac{\partial}{\partial z} \left[-\frac{1}{2} b_0' r - \frac{1}{4} b_2' r^3 - \frac{1}{6} b_4' r^5 - \frac{1}{8} b_6' r^7 - \dots \right] - \frac{\partial}{\partial r} \left[b_0 + b_2 r^2 + b_4 r^4 + b_6 r^6 + b_8 r^8 + \dots \right] = 0$$

$$-\frac{1}{2} b_0'' r - \frac{1}{4} b_2'' r^3 - \frac{1}{6} b_4'' r^5 - \frac{1}{8} b_6'' r^7 - \dots - 2b_2 r - 4b_4 r^3 - 6b_6 r^5 - 8b_8 r^7 - \dots = 0$$

Collecting like powers of r

$$-\left(\frac{1}{2} b_0'' + 2b_2\right) r - \left(\frac{1}{4} b_2'' + 4b_4\right) r^3 - \left(\frac{1}{6} b_4'' + 6b_6\right) r^5 - \left(\frac{1}{8} b_6'' + 8b_8\right) r^7 - \dots = 0$$

if r is non-zero, we must have the coefficients of each power of r zero

$$b_2 = -\frac{1}{2^2} b_0''$$

$$b_4 = -\frac{1}{4^2} b_2'' = \frac{1}{2^2 4^2} b_0'''$$

$$b_6 = -\frac{1}{6^2} b_4'' = -\frac{1}{2^2 4^2 6^2} b_0^{VI}$$

$$b_8 = -\frac{1}{8^2} b_6'' = -\frac{1}{2^2 4^2 6^2 8^2} b_0^{VIII}$$

resulting in the B_z and B_r power series expansions of

$$B_z(r, z) = b_0(z) - \frac{1}{2^2} b_0''(z) r^2 + \frac{1}{2^2 4^2} b_0'''(z) r^4 - \frac{1}{2^2 4^2 6^2} b_0^{VI}(z) r^6 + \dots \quad [5.3]$$

$$B_r(r, z) = -\frac{1}{2} b_0'(z) r + \frac{1}{2^2 4} b_0'''(z) r^3 - \frac{1}{2^2 4^2 6} b_0^V(z) r^5 + \frac{1}{2^2 4^2 6^2 8} b_0^{VII}(z) r^7 - \dots \quad [5.4]$$

In summary,

$$B_z(r, z) = \sum_1^\infty (-1)^{n+1} \left(\frac{r}{2}\right)^{2n-2} \frac{b_0^{(2n-2)}}{[(n-1)!]^2} \quad [5.5]$$

$$B_r(r, z) = \sum_1^\infty \frac{(-1)^n r^{2n-1} b_0^{(2n-1)}}{2^n 2^{2n-2} [(n-1)!]^2} \quad [5.6]$$

$$A_\theta(r, z) = \sum_1^\infty \frac{(-1)^{n+1} b_o^{(2n-2)}}{n[(n-1)!]^2} \left(\frac{r}{2}\right)^{2n-1} \quad [5.7]$$

Consider Maxwell's equation $\nabla \cdot B = 0$ and $\nabla \times B = 0$ in the cylindrical symmetry of the solenoid geometry

$$\nabla \cdot B = \frac{1}{r} \frac{\partial(rB_r)}{\partial r} + \frac{\partial B_z}{\partial z}$$

$$\nabla \times B = \frac{\partial B_z}{\partial z} - \frac{\partial B_r}{\partial r}$$

The divergence equation is satisfied exactly if the field expansions are taken up to some odd order and truncated. The curl equation is satisfied exactly if the field expansions are taken up to some even order and truncated, therefore both of these equations can not be simultaneously satisfied.

FIRST ORDER

Consider equations [5.3] and [5.4] to first order,

$$B_r = -\frac{1}{2} b' r \quad [5.8]$$

$$B_z = b_o(z)$$

THIRD ORDER

If these field equations are taken to third order, then

$$B_r = -\frac{1}{2} b'r + \frac{1}{16} b'''r^3 \quad [5.9]$$

$$B_z = b - \frac{1}{4} b''r^2$$

and Maxwell's equations are satisfied as

$$\nabla \cdot B = 0 \text{ exactly}$$

$$\nabla \times B = \frac{1}{16} b^{IV} r^3 \quad \text{third order in } r$$

SIXTH ORDER

If the field equations are taken to sixth order, then

$$B_r = -\frac{1}{2} b'r + \frac{1}{16} b'''r^3 - \frac{1}{2^2 4^2 6} b^V r^5 + O(7) \quad [5.10]$$

$$B_z = b - \frac{1}{2^2} b''r^2 + \frac{1}{2^2 4^2} b^{IV} r^4 - \frac{1}{2^2 4^2 6^2} b^{VI} r^6 + O(8)$$

and Maxwell's equations become

$$\nabla \cdot B = -\frac{1}{2^2 4^2 6^2} b^{VII} r^6 \quad \text{sixth order in } r$$

$$\nabla \times B = 0 \text{ exactly}$$

The axial field derivatives b' , b'' , b''' , are given by equations [4.7], [4.10], and [4.13] for first, third and sixth order.

Table 13
Maximum field values for Poisson code, and 1st, 3rd, 6th order field expansions.

Radius r(cm)	Maximum Bz(z,r)				Maximum Br(z,r)			
	First order [5.8]	Third order [5.9]	Sixth order [5.10]	Poisson code	First order [5.8]	Third order [5.9]	Sixth order [5.10]	Poisson code
0.00	325.360	325.360	325.360	325.360	0.000	0.000	0.000	0.000
1.00	325.360	325.889	325.890	325.879	7.231	7.245	7.245	7.504
2.00	325.360	327.476	327.491	-	14.463	14.571	14.572	-
3.00	325.360	330.121	330.207	329.911	21.694	22.058	22.067	22.881
4.00	325.360	333.824	334.149	-	28.926	29.788	29.825	-
5.00	325.360	338.585	339.540	338.131	36.157	37.842	37.954	39.418
6.00	325.360	344.404	346.794	-	43.389	46.300	46.579	-
7.00	325.360	351.282	356.608	350.840	50.620	55.244	55.846	58.312
8.00	325.360	359.217	370.074	-	57.851	64.753	65.927	-

These sixth order field expansions based on the fitting equations [3.1] and [3.2] compare well with the Poisson code field values, figures 17 and 18. Remember, the Poisson code calculates the vector potential which is differentiated to give the axial and radial field values. These expansions are subject to the same limits as considered here in developing field components off-axis from the axial field values.

Table 14
Off axis field errors (Referenced to field values calculated by Poisson)

R cm	δB_z percent			δB_r percent		
	First order	Third order	Sixth order	First order	Third order	Sixth order
0.	0.	0.	0.	0.	0.	0.
1.00	0.16	-0.003	0.0034	3.64	3.45	3.45
2.00						
3.00	1.38	-0.064	0.0897	5.19	3.60	3.56
4.00						
5.00	3.78	-0.134	0.417	8.27	4.00	3.71
6.00						
7.00	7.26	-0.126	1.64	13.2	5.26	4.23
8.00						

The apparent "best fit" to third order seen in the above table for the B_z field component is an artifact of the fact that in the field expansion done by Poisson about the actual value of the vector potential calculated at point (z,r) the expansion was carried out by Poisson code only to third order. If real field measured values were used for the actual file, the sixth order values would have generated a "better fit". The constant 3-4 percent field error seen in the B_r component is attributable to the field expansion algorithm used in the Poisson code. The value of the vector potential is calculated at the off-axis coordinates and locally differentiated.

CONCLUSION

sixth order field expansions are ok out to 6 cm radius for FXR

6. Beam Emittance

The ability to focus a beam of particles to a small spot requires that the particles occupy a small volume in phase space. In two dimensions, the area of the beam in $r-r'$ space divided by π is called the two dimensional emittance of the beam. The square of this quantity is the determinant of the sigma matrix parameters describing the elliptical boundary circumscribing all the particles comprising this beam.

The centroid motion of the beam exiting the accelerator can be calculated by the simple vector transformation using the first order linear transformation matrix extending from the accelerator exit to the point of evaluation.

$$V = R V_o \quad [6.1]$$

where V is the vector $(x, x', y, y')^T$ and R is the transformation matrix

$$R = \begin{bmatrix} R_{11} & R_{12} & R_{13} & R_{14} \\ R_{21} & R_{22} & R_{23} & R_{24} \\ R_{31} & R_{32} & R_{33} & R_{34} \\ R_{41} & R_{42} & R_{43} & R_{44} \end{bmatrix}. \quad [6.2]$$

This matrix is the product of the various matrices representing the elements along the beamline.

The beam envelope transforms by this same transformation matrix as a similarity transformation. The sigma matrix is constrained by the invariance of the beam emittance. Let a axially symmetric beam ($x=y$, $x'=y'$, $r_{31}=r_{42}=r_{32}=r_{41}=0$) be defined by the vector $V_o \equiv (r, r')^T$ (This beam is at a waist if we impose the further restriction that $r_{21}=r_{43}=0$.) The phase space bounding the ensemble of particles comprising this beam is given by the ellipse coefficients expressed in the σ matrix

$$V_o^T \sigma_o^{-1} V_o = 1 \quad [6.3]$$

The beam σ then transforms by the above R matrix as

$$\sigma = R \sigma_o R^T \quad [6.4]$$

It can be shown that the square root of the diagonal elements of the sigma matrix are the physical projections of the beam onto the coordinate axes and that the determinant of this matrix is the square of the beam emittance.

$$\det(\sigma) = \epsilon^2 = \sigma_{11}\sigma_{22} - \sigma_{21}^2 \quad [6.5]$$

$$r = \sqrt{\sigma_{11}} = \sqrt{\sigma_{33}}$$

and

$$r' = \sqrt{\sigma_{22}} = \sqrt{\sigma_{44}}$$

For a non-axially symmetric beam, we have

$$\begin{pmatrix} x \\ x' \\ y \\ y' \end{pmatrix} = \begin{pmatrix} \sigma(1, 1)^{\frac{1}{2}} \\ \sigma(2, 2)^{\frac{1}{2}} \\ \sigma(3, 3)^{\frac{1}{2}} \\ \sigma(4, 4)^{\frac{1}{2}} \end{pmatrix} \quad \text{or} \quad \begin{pmatrix} \sigma_{11}^{\frac{1}{2}} \\ \sigma_{22}^{\frac{1}{2}} \\ \sigma_{33}^{\frac{1}{2}} \\ \sigma_{44}^{\frac{1}{2}} \end{pmatrix} \quad [6.6]$$

with possible non-zero correlations between the axis x , x' , y , and y' ($r_{21}, r_{31}, r_{32}, r_{41}, r_{42}, r_{43}$).

Uniform distribution

$$\rho_u(r) \equiv \rho_o \quad [6.7]$$

Let a be the beam edge radius and a' be the edge phase space maximum angle extent. The half width half maximum radius r_h is the same as the edge radius of the beam. The rms beam radius is

$$r_{\text{RMS}}^2 = \frac{\int_0^a \rho_o r^3 dr}{\int_0^a \rho_o r dr} = \frac{1}{2} a^2$$

$$r_{\text{RMS}} = \frac{a}{\sqrt{2}} \quad [6.8]$$

The rms phase space angle is

$$r'_{\text{RMS}} = \frac{a'}{\sqrt{2}} \quad [6.9]$$

and the rms emittance $\epsilon_{\text{RMS}} \equiv r_{\text{RMS}} r'_{\text{RMS}}$ and hard edge beam emittance $\epsilon_{\text{he}} \equiv a a'$ is

$$\begin{aligned} \epsilon_{\text{RMS}} &\equiv r_{\text{RMS}} r'_{\text{RMS}} = \frac{1}{2} a a' \\ \epsilon_{\text{he}} &= 2 \epsilon_{\text{RMS}} \end{aligned} \quad [6.10]$$

Parabolic distribution

$$\rho_p(r) \equiv \rho_o \left[1 - \left(\frac{r}{a} \right)^2 \right] \quad [6.11]$$

The half width half maximum radius r_h is given by

$$\begin{aligned} \frac{\rho_p(r_h)}{\rho_o} &= \frac{1}{2} = 1 - \left(\frac{r_h}{a} \right)^2 \\ r_h &= \frac{a}{\sqrt{2}} \end{aligned} \quad [6.12]$$

The rms beam radius is

$$\begin{aligned} r_{\text{RMS}}^2 &= \frac{\int_0^a \rho_o \left[1 - \left(\frac{r}{a} \right)^2 \right] r^3 dr}{\int_0^a \rho_o \left[1 - \left(\frac{r}{a} \right)^2 \right] r dr} = \frac{1}{3} a^2 \\ r_{\text{RMS}} &= \frac{a}{\sqrt{3}} \end{aligned} \quad [6.13]$$

The amplitude at the rms radius is $2/3$ the peak amplitude. The rms emittance ϵ_{RMS} and hard edge beam emittance ϵ_{he} is

$$\begin{aligned} \epsilon_{\text{RMS}} &= \frac{1}{3} a a' \\ \epsilon_{\text{he}} &= 3 \epsilon_{\text{RMS}} \end{aligned} \quad [6.14]$$

Gaussian distribution

$$\rho_g(r) \equiv \rho_o e^{-r^2/\sigma^2} \quad [6.15]$$

The half width half maximum radius r_h

$$\rho_g(r_h) = \rho_o e^{-(r_h/\sigma)^2}$$

$$\frac{\rho_g(r_h)}{\rho_o} = \frac{1}{2} = e^{-(r_h/\sigma)^2} \rightarrow r_h = \sqrt{\ln 2} \sigma$$

and the rms beam radius is

$$r_{\text{RMS}}^2 \equiv \frac{\int_0^\infty \rho_o e^{-(r/\sigma)^2} r^3 dr}{\int_0^\infty \rho_o e^{-(r/\sigma)^2} r dr} \equiv \sigma^2$$

$$r_{\text{RMS}} = \sigma$$

The rms emittance ϵ_{RMS} is

$$\epsilon_{\text{RMS}} = \sigma \sigma' \quad [6.16]$$

where σ' is the Gaussian with of the phase space angle distribution of the r' coordinate. In order to connect the Gaussian emittance to the beam edge emittance, we must cut off the Gaussian at some amplitude. Consider first truncation of the amplitude at 0.1 maximum value. This determines the Gaussian width σ in terms of the beam hard edge radius a .

$$\frac{\rho_g(a)}{\rho_o} = 0.1$$

$$10 = e^{a^2/\sigma^2} \rightarrow \sigma = \frac{a}{\sqrt{\ln 10}} = 0.6590 a$$

$$\epsilon_{\text{he}} = a a' = \ln 10 \sigma \sigma' = \ln 10 r_{\text{RMS}} r'_{\text{RMS}}$$

$$\epsilon_{\text{he}} = 2.30 \epsilon_{\text{RMS}}$$

Table 15
Comparison between the different distributions

Distribution function	cutoff amplitude	beam edge	r_{rms}	r_h	ϵ_{rms}	ϵ_{he}
uniform	-	a	$a/\sqrt{2}$	a	$1/2 aa'$	$2\epsilon_{\text{rms}}$
parabolic	-	a	$a/\sqrt{3}$	$a/\sqrt{2}$	$1/3 aa'$	$3\epsilon_{\text{rms}}$
Gaussian	-	∞	σ	$\sqrt{\ln 2} \sigma$	$\sigma \sigma'$	-
"	0.13534	$\sqrt{2}$	-	-	-	$2\epsilon_{\text{rms}}$
"	0.1	$\sqrt{\ln 10} \sigma$	-	-	-	$2.30\epsilon_{\text{rms}}$
"	0.0498	$\sqrt{3} \sigma$	-	-	-	$3\epsilon_{\text{rms}}$
"	0.0183	2σ	-	-	-	$4\epsilon_{\text{rms}}$

7. Injector Modeling

The electrode data is divided into two zones. The first zone models the injector from the egun origin to 30 centimeters. The egun origin is the centerline of the bucking coil which coincides with the cathode location giving the largest possible anode cathode gap. The second zone extends from 20 cm to the end of the injector, 355 cm, figures 21 and 22. The on axis magnetic field used in these calculations is the field generated by equations [3.1] and [3.2] summed over all the magnets, figures 11, 18, and 19 for the Lin33, SPU28, and double pulse tunes. The first zone is iteratively solved for a self consistent solution of the emitted beam current from the cathode using Child's law [2.1] and [2.2], figure 22. The particle distribution at 20 cm has the phase space shown in figure 24. The beam parameters, r , dr/dz , e (volts), z , \dot{r} , \dot{z} , t , e_{phi} , $u_{amps}/radian$, and ϕ for each trajectory (axial symmetric cylinder) are taken at 20 cm and used as input to the second run starting at 20 cm and extending to the end of the injector, figure 21. This is a single pass calculation using Ampere's law to determine the beams self magnetic field and Gauss's law to determine the radial space charge field, figure 26. The results of these calculations are post-processed to find the beam emittance along the FXR injector, figure 27.

These calculations have used emission from the cathode that has zero intrinsic temperature. In the next section we will consider the effect on the beam phase space of an initial transverse beam temperature generated by the "felt" cathode. For these $T_e = 0$ zero temperature runs, the phase space at the 20 cm transfer location is described by the following sigma matrix, figure 24:

$$\sigma = \begin{bmatrix} \sigma_{11} & \sigma_{21} \\ \sigma_{21} & \sigma_{22} \end{bmatrix} = \begin{bmatrix} 5.891 & 764.003 \\ 764.003 & 129.722 \end{bmatrix} \quad [7.1]$$

Note that the σ matrix is symmetric, explicitly $\sigma_{12} \equiv \sigma_{21}$.

$$r_{21} \equiv \frac{\sigma_{21}}{\sqrt{\sigma_{11}} \sqrt{\sigma_{22}}} \quad [7.2]$$

where

$$\sigma_{11} = \frac{4}{N} \sum_0^N r^2 \quad [7.3]$$

$$\sigma_{21} = \frac{4}{N} \sum_0^N r r'$$

$$\sigma_{22} = \frac{4}{N} \sum_0^N r'^2$$

are calculated according to the statistical sums¹⁸ of all the N trajectory points shown in figure 24. The bounding ellipse described by σ is also shown in this figure.

$$\epsilon_{Edge}^2 = \sigma_{11} \sigma_{22} - \sigma_{21}^2 \quad [7.4]$$

This is the same equation as [6.5]. The beam emittance is the square root of the determinant of the sigma matrix. From the numerical values of equation [7.1] we have for the Lin33 tune at the 20 cm transfer position:

$$\epsilon_{Edge} = 15.903 \text{ cm} - \text{mr}$$

For Lin33 tune at the end of the injector, $z=355$ cm, we have a beam energy of 1.9280 MeV for 2.1 MV anode potential.

$$\sigma^{1/2} = \begin{bmatrix} \sigma_{11}^{1/2} \\ \sigma_{22}^{1/2} \end{bmatrix} \quad r_{21} = \begin{bmatrix} 4.313 & \text{cm} \\ 25.300 & \text{mr} \end{bmatrix} \quad -0.86920 \quad \text{emittance } 53.96 \text{ cm} - \text{mr.} \quad [7.5]$$

¹⁸ "Statistical Beam Transport for High Intensity Ion Currents", C.Robert Emigh, 1972 Linac Conference.

8. Cathode Temperature

The effect of a finite initial phase space can be included in the EGUN simulations by introducing an initial non-zero value to the transverse momentum coordinate. /" /" new particle load /" kray, Te /" The unit used is the effective cathode temperature in Kelvin. Non-relativistically, the thermal energy of the cathode is converted to transverse momentum by

$$E = \frac{1}{2} m v^2 = k T$$

k the Boltzmann constant (1.38×10^{-23} Joules/Kelvin), m the electron mass, and v the thermal velocity.

$$v = \sqrt{\frac{2 k T}{m}} = \left[\frac{2 k T}{m_0 c^2} \right]^{1/2} c$$

The electron rest energy $m_0 c^2 = 0.511 \times 10^6$ eV $\times 1.6 \times 10^{-19}$ J/eV.

$$v = c \sqrt{T} \quad 1.837 \times 10^{-5} = 5512 \sqrt{T} \text{ m/sec}$$

The energy of a 1073 Kelvin beam is 0.0925 electron volts. When the initial particle load to EGUN includes the thermal temperature of 20,000 Kelvin (1.7 eV), the beam edge emittance at 20 cm is increased to

$$\epsilon_{\text{Edge}} = 33.9 \text{ cm-mr}$$

Table 16
Cathode Temperature and Transverse Energy
Edge emittance at the 20 cm transfer location

Temperature Kelvin	Energy eV	speed m/sec	emittance cm-mr	
0	0	0	15.35	Absolute zero
1,000	0.0925	1.806E5	16.88	typical thermionic cathode
2,000	0.173	2.465E5	18.21	
5,000	0.431	3.898E5	21.72	
10,000	0.863	5.512E5	26.39	
20,000	1.725	7.795E5	33.90	velvet cathode
30,000	2.587	9.547E5	39.79	
50,000	4.312	1.233E6	46.09	

Figure 31 shows the 20 cm phase space for the cathode temperatures of table 16. The temperature that should be used depends on the details of the emission surface. Conventional wisdom says that a velvet cathode would have 1-2 eV transverse emission energy. The self-consistent beam trajectories generated by EGUN with an initial 1.7 eV transverse energy are shown in figure 32 for 0-30 cm. This figure should be compared with figure 23 for a cold beam. The phase space used as initial condition for the EGUN single pass run to the end of the injector is shown in figure 33. The combined trajectories from the emission surface to the end of the injector, 3-355 cm, along with the magnetic field is shown in figure 34. The beam emittance along the injector for 0 and 1.7 eV cathode emission is shown in figures 27 and 35. Surprisingly, these plots are quite similar. The phase space "flexing" generated by the beam flutter dominates the emittance as shown in figure 36 for both a zero temperature and 2e4 Kelvin beams at z of 200 cm, approximately the center of magnet I32. For the zero temperature beam

$$\sigma^{1/2} = \begin{bmatrix} \sigma_{11}^{1/2} & & \\ \sigma_{22}^{1/2} & r_{21} & \end{bmatrix} = \begin{bmatrix} 5.8259 & \text{cm} \\ 125.8808 & \text{mr} & 0.9998 \end{bmatrix}$$

while for the 2e4 Kelvin (1.7 eV) beam

$$\sigma^{1/2} = \begin{bmatrix} \sigma_{11}^{1/2} \\ \sigma_{22}^{1/2} \end{bmatrix}_{r_{21}} = \begin{bmatrix} 5.4284 & \text{cm} \\ 126.3630 & \text{mr} \end{bmatrix} \quad 0.9989$$

with emittance values of

$$\varepsilon_{\text{he}} \begin{cases} 0 & \text{Kelvin} \\ 2 \times 10^4 \text{ Kelvin} \end{cases} = \begin{cases} 15.04 \text{ cm-mr} \\ 33.90 \text{ cm-mr} \end{cases}$$

The conclusion is that the exact value of the cathode temperature is not important in determining the emittance of the FXR injector in the range of emittance in which it is operating.

9. Matching the Beam to the Magnetic Field

In-order to minimize the beam flutter we need the beam matched to the magnetic field for the give beam current and intrinsic emittance. Preceding from the space charge beam envelop equation for a matched beam, $r'' = 0$

$$r'' + k^2 r = \frac{\varepsilon_{\text{he}}^2}{r^3} + \frac{2I}{I_A} \frac{1}{(\beta\gamma)^3} \frac{1}{r} \quad [9.1\text{XX}]$$

We define a beam radius for a zero current beam of the given edge emittance ε_{he} as r_e and a zero emittance beam of the given current I as r_i . Then

$$k^2 r_e^4 \equiv \varepsilon_{\text{he}}^2$$

and

$$k^2 r_i^2 \equiv \frac{2I}{I_A} \frac{1}{(\beta\gamma)^3}$$

For the actual beam of current I and emittance ε_{he}

$$k^2 r^4 = k^2 r_e^4 + k^2 r^2 r_i^2$$

Solving this quadratic equation for r

$$r^2 = \frac{r_i^2}{2} + \sqrt{\frac{r_i^4}{4} + r_e^4} \quad [9.2\text{XX}]$$

Table 17 shows the values of the matched radius for different average values of the magnetic field for a 2.0 MeV, 3.3 KAmp, 70 cm-mr beam.

Table 17
Matched radius

E(MeV)	$\beta\gamma$	I(kA)	ε_{he} (cm-mr)	B(kG)	r_i (cm)	r_e (cm)	r(cm)
2.0	4.8111	3.300	70.000	0.2500	3.8735	2.1429	4.0371
2.0	4.8111	3.300	70.000	0.3000	3.2279	1.9562	3.4167
2.0	4.8111	3.300	70.000	0.3500	2.7668	1.8111	2.9780
2.0	4.8111	3.300	70.000	0.4000	2.4210	1.6941	2.6519
2.0	4.8111	3.300	70.000	0.4500	2.1520	1.5973	2.4002
2.0	4.8111	3.300	70.000	0.5000	1.9368	1.5153	2.2001
2.0	4.8111	3.300	70.000	0.5500	1.7607	1.4448	2.0371
2.0	4.8111	3.300	70.000	0.6000	1.6140	1.3833	1.9019
2.0	4.8111	3.300	70.000	0.6500	1.4898	1.3290	1.7877
2.0	4.8111	3.300	70.000	0.7000	1.3834	1.2806	1.6899
2.0	4.8111	3.300	70.000	0.7500	1.2912	1.2372	1.6052
2.0	4.8111	3.300	70.000	0.8000	1.2105	1.1979	1.5310
2.0	4.8111	3.300	70.000	0.8500	1.1393	1.1622	1.4654
2.0	4.8111	3.300	70.000	0.9000	1.0760	1.1294	1.4070

and for a 2.1 MeV 25 cm-mr beam

Table 18
Matched radius

E(MeV)	$\beta\gamma$	I(kA)	ϵ_{he} (cm-mr)	B(kG)	r _i (cm)	r _e (cm)	r(cm)
2.1000	5.0108	3.300	25.000	0.2500	3.7955	1.3070	3.8218
2.1000	5.0108	3.300	25.000	0.3000	3.1630	1.1931	3.1942
2.1000	5.0108	3.300	25.000	0.3500	2.7111	1.1046	2.7472
2.1000	5.0108	3.300	25.000	0.4000	2.3722	1.0332	2.4131
2.1000	5.0108	3.300	25.000	0.4500	2.1086	0.9742	2.1542
2.1000	5.0108	3.300	25.000	0.5000	1.8978	0.9242	1.9478
2.1000	5.0108	3.300	25.000	0.5500	1.7252	0.8812	1.7796
2.1000	5.0108	3.300	25.000	0.6000	1.5815	0.8436	1.6399
2.1000	5.0108	3.300	25.000	0.6500	1.4598	0.8105	1.5223
2.1000	5.0108	3.300	25.000	0.7000	1.3556	0.7811	1.4218
2.1000	5.0108	3.300	25.000	0.7500	1.2652	0.7546	1.3351
2.1000	5.0108	3.300	25.000	0.8000	1.1861	0.7306	1.2595
2.1000	5.0108	3.300	25.000	0.8500	1.1163	0.7088	1.1931
2.1000	5.0108	3.300	25.000	0.9000	1.0543	0.6888	1.1343

Note that the average B_z for the LIN33 tune in the anode stalk (axial range 800-1050 cm), figure 12, of the FXR injector is around 470 Gauss. From table 17 the matched radius for this field value is around 2.3 cm while the EGUN beam envelop calculations show the radius entering the anode stalk to be closer to 4.0 cm, figures 25, 26. This "mis-match" would be consistent with the beam envelop flutter (oscillations) shown in these figures. For the SPU28 tune, the average B_z in the anode stalk, figure 19, is around 220 Gauss. From tables 17 and 18 the matched radius is around 4.0 cm for 250 Gauss field. Note the better "match" as evidenced by the smaller beam envelop flutter shown in the EGUN calculations, figure 38. Finally, for the double pulse tune, the average B_z in the anode stalk is around 375 Gauss, figure 20. The matched radius for this field value is around 2.5 cm, tables 17 and 18. Note that the EGUN beam envelop calculations show the radius of the beam entering the anode stalk to be about this value, figure 44 and that the envelop does not under go extreme oscillations.

10. Magnetic Field Tunes

FXR has been run under three "standard" tunes referred to as the Lin33, SPU28, and DP tunes. The simulations discussed up to here have all been for the magnetic field used in the Lin33 tune. We now consider the SPU28 and DP tunes. Table 19 give the difference between the three configurations.

Table 19
Tunes

Tune	Lin33	SPU28	DP	ACP1
AK gap (cm)	12.0	13.0	11.0	
Mega Volts	2.1	2.1	1.50	
Magnet	Amperes	Amperes	Amperes	Amperes
I20	-141	-120	-154	
-				
I21	295	265	350	
I22	483	483	300	
I23	109	109	75	
I24	63	63	75	
I25	63	63	75	
I31	170	100	158	
I32	196	100	158	
I33	196	100	158	
I34	94	50	80	
I35	425	200	400	
-				
J21	100	53	80	
J22	116	56	89	
J23	125	59	94	
J24	131	62	98	
-				
J25	230	80	191	

Note that the DP (Double pulse) tune has a smaller AK gap to help boost the current for the reduced anode voltage. The magnetic field profile for these three tunes is overplotted in figure 49. The main performance difference between these tunes is summarized in table 20 at the exit of the injector, location of bug I35.

Table 20
Performance

Parameter	Lin33	SPU28	DP	Unit
Cathode Current	3624	3184	2523	Amperes
Bug I35 Current	3431	3069	2520	Amperes
z	355	355	355	cm
Energy	1.9600	1.9732	1.3952	MeV
Emittance (edge)	58.03	76.26	67.70	cm-mr
$r = \sqrt{\sigma_{11}}$	3.0282	4.819	2.866	cm
$r' = \sqrt{\sigma_{22}}$	45.8441	35.437	87.697	mr
r_{21}	0.90844	-0.89476	0.96304	
Flutter				
Measured Values				
I35 Current	3300	2800	2500	Amperes
z	1045.5	1045.5	1045.5	cm
RMS Emittance	47.9 ± 8.6			cm-mr
RMS radius	2.5 ± 0.2			cm

In some region of beam transport, measure the minimum and maximum beam radius. The beam flutter in this region is defined as

$$f_{lut} = \frac{r_{max} - r_{min}}{r_{max} + r_{min}} \quad [10.1]$$

The region should exceed a betatron wave length for the flutter to be a meaningful gage of match. For a beam perfectly matched to the magnetic field, the flutter is zero. For the flutter given in table 20, the axial range used is the injector anode stalk extending from about 800 to 1000 cm in figures 26, 38, and 44 for the three tunes.

SPU28

This tune scraps some beam on the anode between coils I25 and I31. The overall magnetic field in the injector is lower than in the Lin33 tune leading to a larger beam radius and better match to the magnetic field as evidenced by a lower value of beam flutter calculated in the EGUN runs. The data for the SPU28 runs is shown in table 21. This data is essentially the same as the Lin33 data, table 7 with the exception of the magnetic field and the change in location of the cathode.

The EGUN runs generated figures 37 and 38 showing the 0-30 cm iterative solution and the trajectories transferred at 20 cm and run to the end of the injector. These two figures should be compared with figures 23 and 26 for the Lin33 tune. The beam emittance along the injector is shown in figure 39.

Figure 42 shows the beam phase space at the 20 cm transfer position and at the end of the injector. This should be compared with figure 24 for the Lin33 tune. Figures 39, 40, and 41 show the emittance, transmitted beam current, and magnetic field along the injector for the SPU28 tune. The phase space at 20 and 355 cm (100 and 1341 mesh units) are characterized by the sigma matrices

$$\sigma^{1/2} = \begin{bmatrix} \sigma_{11}^{1/2} & \\ \sigma_{22}^{1/2} & r_{21} \end{bmatrix} = \begin{bmatrix} 5.7717 & \text{cm} \\ 117.002 & \text{mr} & 0.999762 \end{bmatrix} \quad [10.2]$$

with emittance of 14.73 cm-mr and

$$\sigma^{1/2} = \begin{bmatrix} \sigma_{11}^{1/2} & \\ \sigma_{22}^{1/2} & r_{21} \end{bmatrix} = \begin{bmatrix} 4.819 & \text{cm} \\ 35.048 & \text{mr} & -0.89885 \end{bmatrix} \quad [10.3]$$

with emittance of 74.02 cm-mr.

Table 21
EGUN SPU28 data

FXR Injector study 2mm grid SPU28 13cm AK gap	0 41 76 0. 2.
bscale 1.0	2 40 76 2. 0.7
jinput1	2 39 76 -0.1 0.05
fudge = -1.0	2 38 75 2. 0.7
converge 1.0e-6 400	2 37 75 2. 0.4
rlim=41 zlim=151	2 36 75 2. 0.2
mi=4	2 35 75 2. 0.05
mpot=1.0e5	2 34 75 2. 0.01
potn=5	2 33 75 2. 0.05
pot=0. 2.1e6 0. 0. 0.	2 32 75 2. 0.15
zphase=100.0	2 31 75 2. 0.5
magsig = -1	2 30 76 0.01 0.01
jend1	2 29 76 2. 0.8
-14.129 -13.348 -12.547 -11.725 -10.88 -10.018 -9.13 -8.226	2 28 77 0.8 2.
-7.297 -6.346 -5.373 -4.377 -3.359 -2.317 -1.252 -0.163	2 28 78 0.01 0.01
0.950 2.087 3.249 4.436 5.648 6.886 8.149 9.439	2 27 79 0.5 2.
10.756 12.099 13.470 14.869 16.296 17.751 19.236 20.750	2 27 80 0.2 2.
22.293 23.867 25.471 27.106 28.773 30.472 32.202 33.966	2 27 81 0.01 2.
35.762 37.593 39.457 41.356 43.289 45.258 47.263 49.304	2 27 82 0.01 2.
51.381 53.496 55.648 57.839 60.067 62.335 64.641 66.988	2 27 83 0.2 2.
69.374 71.801 74.268 76.777 79.327 81.919 84.553 87.230	2 27 84 0.6 2.
89.949 92.71 95.518 98.367 101.26 104.198 107.179 110.204	2 27 85 0.99 2.
113.274 116.388 119.547 122.75 125.998 129.289 132.625 136.006	2 28 86 0.6 2
139.430 142.897 146.408 149.962 153.559 157.197 160.878 164.599	2 31 91 0. 0
168.361 172.163 176.003 179.882 183.798 187.751 191.739 195.761	2 33 96 0.5 2
199.817 203.90 208.02 212.17 216.345 220.547 224.77 229.023	2 34 97 0.1 -0.2
233.294 237.585 241.89 246.217 250.555 254.904 259.264 263.63	2 34 98 0.3 2.
268.00 272.376 276.75 281.124 285.49 289.854 294.206 298.546	2 34 122 0.3 2.
302.87 307.180 311.468 315.734 319.974 324.187 328.370 332.519	2 34 150 0.3 2
336.633 340.709 344.744 348.736 352.682 356.580 360.429 364.225	2 34 151 0.3 0
367.966 371.65 375.277 378.84 382.347 385.787 389.16 392.469	0 15 151 2. 0
395.709 398.880 401.981 405.010 407.968 410.853 413.665 416.403	0 0 151 0. 0
419.068 421.660 424.177 426.621 428.992 431.289 433.515 435.669	0 0 110 0. 0
437.751 439.764	0 0 11 0. 0.
s	888
1 0 10 0. -0.99	noinital
1 10 10 2. -0.99	jinput5
1 27 10 2. -0.99	av=15
1 28 10 2. -0.99	avr=0.5
5 29 10 2. -0.6	hold=5
5 30 10 0.5 -0.1	pervo=1.0
5 31 11 2. -0.8	ns=20
5 32 11 0.8 -0.4	cl=27.0
5 34 12 0. 0.	spc=0.5
5 35 13 0.5 -0.4	zc=16.7
5 36 14 2. -0.7	zc=11.7
5 37 14 0.2 -0.15	rmag=5
5 38 15 2. -0.7	maxray=84
5 39 15 0.5 -0.2	bscale=1.000
5 40 16 2. -0.8	magord=6
5 41 16 0. -0.4	punch=100
0 41 17 0. 2.	unit=0.002
0 41 50 0. 2.	jend5
0 41 74 0. 2.	end
0 41 75 0. 2.	end

Double Pulse

The injector and accelerator is triggered in such a fashion so as to allow two half energy beam pulses to be generated with a given temporal separation between them. In order to increase the current at half energy the anode cathode gap is reduced to 11 cm. Scaling the Marx generator charge and using the estimate of 2.1 MV for LIN33ec, the beam output energy from the injector should be between 1.4 and 1.5 MeV, Jan Zentlers estimate in 1999 was 1.4 MeV.

The EGUN runs generated figures 43 and 44 showing the 0-30 cm iterative solution and the trajectories transferred at 20 cm and run to the end of the injector. These two figures should be compared to figures 23 and 26 for the Lin33 tune. The beam emittance along the injector is shown in figure 45.

Figure 48 shows the beam phase space at the 20 cm transfer position. Figures 45, 46, and 47 show the emittance, transmitted beam current, and magnetic field along the injector for the Double pulse tune. The phase space at 20 cm is characterized by the sigma matrix

$$\sigma^{1/2} = \begin{bmatrix} \sigma_{11}^{1/2} & & \\ \sigma_{22}^{1/2} & r_{21} \end{bmatrix} = \begin{bmatrix} 6.2936 & \text{cm} \\ 153.2873 & \text{mr} & 0.999863 \end{bmatrix} \quad [10.4]$$

with emittance of 15.96 cm-mr .

$$\sigma^{1/2} = \begin{bmatrix} \sigma_{11}^{1/2} & & \\ \sigma_{22}^{1/2} & r_{21} \end{bmatrix} = \begin{bmatrix} & \text{cm} \\ & \text{mr} \end{bmatrix} \quad [10.5]$$

with emittance of XXXX cm-mr.

Table 22
EGUN Double Pulse data

FXR Injector study 2mm grid DP 11cm AK gap	0 41 76 0. 2.
bscale 1.0	2 40 76 2. 0.7
jinput1	2 39 76 -0.1 0.05
fudge = -1.0	2 38 75 2. 0.7
converge 1.0e-6 400	2 37 75 2. 0.4
rlim=41 zlim=151	2 36 75 2. 0.2
mi=4	2 35 75 2. 0.05
mpot=1.0e5	2 34 75 2. 0.01
potn=5	2 33 75 2. 0.05
pot=0. 1.4e6 0. 0. 0.	2 32 75 2. 0.15
zphase=100.0	2 31 75 2. 0.5
magsig = -1	2 30 76 0.01 0.01
jend1	2 29 76 2. 0.8
-23.595 -22.668 -21.717 -20.739 -19.737 -18.708 -17.65 -16.57	2 28 77 0.8 2
-15.465 -14.33 -13.168 -11.979 -10.76 -9.517 -8.24 -6.94	2 28 78 0.01 0.01
-5.609 -4.248 -2.857 -1.436 0.016 1.499 3.013 4.560	2 27 79 0.5 2
6.138 7.749 9.394 11.072 12.783 14.530 16.311 18.128	2 27 80 0.2 2.
19.98 21.869 23.795 25.758 27.759 29.798 31.876 33.993	2 27 81 0.01 2
36.15 38.347 40.585 42.864 45.185 47.548 49.954 52.403	2 27 82 0.01 2.
54.896 57.433 60.015 62.642 65.315 68.033 70.798 73.61	2 27 83 0.2 2.
76.470 79.377 82.332 85.335 88.388 91.489 94.640 97.841	2 27 84 0.6 2.
101.09 104.39 107.744 111.146 114.599 118.1 121.657 125.26	2 27 85 0.99 2.
128.918 132.625 136.38 140.19 144.049 147.957 151.916 155.923	2 28 86 0.6 2
159.979 164.084 168.237 172.436 176.68 180.974 185.31 189.69	2 31 91 0. 0.
194.114 198.579 203.084 207.628 212.21 216.829 221.48 226.169	2 33 96 0.5 2
230.886 235.634 240.409 245.209 250.03 254.877 259.74 264.62	2 34 97 0.1 -0.2
269.515 274.420 279.333 284.252 289.173 294.094 299.01 303.92	2 34 98 0.3 2
308.824 313.71 318.58 323.434 328.26 333.06 337.83 342.566	2 34 122 0.3 2
347.263 351.917 356.526 361.086 365.59 370.04 374.43 378.754	2 34 150 0.3 2
383.01 387.195 391.304 395.335 399.28 403.146 406.92 410.60	2 34 151 0.3 0.
414.19 417.68 421.069 424.355 427.536 430.609 433.57 436.42	0 15 151 2. 0.
439.16 441.78 444.287 446.675 448.944 451.093 453.12 455.03	0 0 151 0. 0.
456.817 458.483 460.029 461.455 462.76 463.948 465.017 465.97	0 0 110 0. 0
466.807 467.530	0 0 21 0. 0.
s	888
1 0 20 0. -0.99	noinital
1 10 20 2. -0.99	jinput5
1 27 20 2. -0.99	av=15
1 28 20 2. -0.99	avr=0.5
5 29 20 2. -0.6	hold=5
5 30 20 0.5 -0.1	pervo=1.0
5 31 21 2. -0.8	ns=20
5 32 21 0.8 -0.4	cl=27.0
5 34 22 0. 0.	spe=0.5
5 35 23 0.5 -0.4	zc=16.7
5 36 24 2. -0.7	zc=21.7
5 37 24 0.2 -0.15	rimage=5
5 38 25 2. -0.7	maxray=84
5 39 25 0.5 -0.2	bscale=1.000
5 40 26 2. -0.8	magord=6
5 41 26 0. -0.4	punch=100
0 41 27 0. 2.	unit=0.002
0 41 50 0. 2.	jend5
0 41 74 0. 2.	end
0 41 75 0. 2.	end

11. Zentler Scans

Jan Zentler performed a "magnetic field tune vs beam current" survey where the first injector magnet I21, was scanned from 235 to 430 Amperes in 15 Ampere steps. Magnet coils I22, I23, I24, and I25 were run at the nominal Lin33 values of 483, 109, 63, and 63 Amperes. The bucking coil, I20, was adjusted for zero field on the cathode. Three such surveys were performed affectionately called Series 1, Series 2, and Series 3. In each of these series, the field of the injector magnets I31-I35 was progressively weakened, with values given in table 25.

Table 25
Zentler Scans, Series 1, 2, and 3.

Series	I31=I32=I33 Amperes	I34 Amperes	I35 Amperes
1)	150	75	380
2)	120	60	310
3)	100	50	290
Series	Bz(kG) CL(I21)	Ave Bz(kG) I31-I34	
Lin33	497	439	--
1)	480-657	369	--
2)	480-623	308	--
3)	481-543	271	--

The magnetic field profile from the cathode to Bug I35 for these scan series and the standard Lin33 configuration is shown in figure 50. The average value of the anode stalk field, table 25 was calculated over the axial extent of 764 to 1069 cm. The range in field value at the center position of the first injector magnet, I21 is given for the scans.

The beam current at bug I35 was recorded for each of the series vs the setting of the first anode magnets, I21. Table 26 summarizes the experimental results. The beam current given in the table is extracted from the oscilloscope trace of current vs time, with the value as close to the nominal center of the beam flat top for each shot as possible. For comparison, the normal Lin33 value is shown as shot 0.

Table 26
Beam current Measured at Bug I35.

Shot number	Lin33		Zentler Series 1		Zentler Series 2		Zentler Series 3	
	I21(A)	Beam(A)	I21(A)	Beam(A)	I21(A)	Beam(A)	I21	Beam(A)
0)	320.28	3248.52	-	-	-	-	-	-
1)			235.	2565.79	235.	2833.33	235.	2720.
2)			250.	3000.	250.	3000.	250.	2872.34
3)			265.	3000.	265.	3000.	265.	2881.58
4)			280.	3000.	280.	3000.	280.	2901.10
5)			295.	3000.	295.	3126.76	295.	2716.22
6)			310.	3000.	310.	3041.67	310.	2393.62
7)			325.	3000.	325.	3000.	-	-
8)			340.	2921.05	340.	3000.	-	-
9)			355.	3081.08	355.	2617.02	-	-
10)			370.	3000.	-	-	-	-
11)			385.	3000.	385.	2027.03	-	-
12)			400.	2802.63	-	-	-	-
13)			415.	2630.14	-	-	-	-

The 29 shots summarized in the above table were run with the EGUN code and the current reaching bug I35 calculated. The assumption was made that the beam current density profile is uniform. Other profiles could have been tried, but considering the uncertainties of the non-iterative simulation caring the beam to 1055 cm, such fine tuning was not warranted. These calculations were repeated at 1.9, 2.0, 2.1, and 2.2 MV

anode potentials. The "best" fit to the measured profiles of beam current to magnetic I21 excitation occurs for 2.1 MV, figure 55, 56, 57, and 58.

12. Transport To End of Accelerator

The beam transport code TRANSPORT can be used to run a space charge beam along a series of magnets use matrix manipulation. It would be ideal to start this calculation at the exit of the injector. However, the EGUN non-iterative calculation used to push the particles from the 20 cm location pass the cathode to the end of the injector, some 355 cm is not self consistent. So just for the fun of it, we will take the beam at 20 cm represented by its sigma matrix, use a stair step approximation to the field in the injector, and transport this beam to the end of the injector, and then through the entire FXR accelerator to the end of the machine.

The emittance at the end of the accelerator is adiabatically damped by $\beta\gamma$ ratio between the accelerator exit value and the injector value. Taking the nominal injector anode potential of 2.1 MV with space charge depressed beam energy of 1.9 MeV, and the accelerate output energy of 18.4 MeV, we have

$$\varepsilon = 80 \frac{\beta\gamma(\text{injector})}{\beta\gamma(\text{accelerexit})} = 80 \frac{4.611}{37.0} = 9.97 \text{ cm-mr}$$

The transport code simulates this damping of the phase space by matrix representation of the accelerator gaps

$$R = \begin{bmatrix} 1 & \frac{LP}{dP \cos \phi} \ln[1 + dP \cos \phi / P] & 0 & 0 & 0 & 0 \\ 0 & \frac{P}{P + dP \cos \phi} & 0 & 0 & 0 & 0 \\ 0 & 0 & 1 & \frac{LP}{dP \cos \phi} \ln[1 + dP \cos \phi / P] & 0 & 0 \\ 0 & 0 & 0 & \frac{P}{P + dP \cos \phi} & 0 & 0 \\ 0 & 0 & 0 & 0 & 1 & 0 \\ 0 & 0 & 0 & 0 & \frac{dP \sin 2\pi\phi}{(P + dP \cos \phi)\lambda} & \frac{P}{P + dP \cos \phi} \end{bmatrix}$$

Note that the determinant of this matrix is less than unity. This is the mathematical formulation of phase space adiabatic damping.

Approximation to the Magnetic Fields

A stair step approximation to the actual field profile is given in table 27. Although this is the summation of equation 3.1 for all injector magnets, with the exception of I20 (the bucking coil) only the nearest neighbors are actually required. The field given in table 27 is plotted in figure 50 for the Lin33 tune. These stair step approximations are used by the TRANSPORT envelope code TRAN3, figure 51. The beam is expressed by the sigma matrix parameters at the 20 cm transfer location.

Table 27
Ideal Stair Step Field Approximation
for the TRANSPORT envelope code - 5 cm segments

Magnet region	z(m)	Lin33 Gauss	SPU28 Gauss	DP Gauss	Magnet region	z(m)	Lin33 Gauss	SPU28 Gauss	DP Gauss
I20	6.0000	-8.51	-7.20	-9.36	I31	8.2500	461.83	273.85	430.03
	6.0500	-9.91	-8.38	-10.90	I31	8.3000	513.16	303.23	477.25
	6.1000	-11.54	-9.76	-12.69	I31	8.3500	532.44	313.96	494.75
	6.1500	-13.40	-11.34	-14.75	I31	8.4000	531.63	312.95	493.51
	6.2000	-15.53	-13.13	-17.09	I31	8.4500	510.42	299.81	473.00
	6.2500	-17.85	-15.08	-19.65	I31	8.5000	456.31	266.90	421.18
	6.3000	-20.07	-16.94	-22.10	I31	8.5500	361.60	209.01	329.83
	6.3500	-21.01	-17.71	-23.16		8.6000	285.29	159.41	251.56
	6.4000	-16.87	-14.14	-18.69		8.6500	311.38	165.58	261.38
	6.4500	-5.43	-4.34	-6.25	I32	8.7000	427.12	221.09	349.13
	6.5000	1.55	1.69	1.31	I32	8.7500	535.10	274.57	433.67
	6.5500	1.48	1.75	1.15	I32	8.8000	591.86	302.79	478.28
	6.6000	-3.61	-2.41	-4.50	I32	8.8500	614.70	314.08	496.15
	6.6500	-12.99	-10.15	-14.87	I32	8.9000	614.51	313.80	495.72
	6.7000	-27.40	-22.05	-30.74	I32	8.9500	591.30	301.85	476.86
	6.7500	-36.38	-29.14	-40.69	I32	9.0000	534.06	272.59	430.64
	6.8000	-30.14	-22.97	-34.01	I32	9.0500	427.43	218.15	344.63
	6.8500	-9.89	-4.38	-11.98		9.1000	321.39	164.02	259.13
I21	6.9000	26.51	28.77	27.75		9.1500	316.78	161.66	255.40
	6.9500	84.88	81.91	91.48	I33	9.2000	418.61	213.61	337.49
	7.0000	171.37	160.86	185.29	I33	9.2500	527.89	269.37	425.59
	7.0500	283.27	263.60	303.89	I33	9.3000	588.16	300.13	474.21
	7.1000	395.21	367.94	414.16	I33	9.3500	613.45	313.05	494.65
I21	7.1500	468.59	439.74	467.52	I33	9.4000	615.37	314.07	496.29
I22	7.2000	494.56	470.77	455.42	I33	9.4500	594.47	303.49	479.64
I22	7.2500	490.99	474.78	412.10	I33	9.5000	541.87	276.85	437.65
I22	7.3000	460.88	451.17	360.13	I33	9.5500	439.68	225.14	356.20
I23	7.3500	407.80	402.47	307.82		9.6000	325.57	167.94	266.37
I23	7.4000	350.56	347.88	265.07		9.6500	305.47	159.88	254.80
I23	7.4500	299.21	298.05	234.74	I34	9.7000	403.66	213.44	341.27
I23	7.5000	255.21	254.88	214.93	I34	9.7500	518.83	275.25	440.67
I24	7.5500	222.13	222.21	204.58	I34	9.8000	581.93	308.94	495.15
I24	7.6000	199.56	199.82	199.26	I34	9.8500	610.91	324.21	520.49
I24	7.6500	182.90	183.19	193.56	I34	9.9000	622.27	329.73	531.15
I24	7.7000	169.46	169.66	186.28	I34	9.9500	621.78	328.26	532.61
I25	7.7500	158.94	158.93	179.00	I34	10.0000	610.10	319.53	526.43
I25	7.8000	148.57	148.20	169.78	I34	10.0500	568.48	292.92	497.61
I25	7.8500	132.85	131.84	152.78		10.1000	503.39	252.17	451.21
I25	7.9000	110.38	108.20	126.67		10.1500	482.78	234.59	443.35
	7.9500	87.34	82.88	98.72		10.2000	521.22	248.77	485.19
	8.0000	73.80	64.54	80.19	I35	10.2500	568.43	269.46	531.68
	8.0500	80.87	61.10	82.38	I35	10.3000	564.61	267.36	528.11
	8.1000	124.48	81.74	120.04		10.3500	505.23	240.10	470.31
I31	8.1500	222.93	136.51	209.77		10.4000	440.91	212.06	404.32
I31	8.2000	357.72	213.85	333.95		10.4500	422.17	208.54	374.04

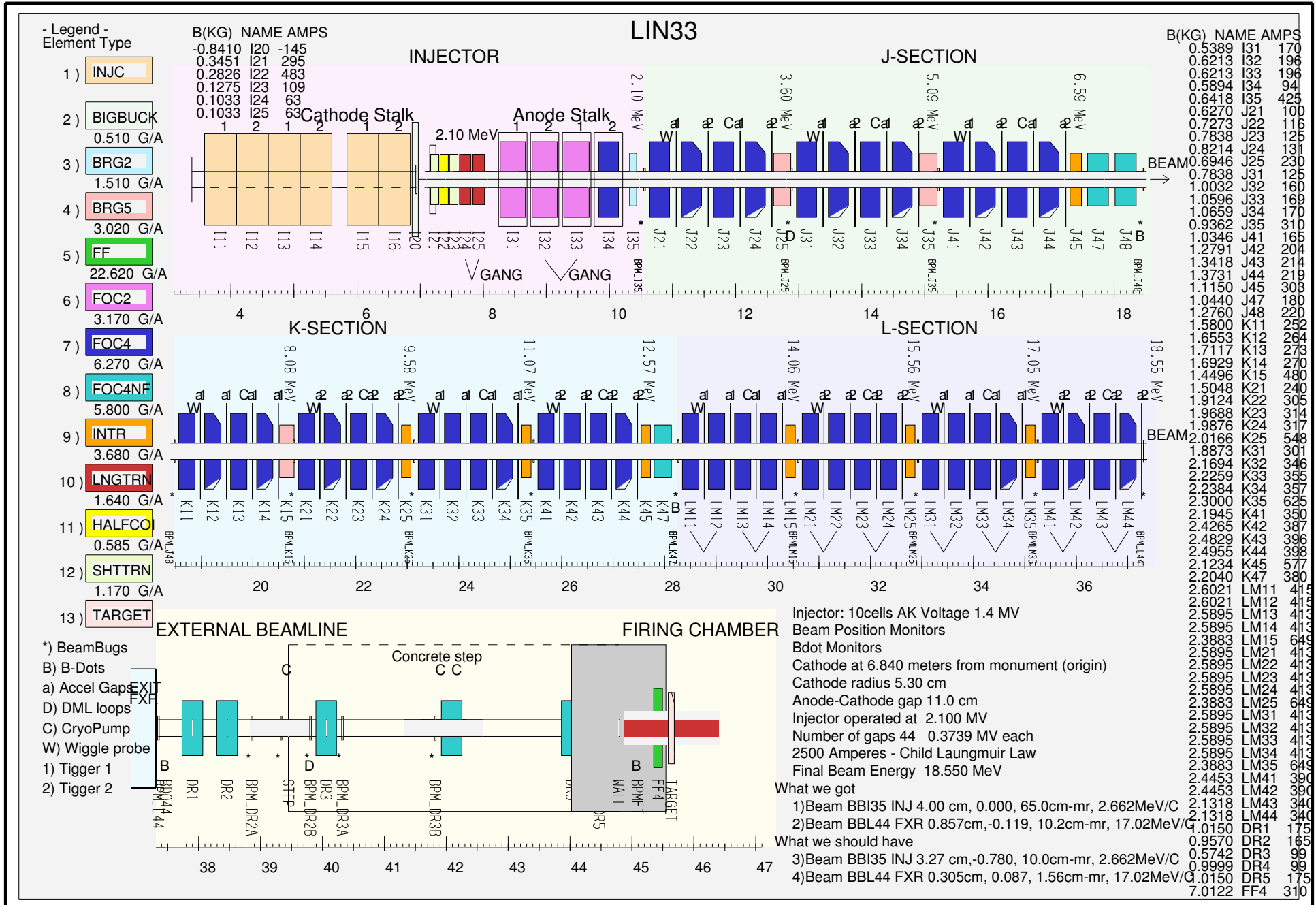
Table 28
Transport Data

FXR Injector - Lin33 tune from 0.20 meters	19	0.0500	0.2857 space
0	19	0.0500	0.3117 space
13 2.1	6 7 8.25 19		
15 0 0 0	19	0.0500	0.4274 I32
15 7 Amps 1.	19	0.0500	0.5354 I32
15 11 MeV 0.001	19	0.0500	0.5921 I32
16 3 1	19	0.0500	0.6149 I32
16 6 7.0610	19	0.0500	0.6147 I32
16 38 1 pipe	19	0.0500	0.5915 I32
24 8 0 0 7.0610	19	0.0500	0.5342 I32
16 6 7.3	19	0.0500	0.4276 I32
24 8 0 0 7.3	6 7 9.55 19		
24 0 10 10	19	0.0500	0.3215 space
1 5.8 60 5.8 60 0 0 2.4	19	0.0500	0.3169 space
12 0.9997 0r4 0.9997 0 0r7	6 7 8.25 19		
26 0.01 3300	19	0.0500	0.4187 I33
13 1	19	0.0500	0.5280 I33
19 0.0500 0.4607 I22	19	0.0500	0.5882 I33
6 7 9.55 19	19	0.0500	0.6135 I33
19 0.0500 0.4072 space	19	0.0500	0.6154 I33
6 7 8.25 19	19	0.0500	0.5945 I33
19 0.0500 0.3501 I23	19	0.0500	0.5418 I33
19 0.0500 0.2991 I23	19	0.0500	0.4396 I33
19 0.0500 0.2553 I23	6 7 9.55 19		
19 0.0500 0.2224 I24	19	0.0500	0.3254 space
19 0.0500 0.1998 I24	19	0.0500	0.3051 space
19 0.0500 0.1830 I24	6 7 8.25 19		
19 0.0500 0.1694 I24	19	0.0500	0.4030 I34
19 0.0500 0.1587 I25	19	0.0500	0.5177 I34
19 0.0500 0.1483 I25	19	0.0500	0.5798 I34
19 0.0500 0.1326 I25	19	0.0500	0.6067 I34
19 0.0500 0.1103 I25	19	0.0500	0.6136 I34
6 7 9.55 19	19	0.0500	0.6036 I34
19 0.0500 0.0875 space	19	0.0500	0.5731 I34
19 0.0500 0.0742 space	19	0.0500	0.5050 I34
19 0.0500 0.0813 space	6 7 9.55 19		
19 0.0500 0.1253 space	19	0.0500	0.4278 space
19 0.0500 0.2238 space	19	0.0500	0.4449 space
6 7 8.25 19	19	0.0500	0.5867 space
19 0.0500 0.3585 I31	6 7 8.25 19		
19 0.0500 0.4626 I31	19	0.0500	0.7575 I35
19 0.0500 0.5139 I31	19	0.0500	0.7554 I35
19 0.0500 0.5331 I31	19	0.0500	0.5732
19 0.0500 0.5323 I31	19	0.0550	0.4043
19 0.0500 0.5110 I31	6 8 6 6 bug35		
19 0.0500 0.4568 I31	13 1		
19 0.0500 0.3620 I31	19 0.0450 0.3464		
6 7 9.55 19	19 0.0500 0.4146		
	73		

Note that the transport runs do not include all the relevant physics, mainly the space charge energy depression caused by the beam radius changing inside a conductive wall. This, and the other approximations inherent in an envelop calculation are the main reasons that the beam envelop from transport does not show the same magnitude of flutter as the EGUN calculations which do include the beam energy variations.

The initial conditions for the beam is taken at the exit of the injector for the transport calculations, equations 7.5, 10.3, and 10.6 for the Lin33, SPU28 and DP tunes respectively.

FXR ACCELERATOR



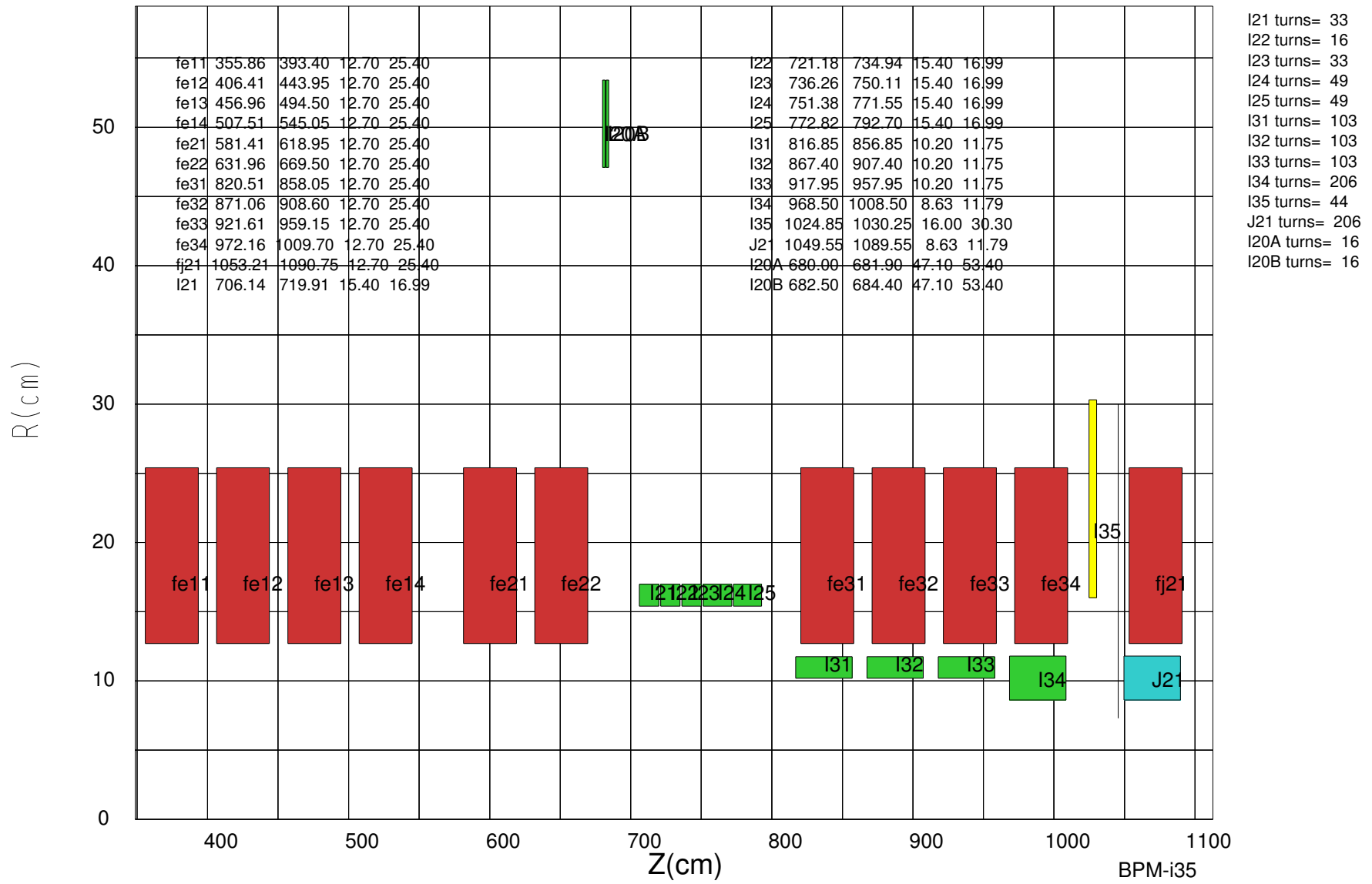


Figure 2) Injector Coil and Ferrite core positions used by POISSON code to calculating the magnetic field. Only the nearest neighbors were used, e.g., coil I33 and cores fe32, fe33, and fe34, etc. except for I20. The bucking coils large radius requires next nearest neighbors, fe21, fe22, fe31, and fe32.

Ferrite and coil data extracted from automesh data files Beam envelope extracted from EGUN tape99 file
 Magnetic field profile synthsized from $B_z(z)$ functions
 Electrode data taken from EGUN generator code FXR data from 'FXR Parameters' dated 9/4/98

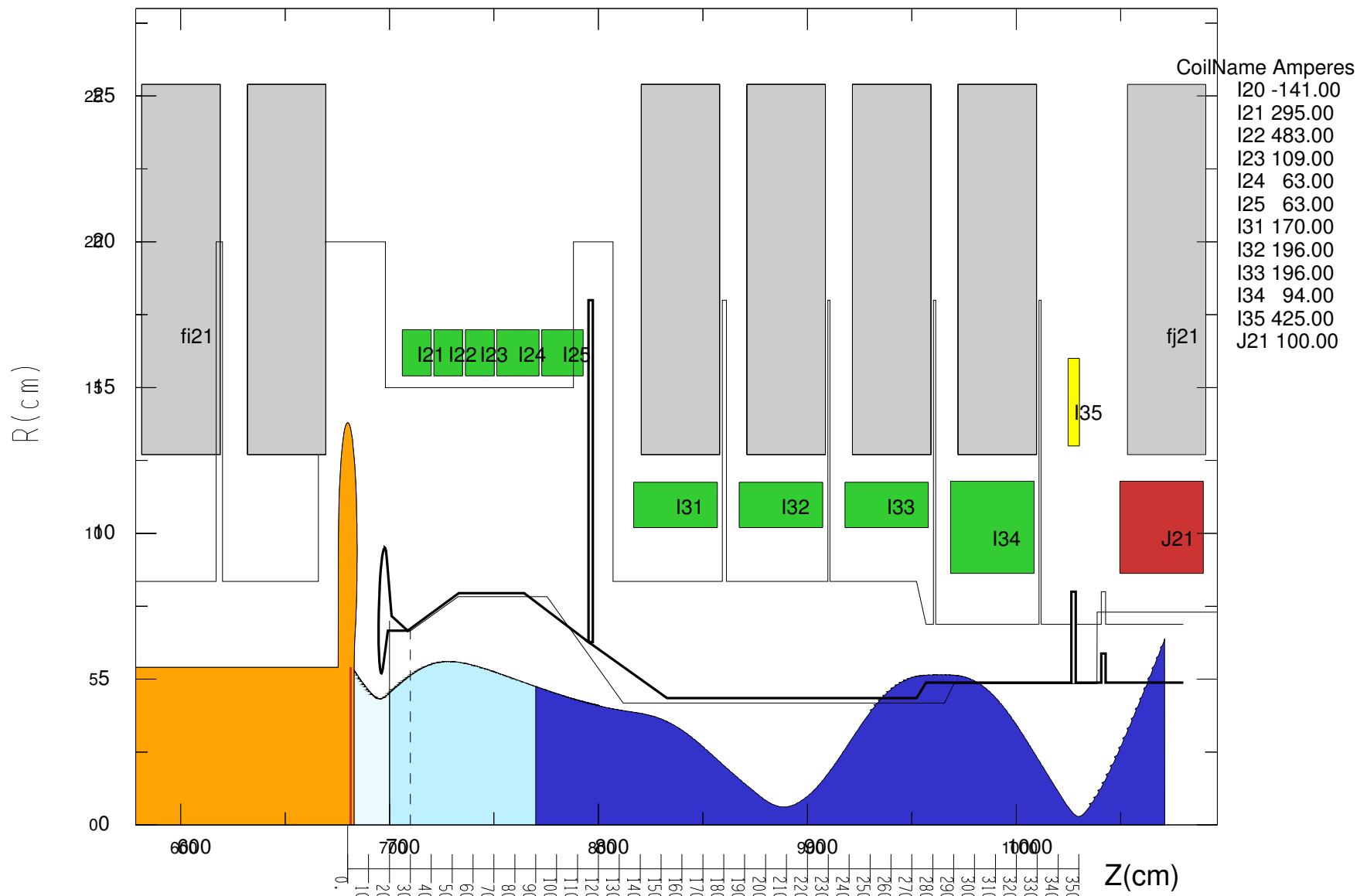


Figure 3) Ferrite, coils and beam envelope Magnetic Field Configuration Lin33. Egun 3362 Amperes Beam energy 2.332 MeV
 Beam emittance at 100 MU ($z=20\text{cm}$) $19.83 \text{ cm}\cdot\text{mr}$. Cathode 683.60 cm R Cathode 5.40 cm Anode 698.80 cm Zhook 800.31 cm A

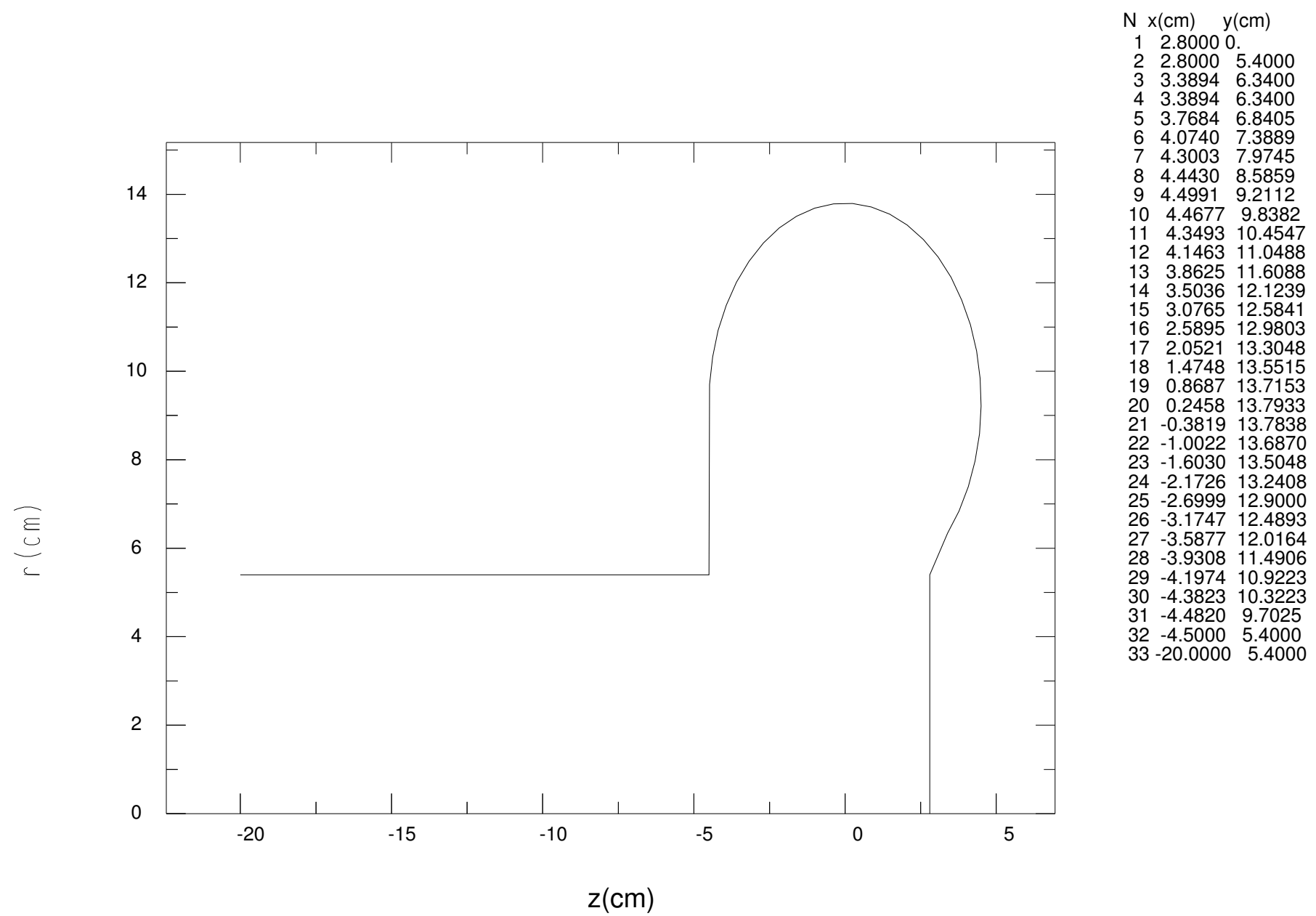


Figure 4) Cathode shroud

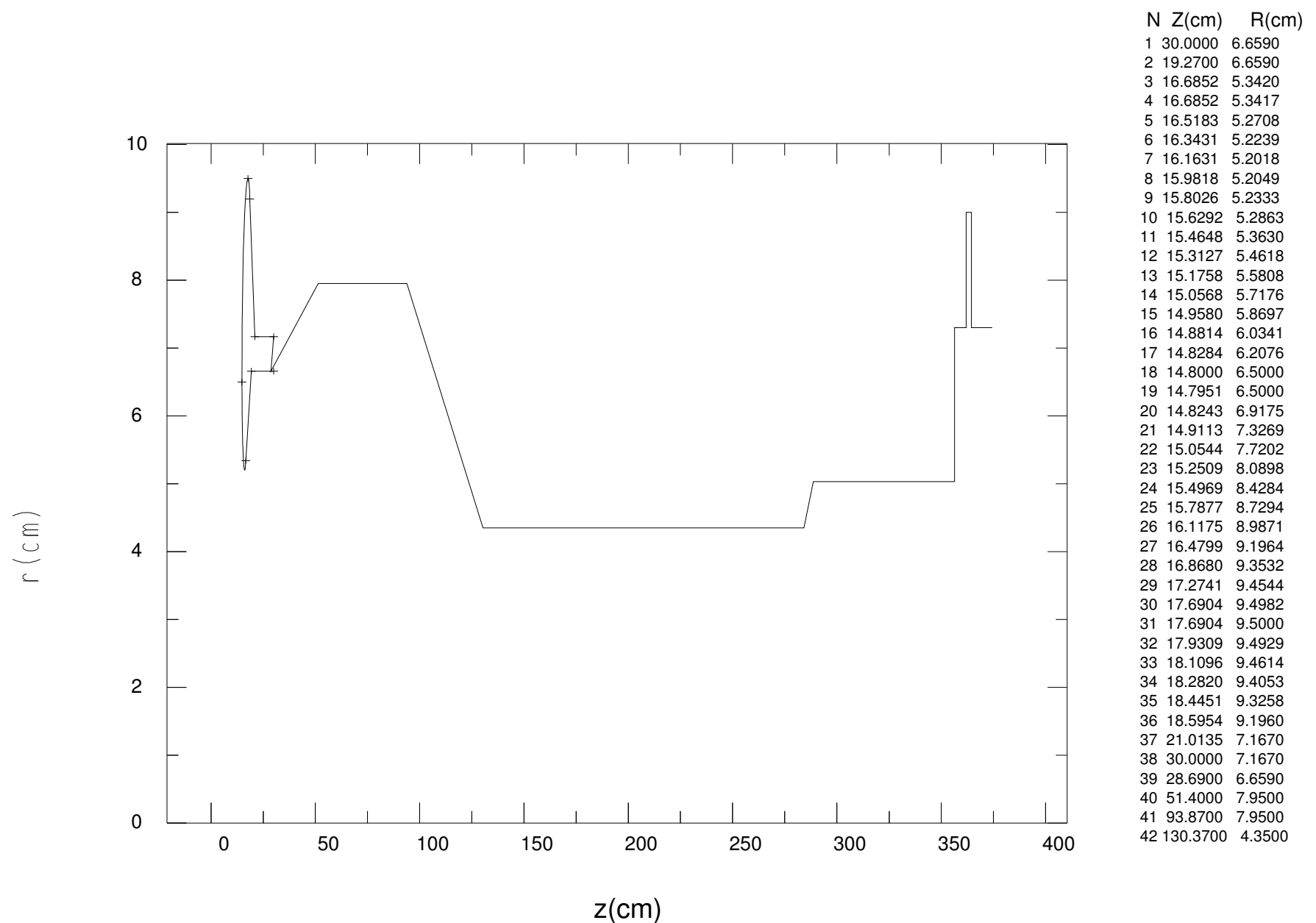


Figure 5) Anode Shroud

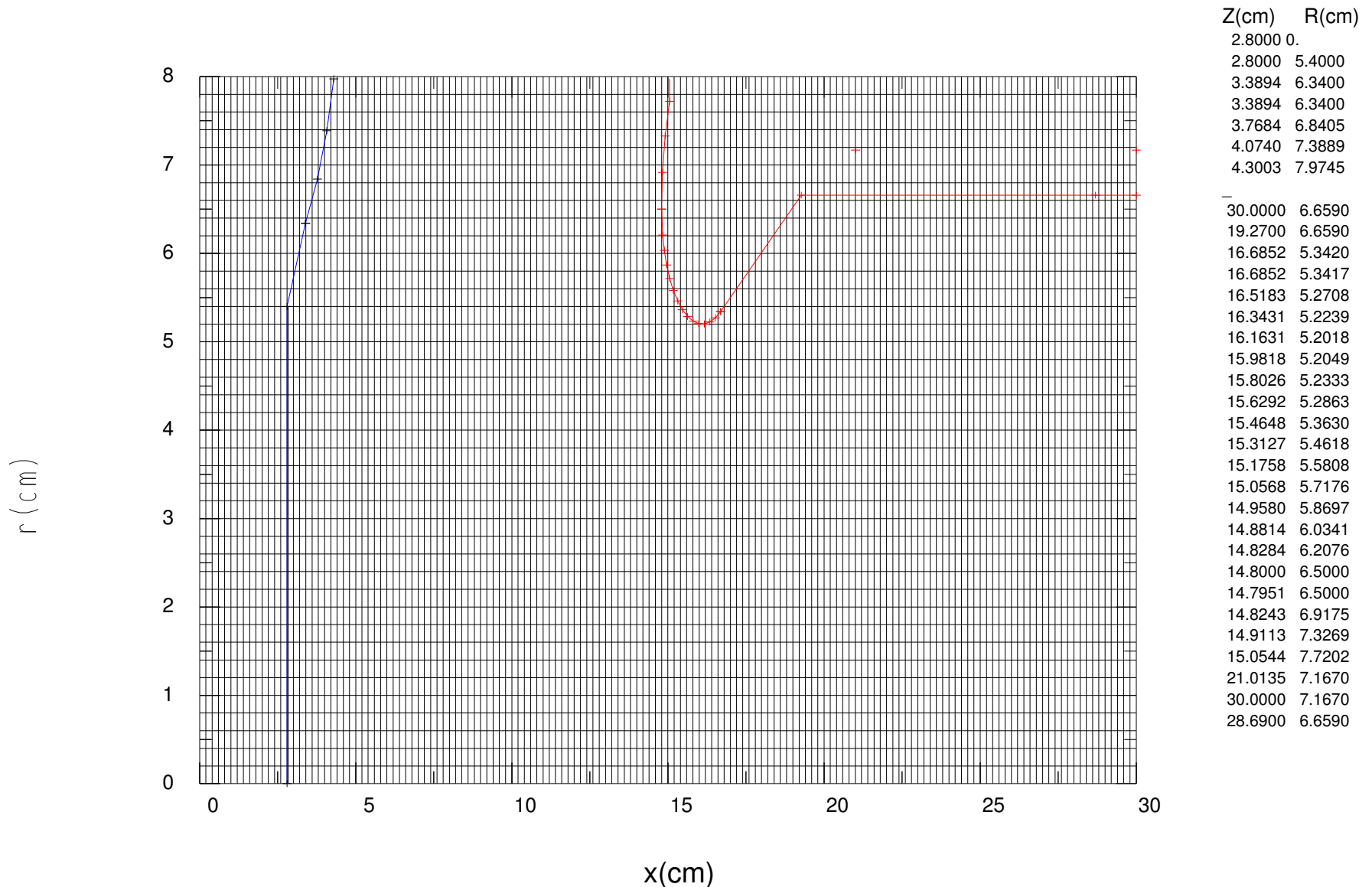


Figure 6) FXR Electrode Region showing the EGUN mesh and the cathode and anode electrodes for the first section of the egun calculations extending from 0 to 30 cm. The trajectories are transferred at 20 cm to the second calculational

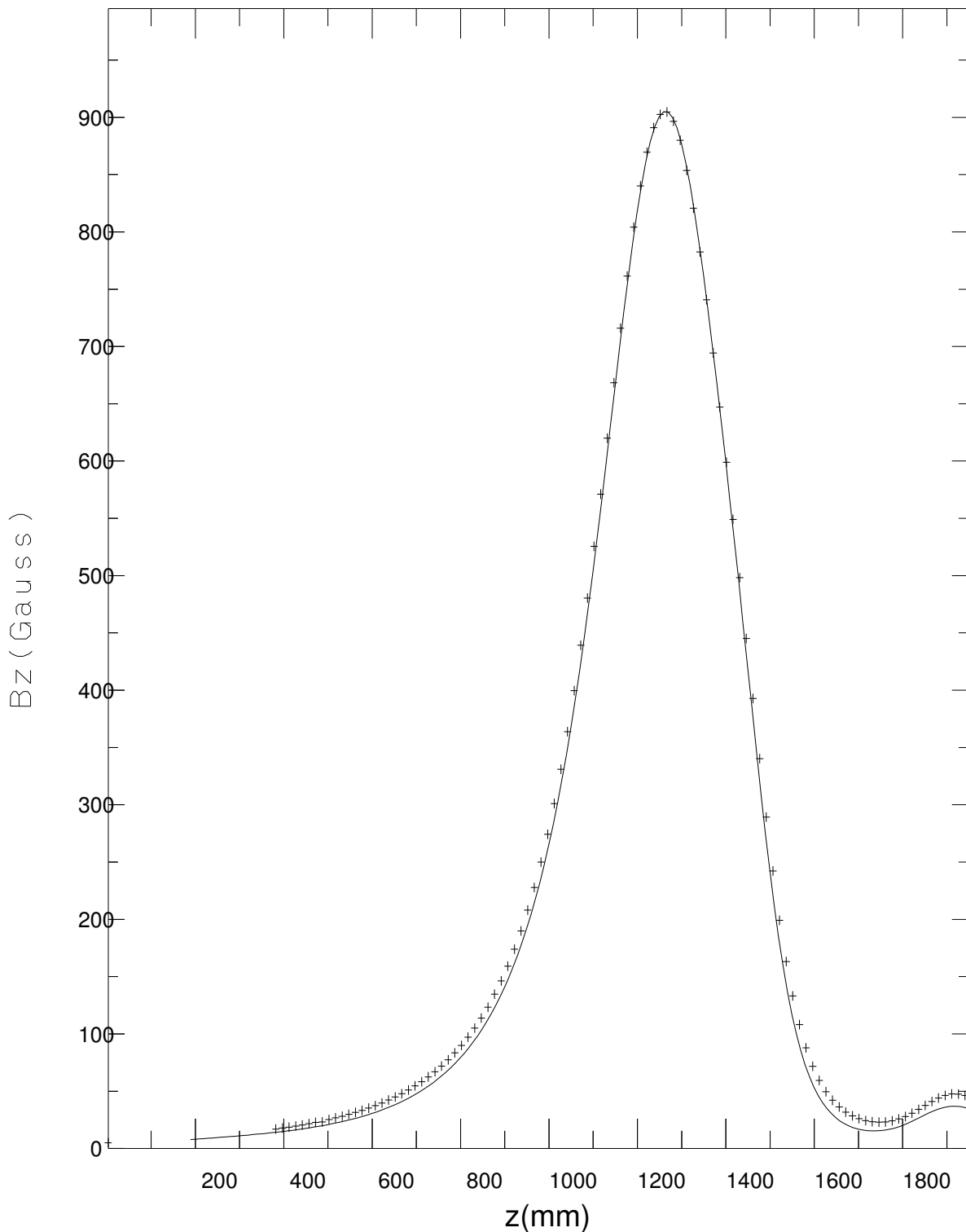


Figure 7) FXR J25 Measured magnetic field profile at 300 Amperes with adjacent ferrites FeJ22, FeJ23, and FeJ24. Poisson calculation at 10,000 Ampere turns, 90.91 Amperes. Ratio of peak fields 3.3289, ratio of currents 3.300. Poisson profile scaled by 3.30 and shifted by 7.80 Gauss. Note ferrite bump at 1900 mm.

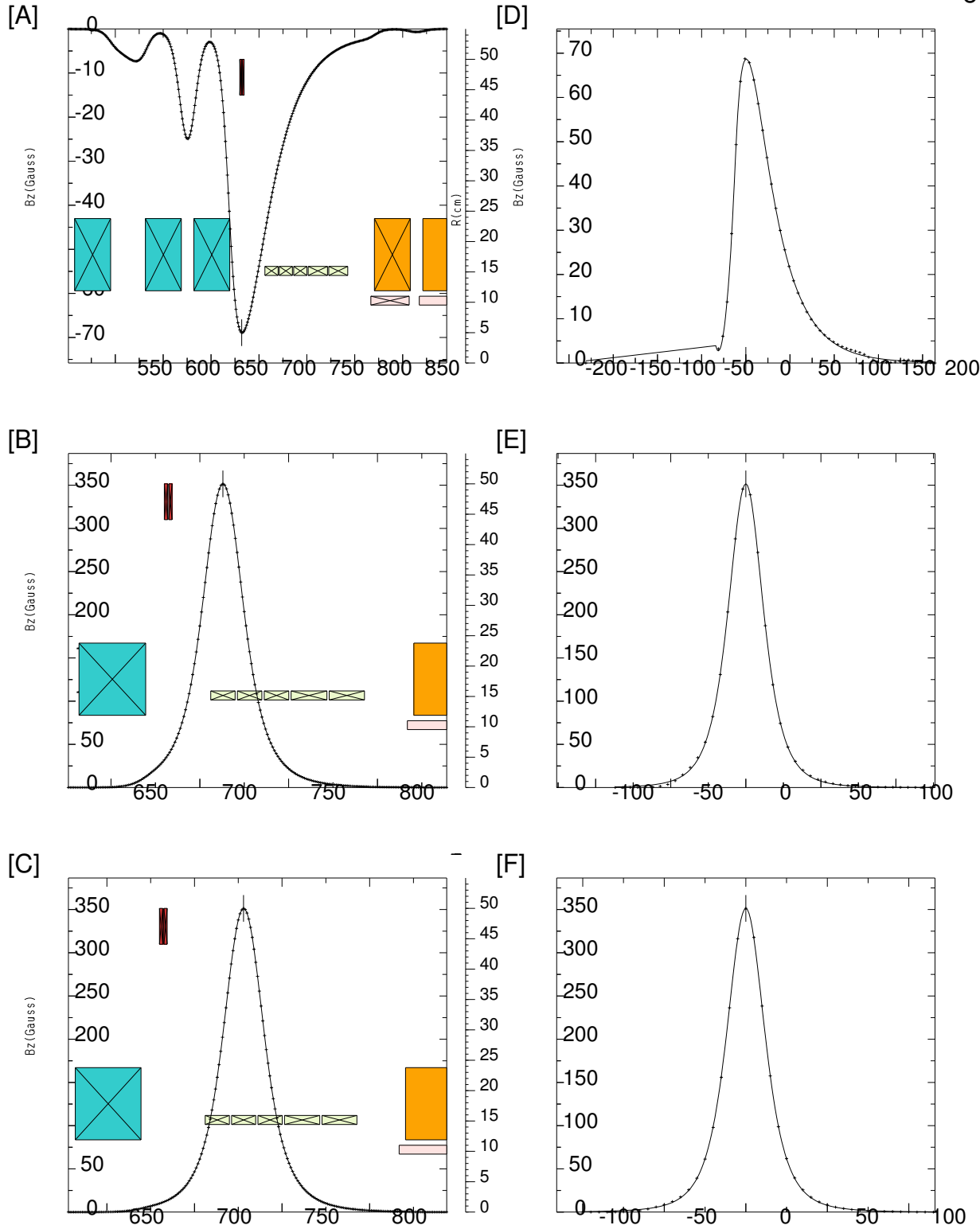


FIGURE 8 $B_z(z) = B_0 / (1 + c1^*z^2 + c2^*z^4 + c3^*z^6)$

Each individual coil is excited, nearest neighbor ferrite cores included in the Poisson calculations. Coil I20, the bucking coil, is asymmetric and fit to a double function. Coils I21-I34 are fit to a single function. The field synthesized from the fitting function and symmetrized about zero is shown to the right.

(A) Coil I20 Poisson field, (D) fitted field: see table 11 for the bucking coil fitting coefficients.

(B) Coil I21 Poisson field, (E) fitted field: coefficients: 351.57, 4.3815e-3, 4.6034e-6, 4.6122e-10.

(C) Coil I22 Poisson field, (F) fitted field: coefficients: 351.35, 4.3379e-3, 5.0122e-6, 1.0866e-10.

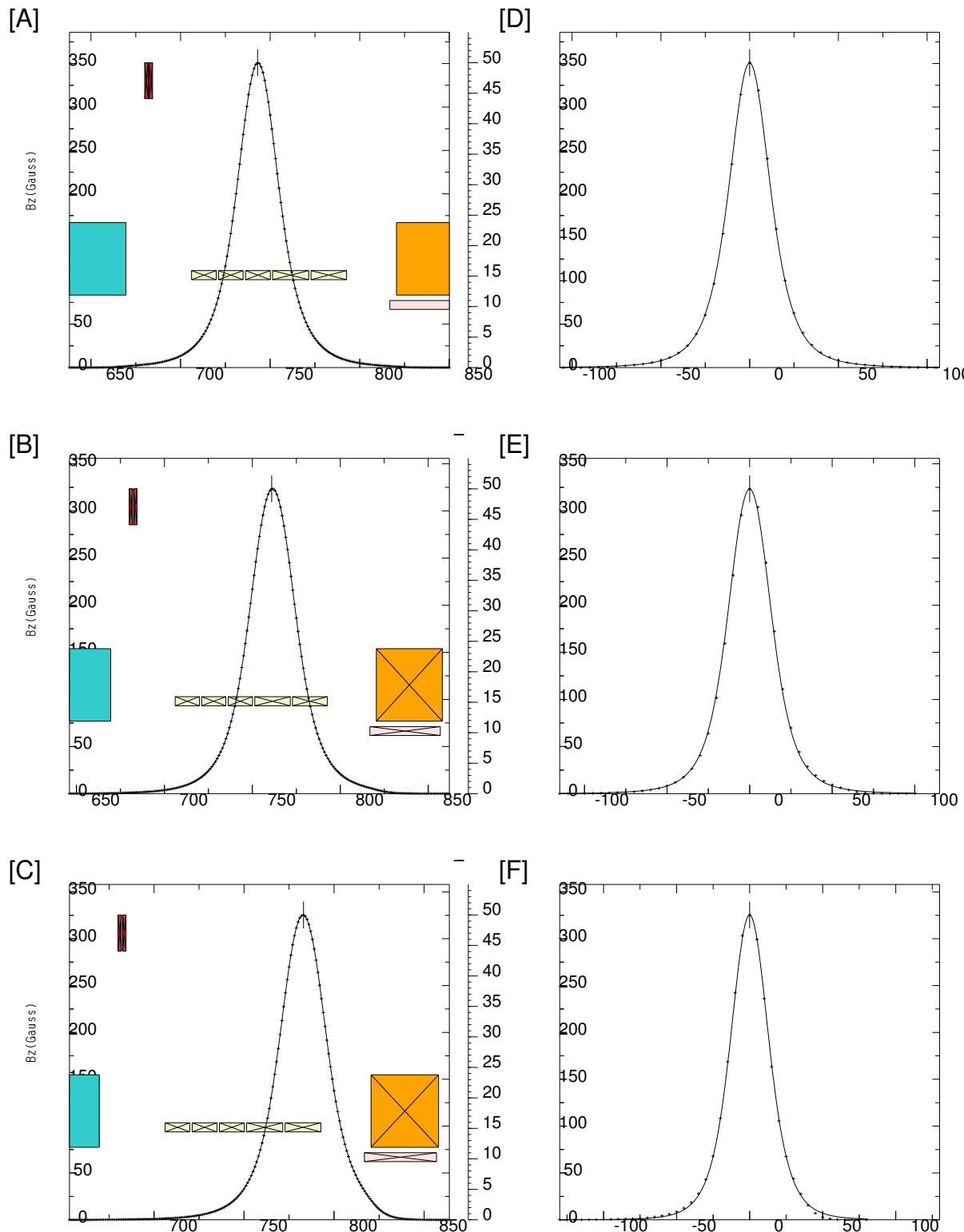


FIGURE 9 $B_z(z) = B_0 / (1 + c1^*z^2 + c2^*z^4 + c3^*z^6)$

Each individual coil is excited, nearest neighbor ferrite cores included in the Poisson calculations. The field synthesized from the fitting function and symmetrized about zero is shown to the right.
 (A) Coil I23 Poisson calculated field, (D) fitted field: 350.94, 4.3087e-03, 5.0920e-06, 5.3037e-11
 (B) Coil I24 Poisson calculated field, (E) fitted field: 323.38, 3.1334e-03, 4.7381e-06, 5.6616e-11
 (C) Coil I25 Poisson calculated field, (F) fitted field: 325.36, 3.2520e-03, 4.1017e-06, 7.2716e-10

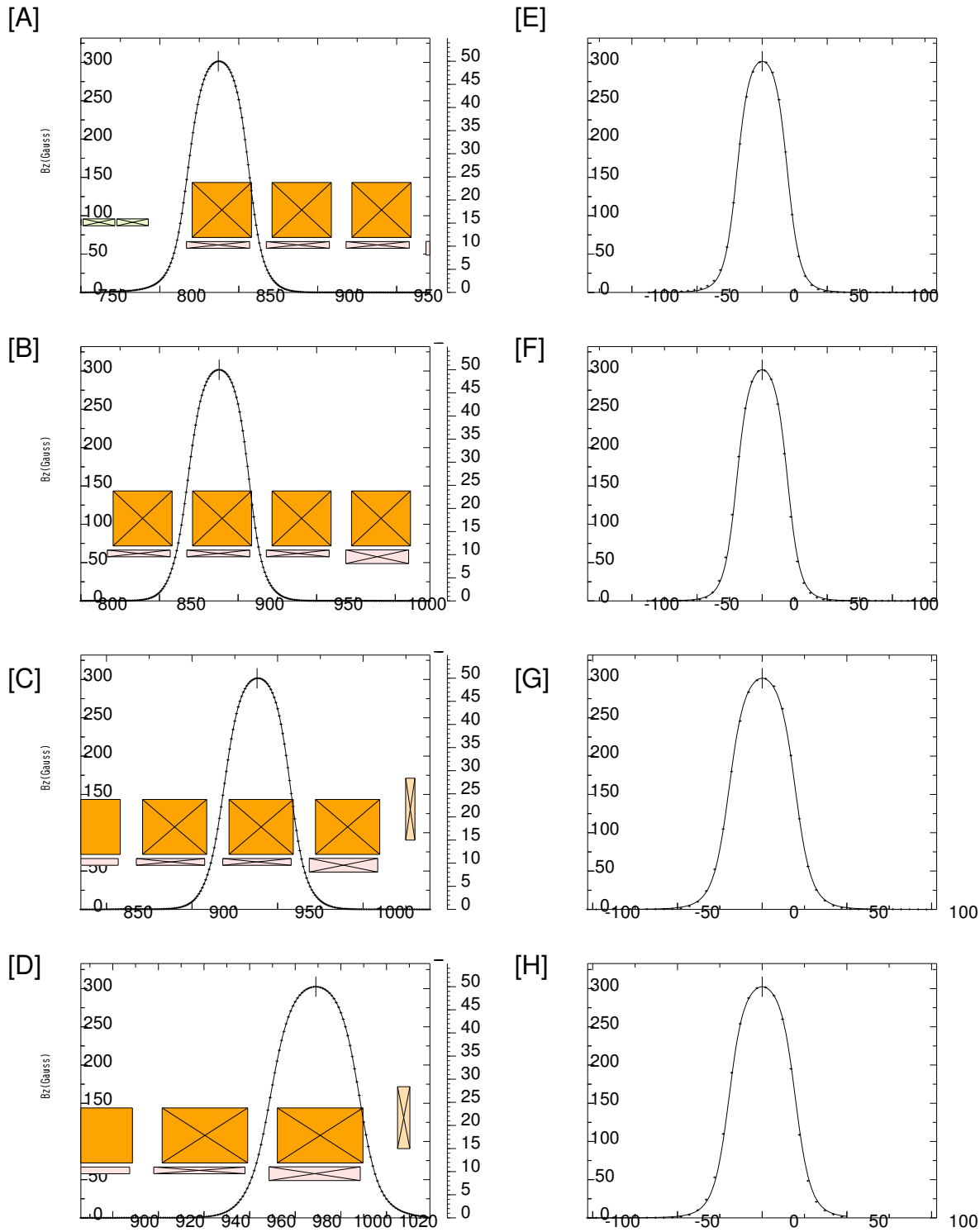


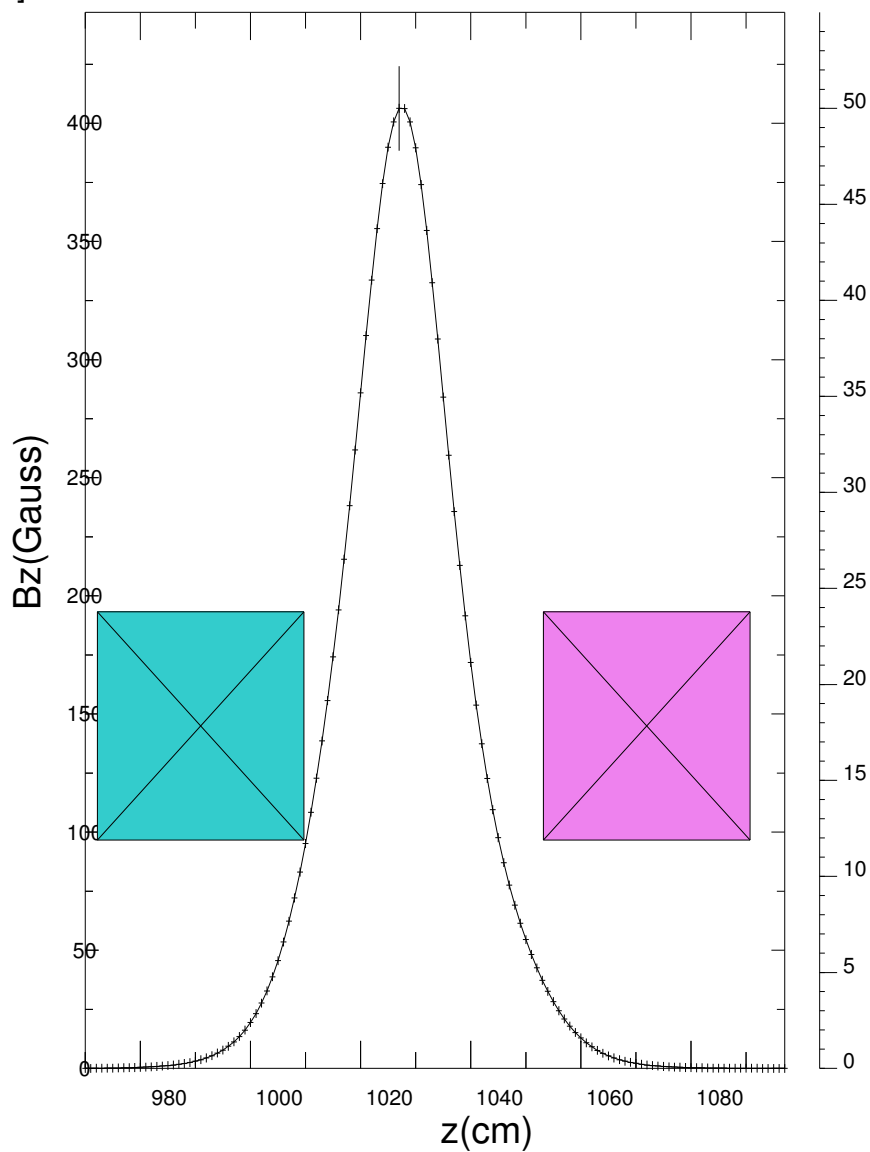
FIGURE 10 $B_z(z) = B_0 / (1 + c1*z^2 + c2*z^4 + c3*z^6)$

Each individual coil is excited, nearest neighbor ferrite cores included in the Poisson calculations. The field synthesized from the fitting function and symmetrized about zero is shown to the right.

(A) Coil I31 Poisson calculated field, (E) fitted field: 301.47, 7.6863e-04, 1.7006e-06, 7.1508e-09
 (B) Coil I32 Poisson calculated field, (F) fitted field: 301.66, 8.1476e-04, 1.2614e-06, 7.6065e-09
 (C) Coil I33 Poisson calculated field, (G) fitted field: 301.62, 8.2509e-04, 1.1379e-06, 7.7810e-09
 (D) Coil I34 Poisson calculated field, (H) fitted field: 302.52, 7.8165e-04, 7.7172e-07, 9.1144e-09

Solid curve - Fitting function
 + Every fifth Poisson point
 Coil center at 1027.5000 cm

[A]



[B]

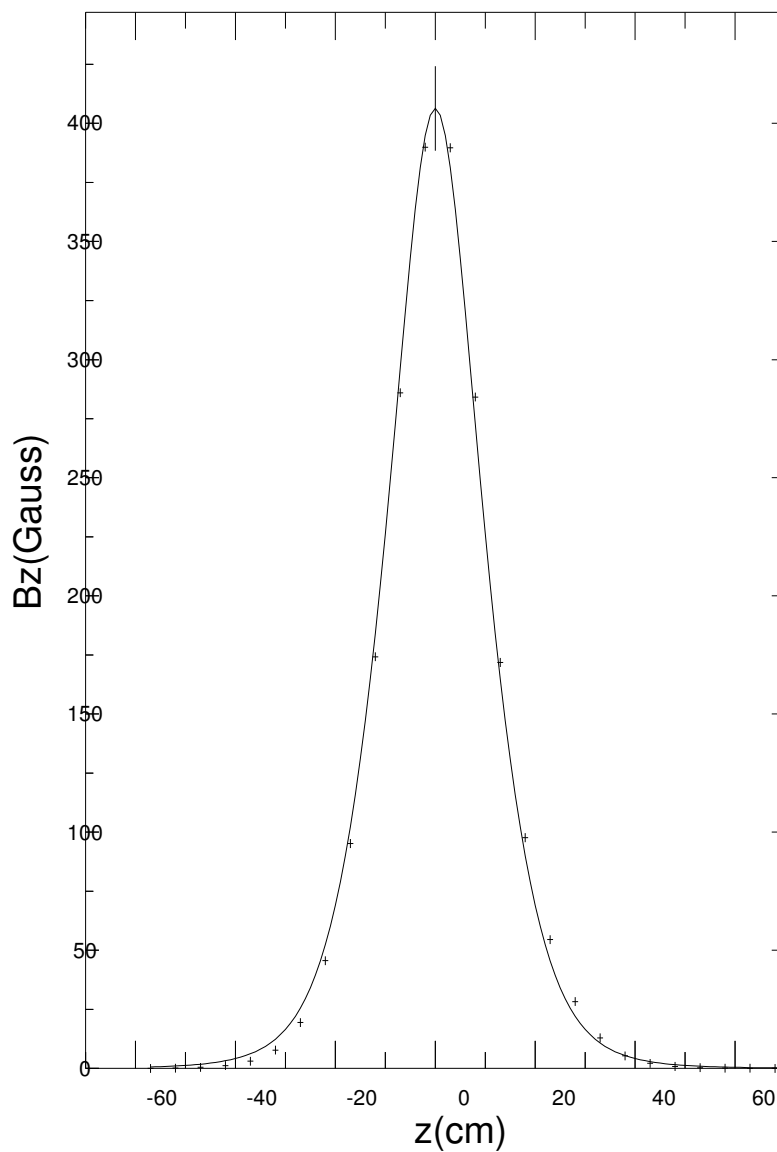


FIGURE 11 $B_z(z) = B_0 / (1 + c1 \cdot z^2 + c2 \cdot z^4 + c3 \cdot z^6)$

(A) Coil I35 Poisson calculated field, the coil is bracketted by ferrite cores Fe34 and Fj21.

(B) Coil I35 fitted field: 292.62, 3.1523e-03, -7.5555e-07, 8.7111e-09, every fifth poisson data point is indicated on the solid fitted curve.

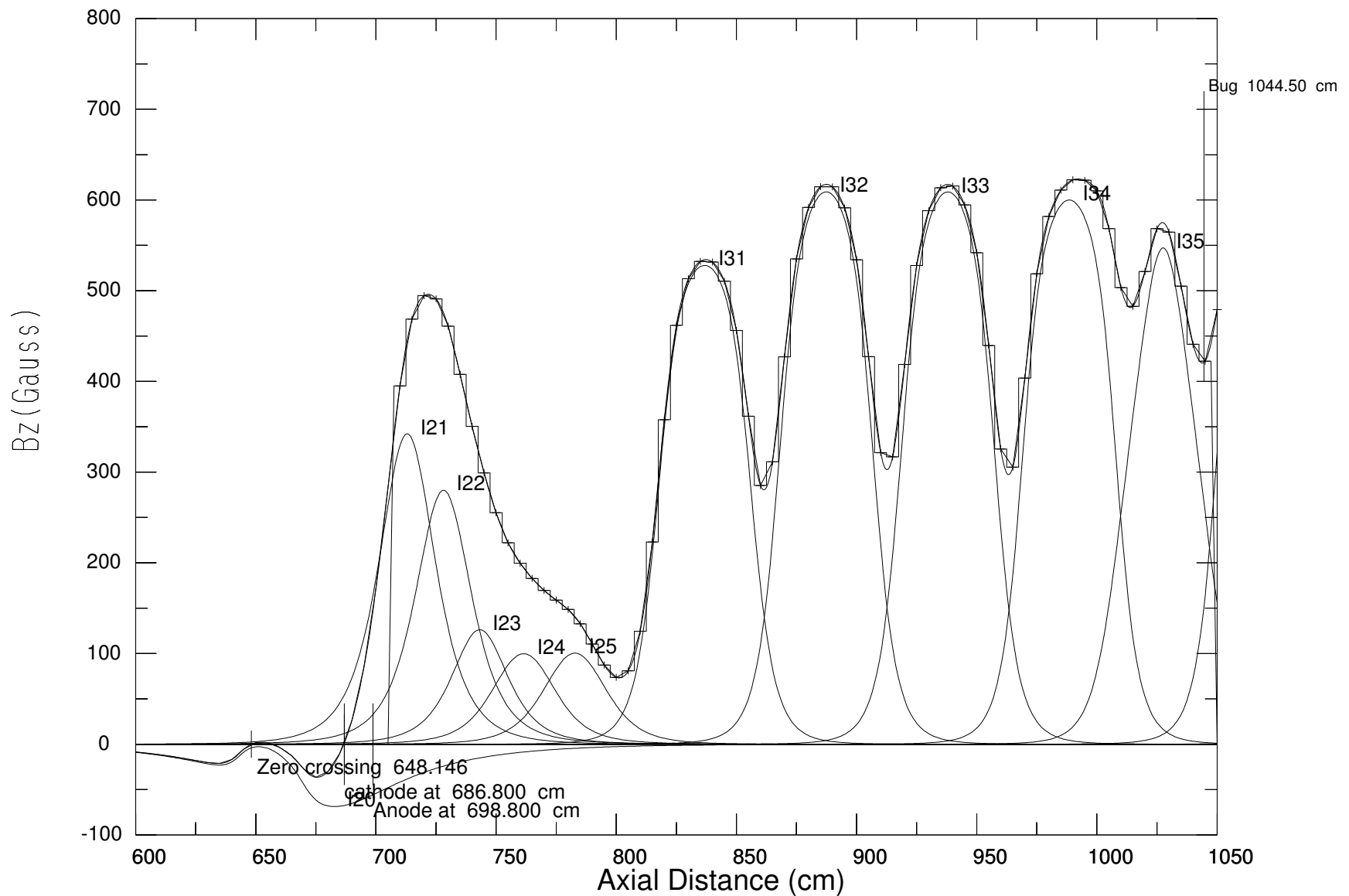


Figure 12 FXR Injector synthesized $B_z(z)$ field for the Lin33 tune. The cathode is located at 686.8 cm, and the Anode at 698.8 cm. The transport solenoid approximation is overplotted as the histogram. The bucking coil field generated from fitting func
Injector Anode coils I21,I22,... I34 fields are also enetered from fitting functions. The location of the I35 beam bug

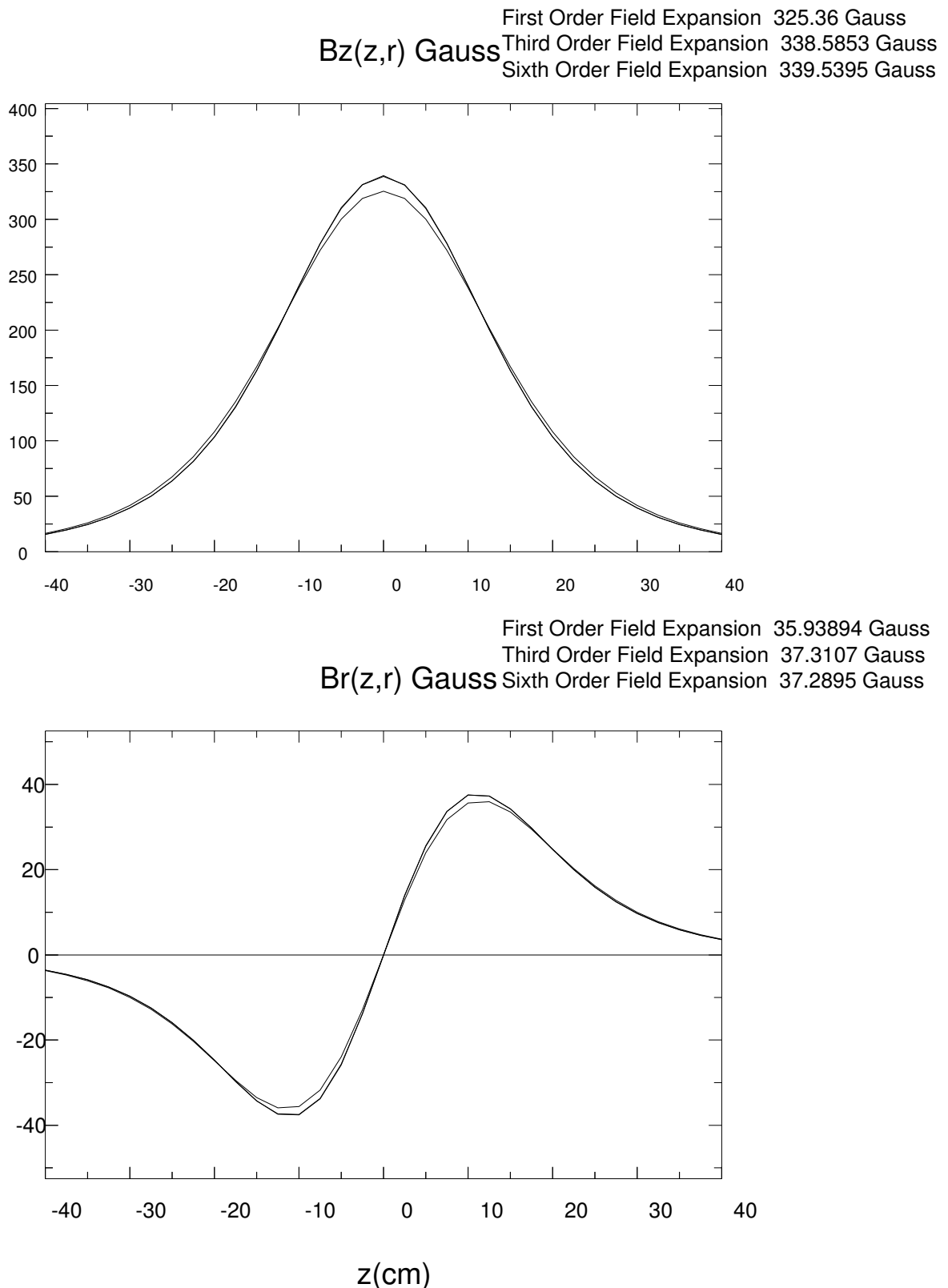


Figure 13) The radial and axial fields derived from $B_z(z) = B_0 / (1 + c1*z^2 + c2*z^4 + c3*z^6)$ for radius of 0 and 5 cm for solenoid I25. The expansion coefficients are given in table 11. Note that the third and sixth order expansions give essentially the same results.

Fourth Order Lagangian Interpolations

14

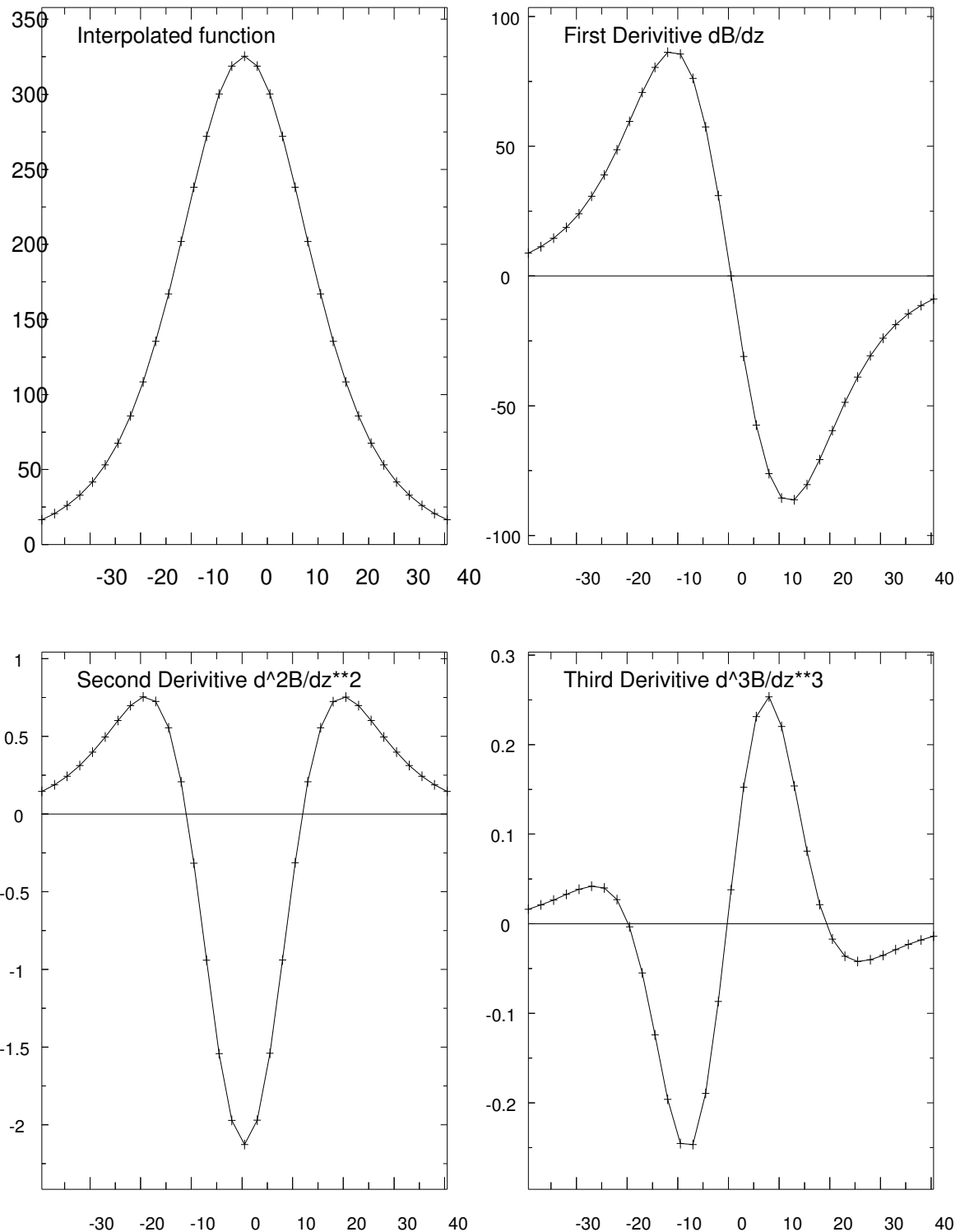


Figure 14) Magnetic field components $B_z(r,z)$ and $B_r(r,z)$ are calculated off axis by field expansions satisfying Maxwell's equations. These involve the derivatives of the axial field based on the interpolation equation $B_z(z) = B_0 / (1 + c_1 z^2 + c_2 z^4 + c_3 z^6)$. Here the derivatives are carried out through fourth order.

Sixth Order Lagangian Interpolations

15

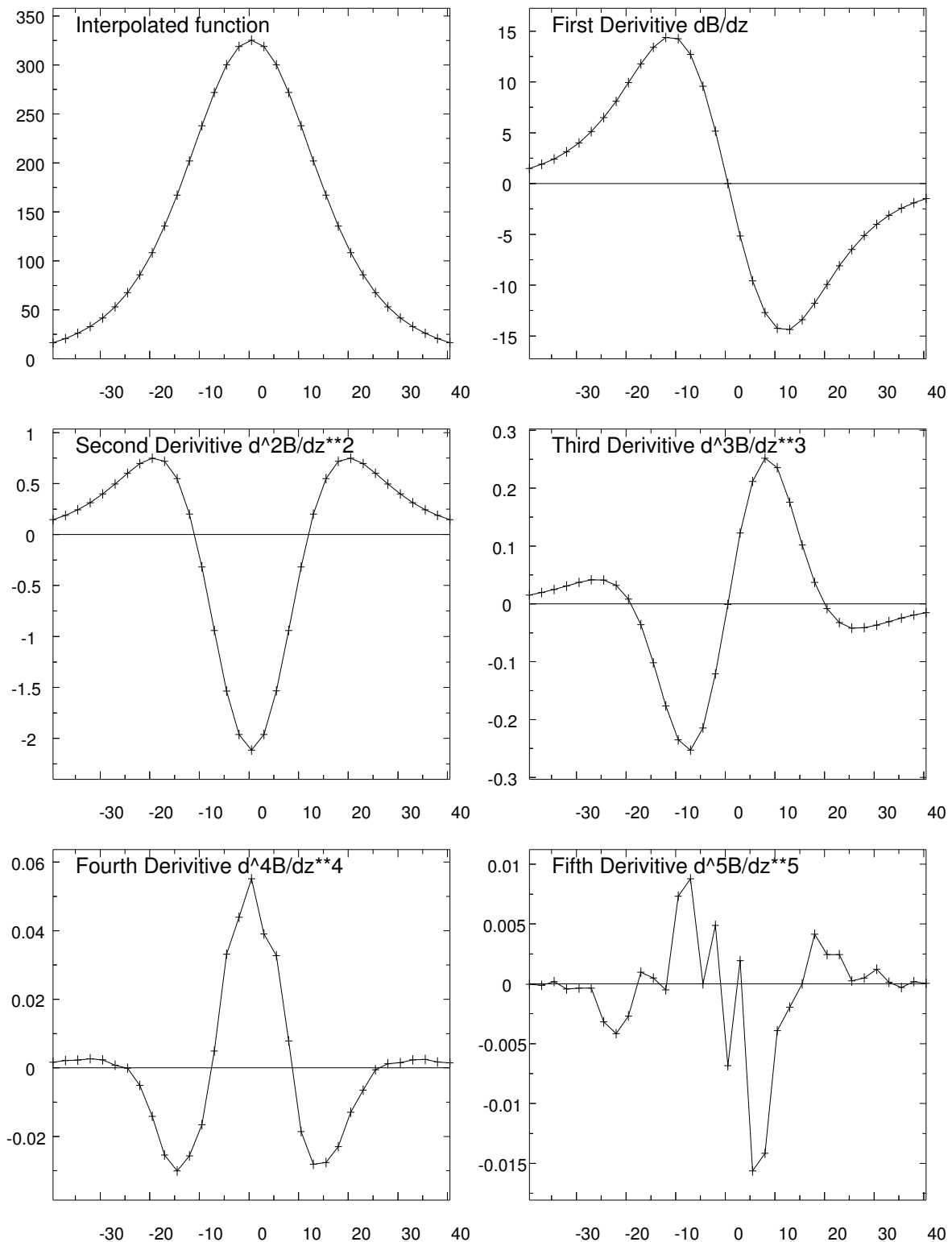


Figure 15) Magnetic field components $B_z(r,z)$ and $B_r(r,z)$ are calculated off axis by field expansions satisfying Maxwell's equations. These involve the derivatives of the axial field based on the interpolation equation $B_z(z) = B_0 / (1 + c_1 z^2 + c_2 z^4 + c_3 z^6)$. Here the derivatives are carried out through sixth order.

Eighth Order Lagangian Interpolations

16

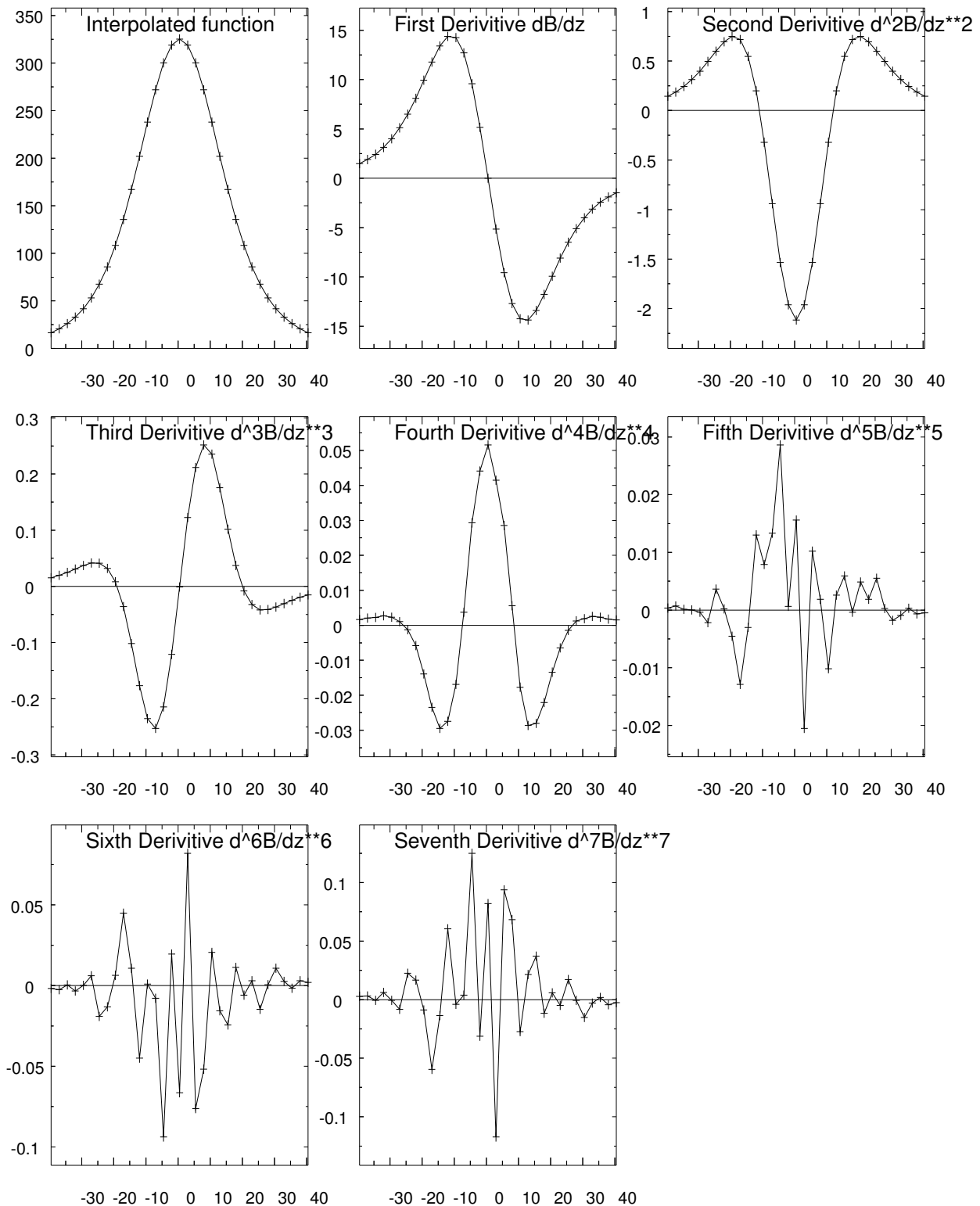


Figure 16) Magnetic field components $B_z(r,z)$ and $B_r(r,z)$ are calculated off axis by field expansions satisfying Maxwells equations. These involve the derivatives of the axial field based on the interpolation equation $B_z(z) = B_0 / (1 + c_1 z^2 + c_2 z^4 + c_3 z^6)$. Here the derivatives are carried out through eighth order.

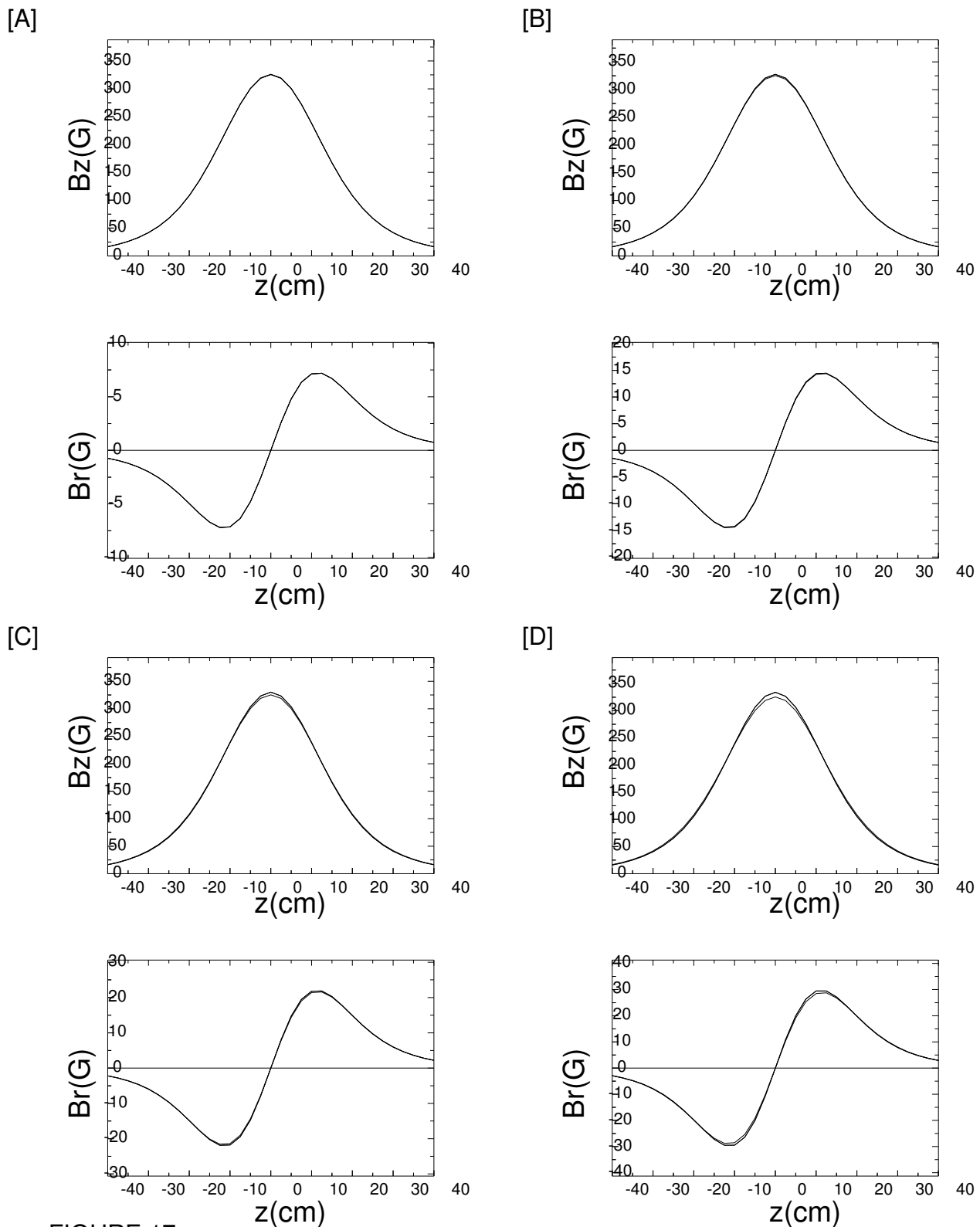


FIGURE 17

Off axis field errors overplotting the first, third and sixth order expansions.

- (A) $B_z(r=1 \text{ cm})$ 1st, 3rd, and 6th Order Field Expansion 325.36, 325.889, 325.8898 Gauss
 $B_r(r=1 \text{ cm})$ 1st, 3rd, and 6th Order Field Expansion 7.187788, 7.198762, 7.198755 Gauss
- (B) $B_z(r=2 \text{ cm})$ 1st, 3rd, and 6th Order Field Expansion 325.36, 327.476, 327.4908 Gauss
 $B_r(r=1 \text{ cm})$ 1st, 3rd, and 6th Order Field Expansion 14.37558, 14.46337, 14.46315 Gauss
- (C) $B_z(r=3 \text{ cm})$ 1st, 3rd, and 6th Order Field Expansion 325.36, 330.1211, 330.2074 Gauss
 $B_r(r=1 \text{ cm})$ 1st, 3rd, and 6th Order Field Expansion 21.56336, 21.85966, 21.85802 Gauss
- (D) $B_z(r=4 \text{ cm})$ 1st, 3rd, and 6th Order Field Expansion 325.36, 333.8242, 334.1486 Gauss
 $B_r(r=1 \text{ cm})$ 1st, 3rd, and 6th Order Field Expansion 28.75115, 29.45349, 29.44655 Gauss

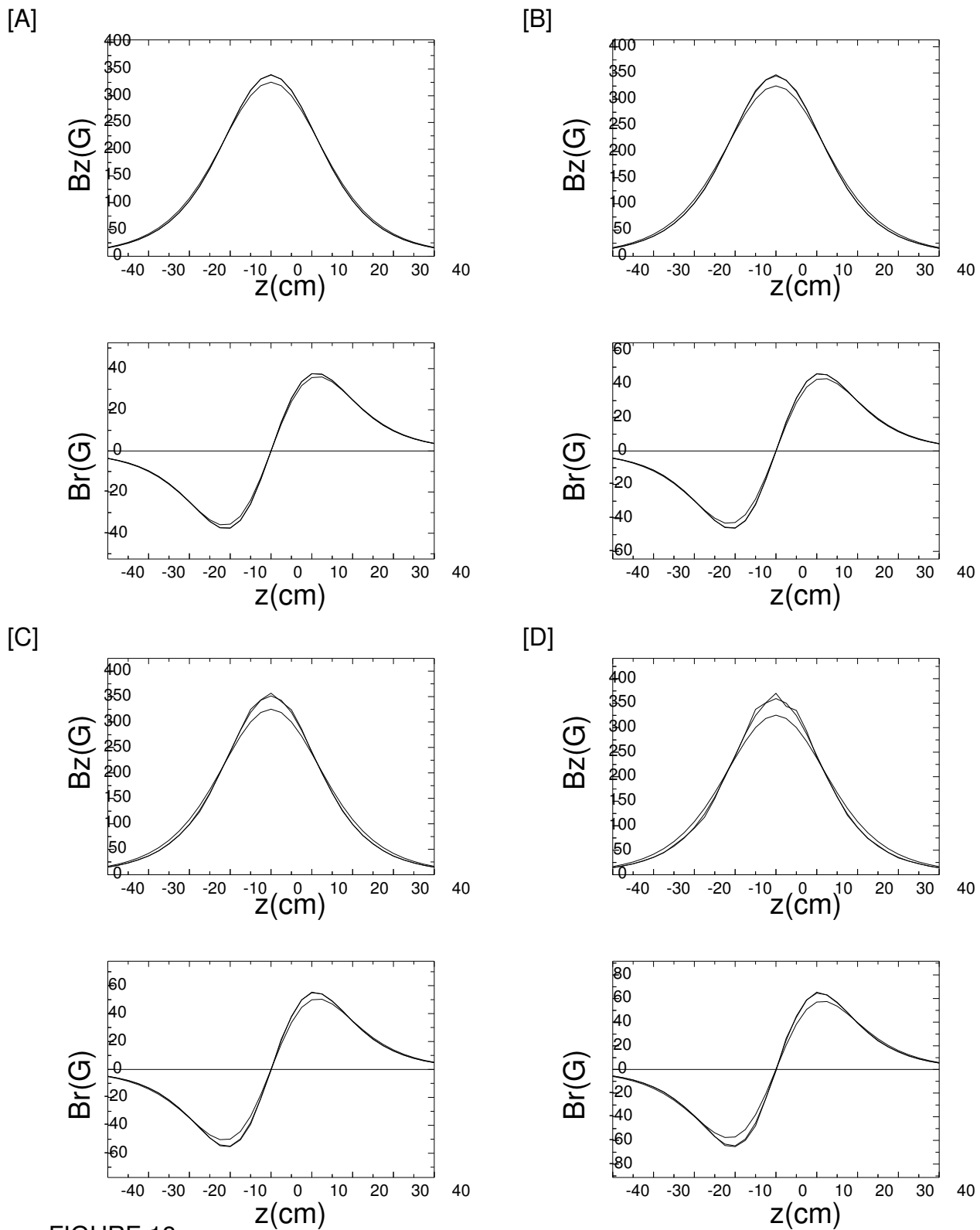


FIGURE 18

Off axis field errors overplotting the first, third and sixth order expansions.

- (A) $B_z(r=5 \text{ cm})$ 1st, 3rd, and 6th Order Field Expansion 325.36, 338.5853, 339.5395 Gauss
 $Br(r=5 \text{ cm})$ 1st, 3rd, and 6th Order Field Expansion 35.93894, 37.3107, 37.2895 Gauss
- (B) $B_z(r=6 \text{ cm})$ 1st, 3rd, and 6th Order Field Expansion 325.36, 344.4045, 346.794 Gauss
 $Br(r=5 \text{ cm})$ 1st, 3rd, and 6th Order Field Expansion 43.12673, 45.49712, 45.44439 Gauss
- (C) $B_z(r=7 \text{ cm})$ 1st, 3rd, and 6th Order Field Expansion 325.36, 351.2816, 356.6082 Gauss
 $Br(r=5 \text{ cm})$ 1st, 3rd, and 6th Order Field Expansion 50.31451, 54.07862, 53.96464 Gauss
- (D) $B_z(r=8 \text{ cm})$ 1st, 3rd, and 6th Order Field Expansion 325.36, 359.2169, 370.0745 Gauss
 $Br(r=5 \text{ cm})$ 1st, 3rd, and 6th Order Field Expansion 57.5023, 63.12102, 62.8988 Gauss

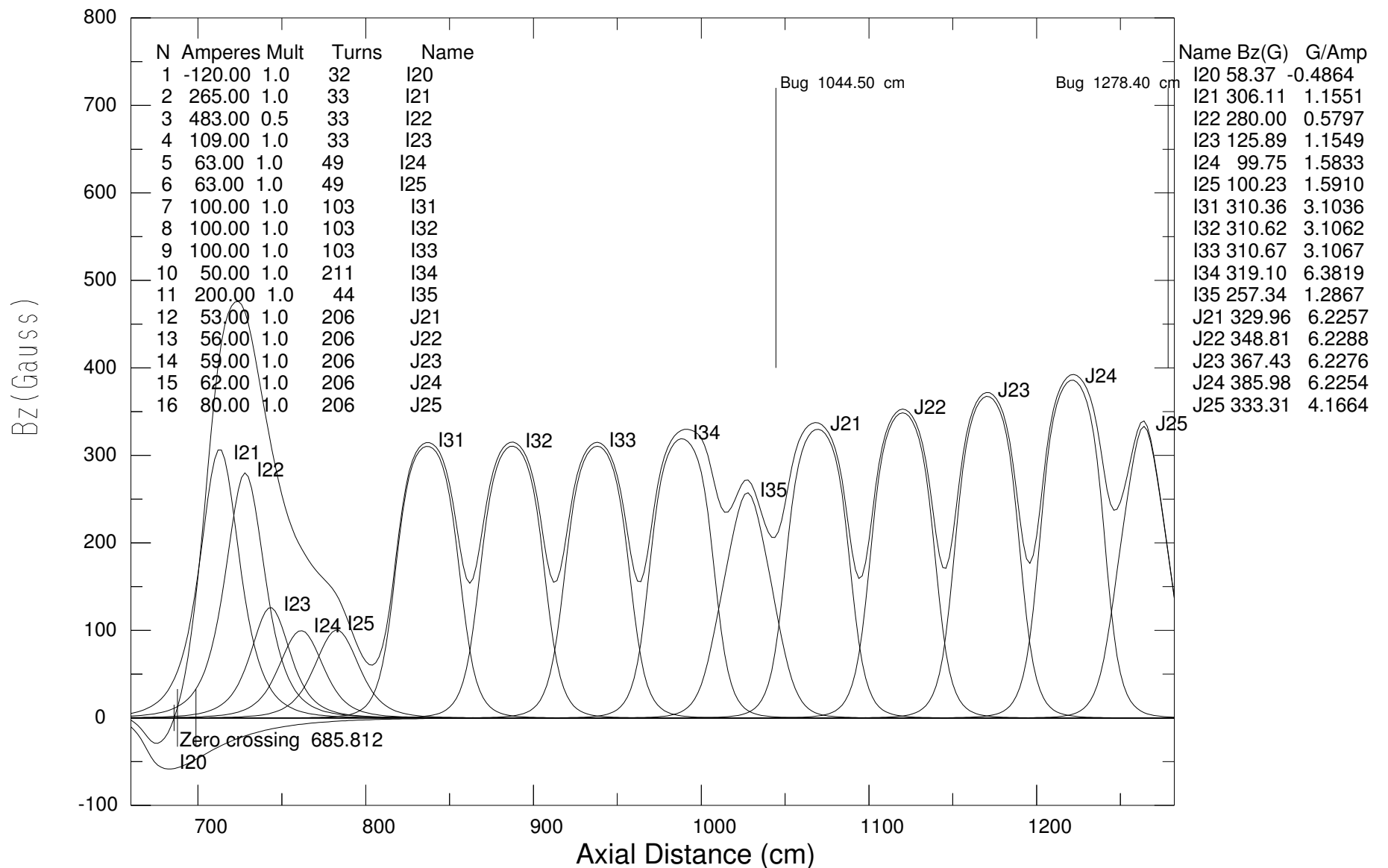


Figure 19) FXR tune SPU28. Cathode located at 687.8 cm and anode shroud starting at 698.800 cm from alignment monument. The bucking coil and injector coil fields were synthesized from the fitting function for $B_z(z)=B_0/(1+c_1 z^2 + c_2 z^4 + c_3 z^6)$ and summed over all the coils for each axial position.

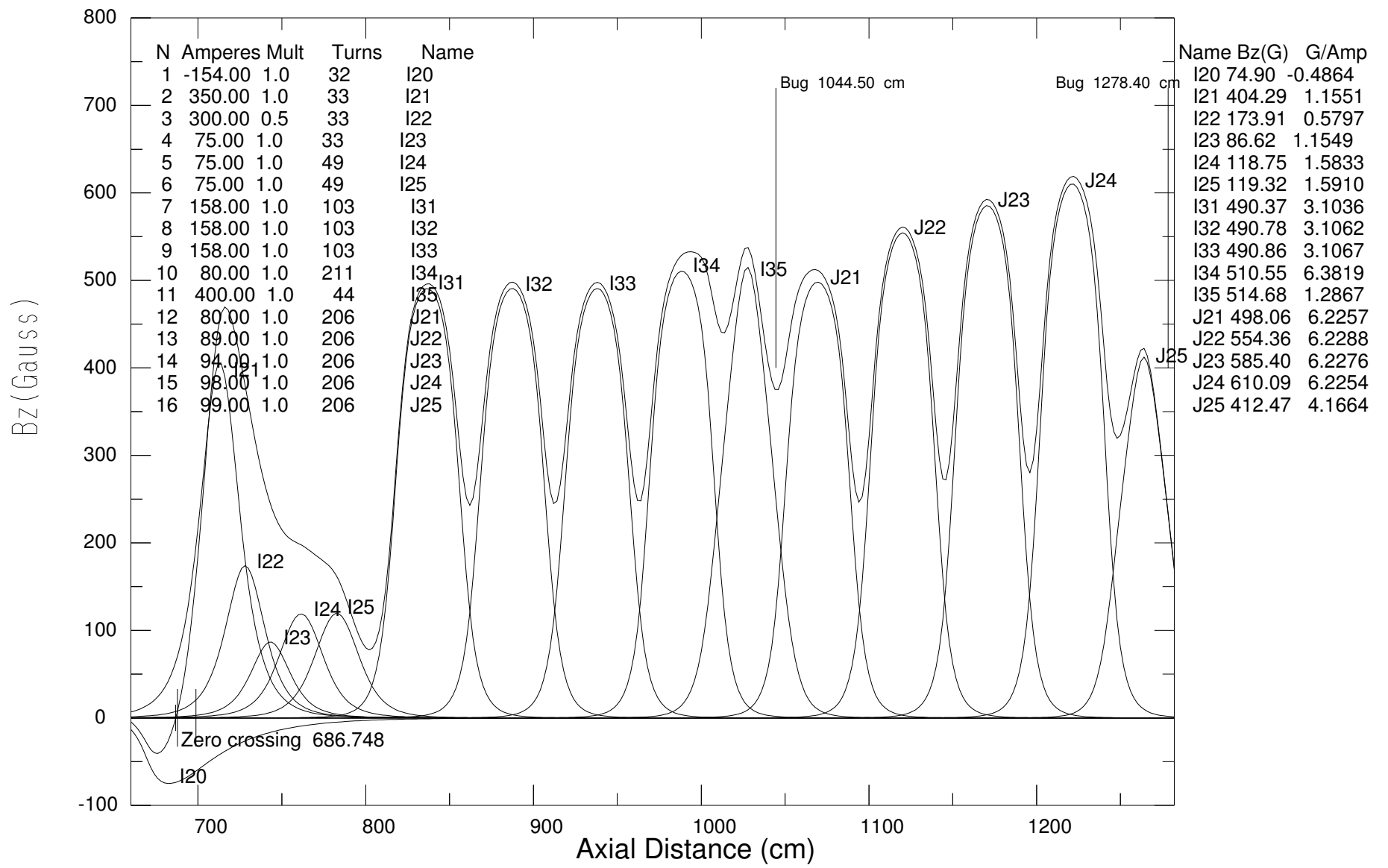


Figure 20) FXR Double Pulse Synthesized $B_z(z)$ Field dp1170 tune. Cathode at 687.8 cm Anode at 698.8 cm from the alignment monument. The bucking coil and injector coil fields were generated from the fitting function for $B_z(z)=B_0/(1+c_1*z^2+c_2*z^4+c_3*z^6)$ and summed over all the coils for each axial position.

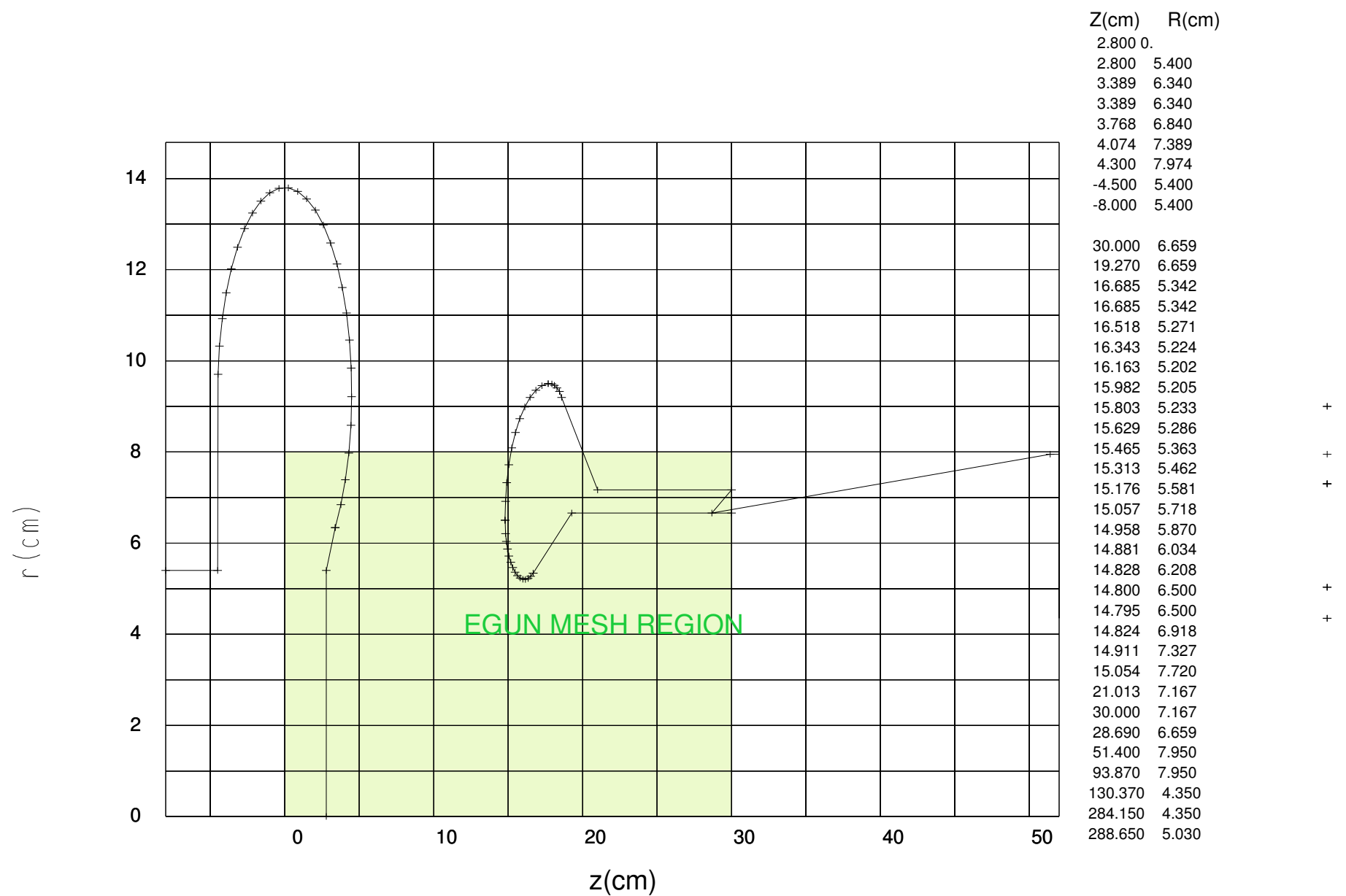


Figure 21) EGUN mesh Number of mesh points 6190 Egun mesh cell 0.2000 0.2000 cm

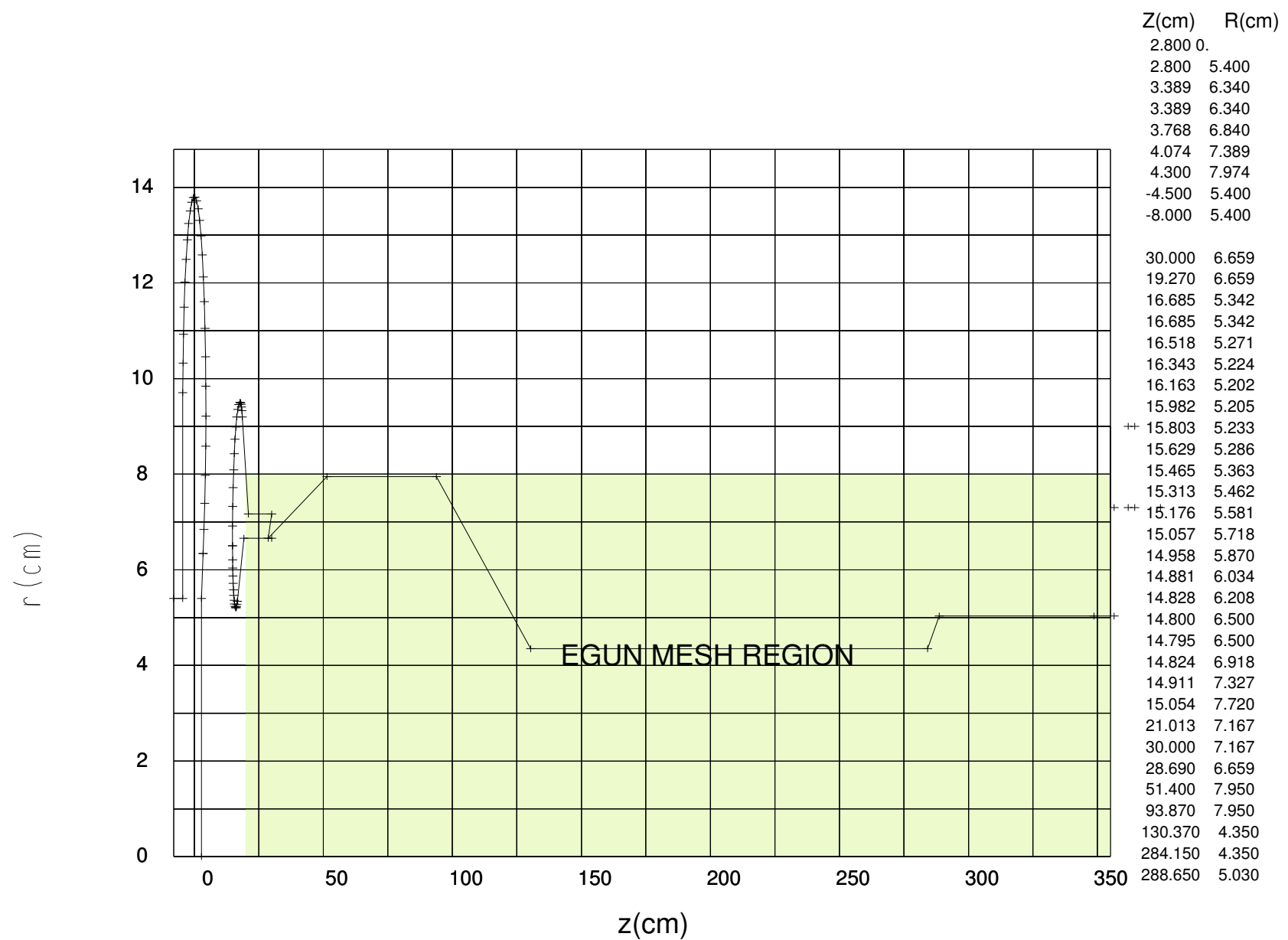


Figure 22) 20-355 cm egun mesh Number of mesh points 11407 Egun mesh cell 0.5000 0.5000 cm

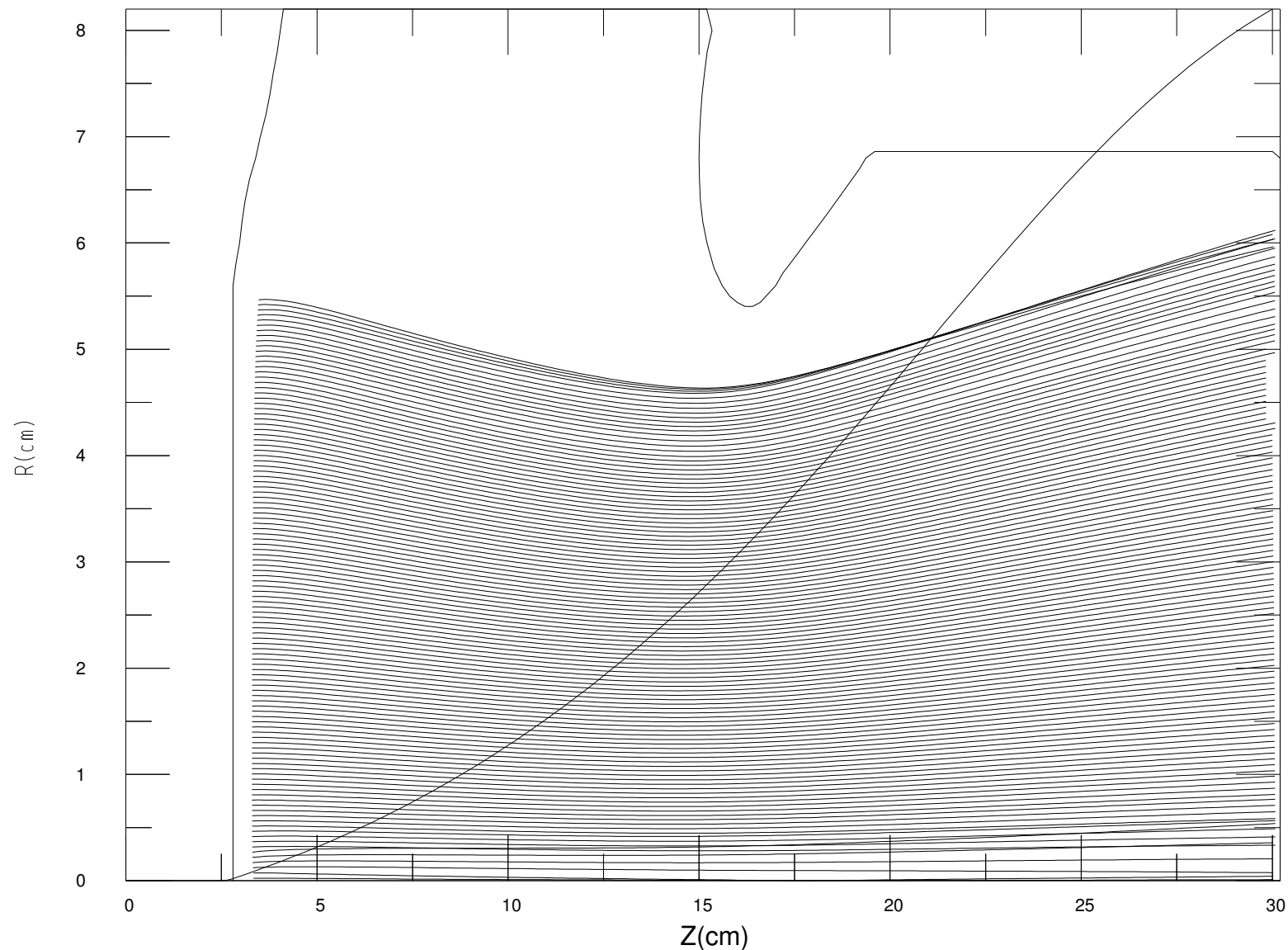


Figure 23) Egun iteration 19, 2.1 MV Anode potential, 2.00E-03 meters/Mesh_Unit Beam current 3624 Amperes
 Beam run from cathode to 30 cm with phase space transferred at 20 cm to the continuation problem.
 The magnetic field is overplotted. Note it is zero at the cathode.

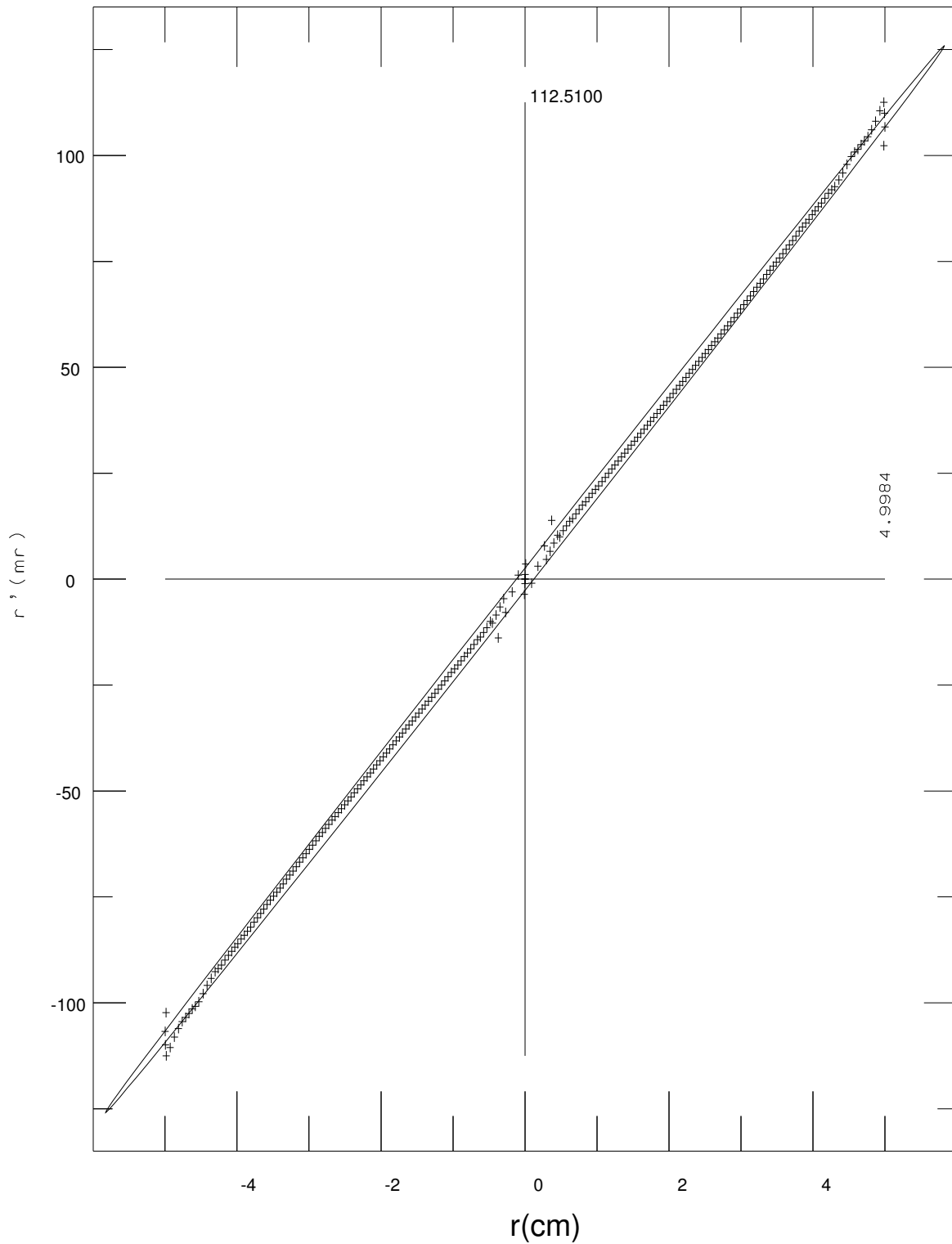


Figure 24) Phase space plot at 20 cm from cathode. Anode potential 2.1 MV, Beam energy 1.944 MeV and current of 3624 Amperes. Beam characterized by r, r_{21}, r' of 5.8259 cm, 0.9998, 125.8808 mr and emittance of 15.461 cm-mr.

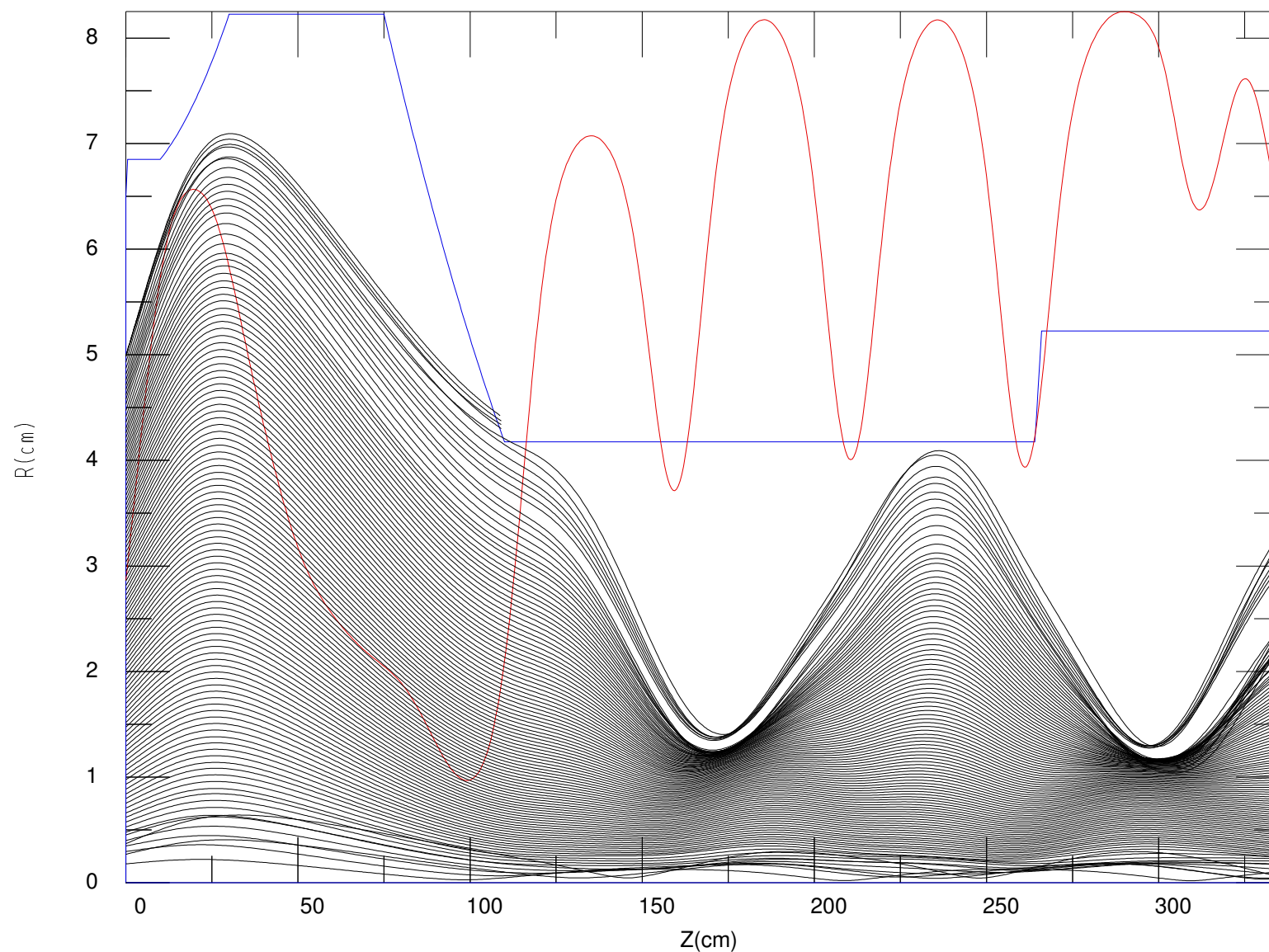


Figure 25) EGUN continuation Lin33 Tune, transfere point at 100 MU (20.0 cm) 2.50E-03 meters/Mesh_Unit
Beam Current 3624. Amperes and 1.96 MeV with 2.1 MV anode potential.

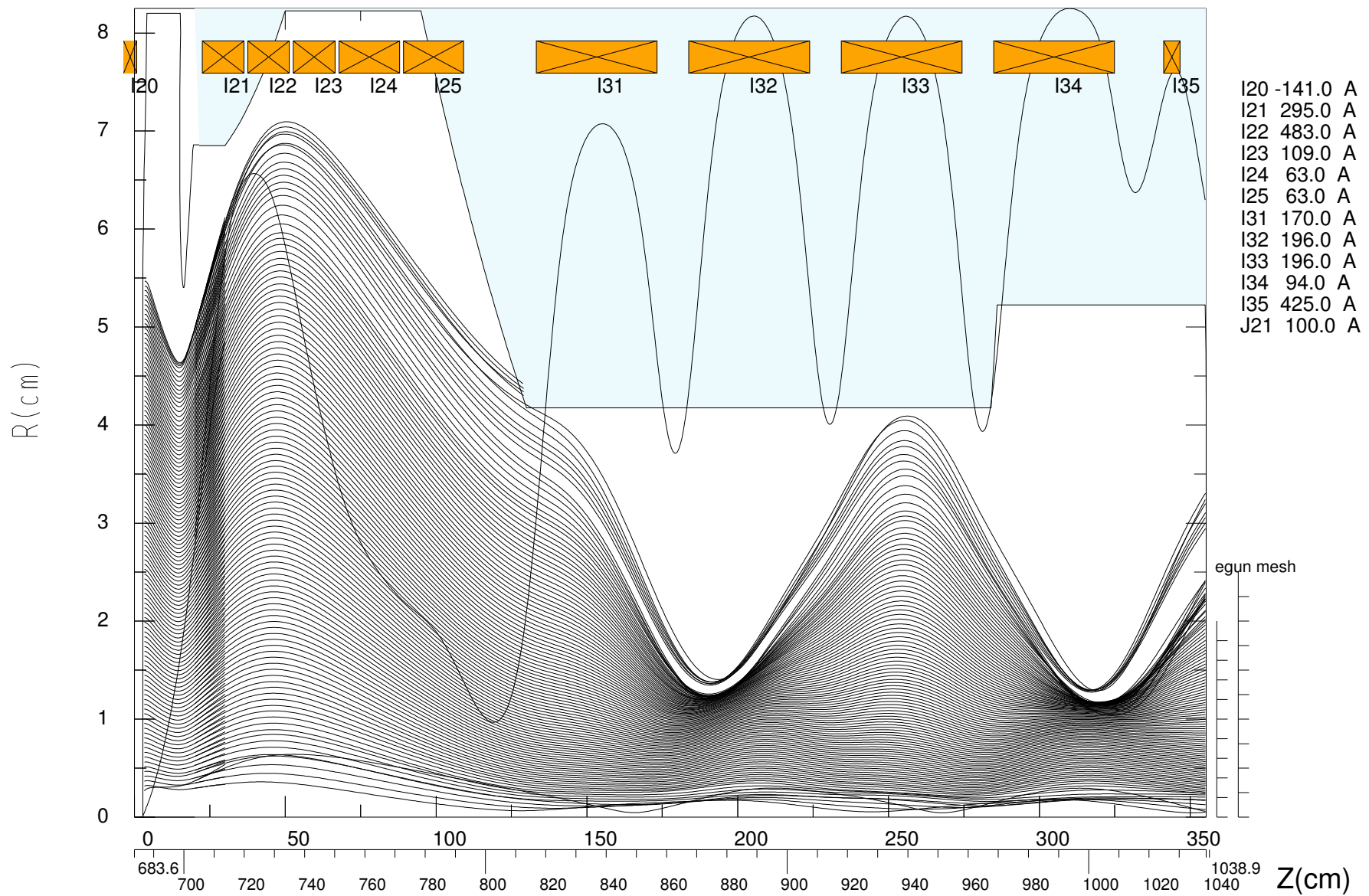


Figure 26) FXR Injector 2 mm grid Lin33 tune, 12cm AK gap Anode 2.10 MV cathode 386.8 anode 698.8 cm 3624.5 Amperes beam current LIN33 Magnetic field profile. Beam current reaching end 3431.22 Amperes

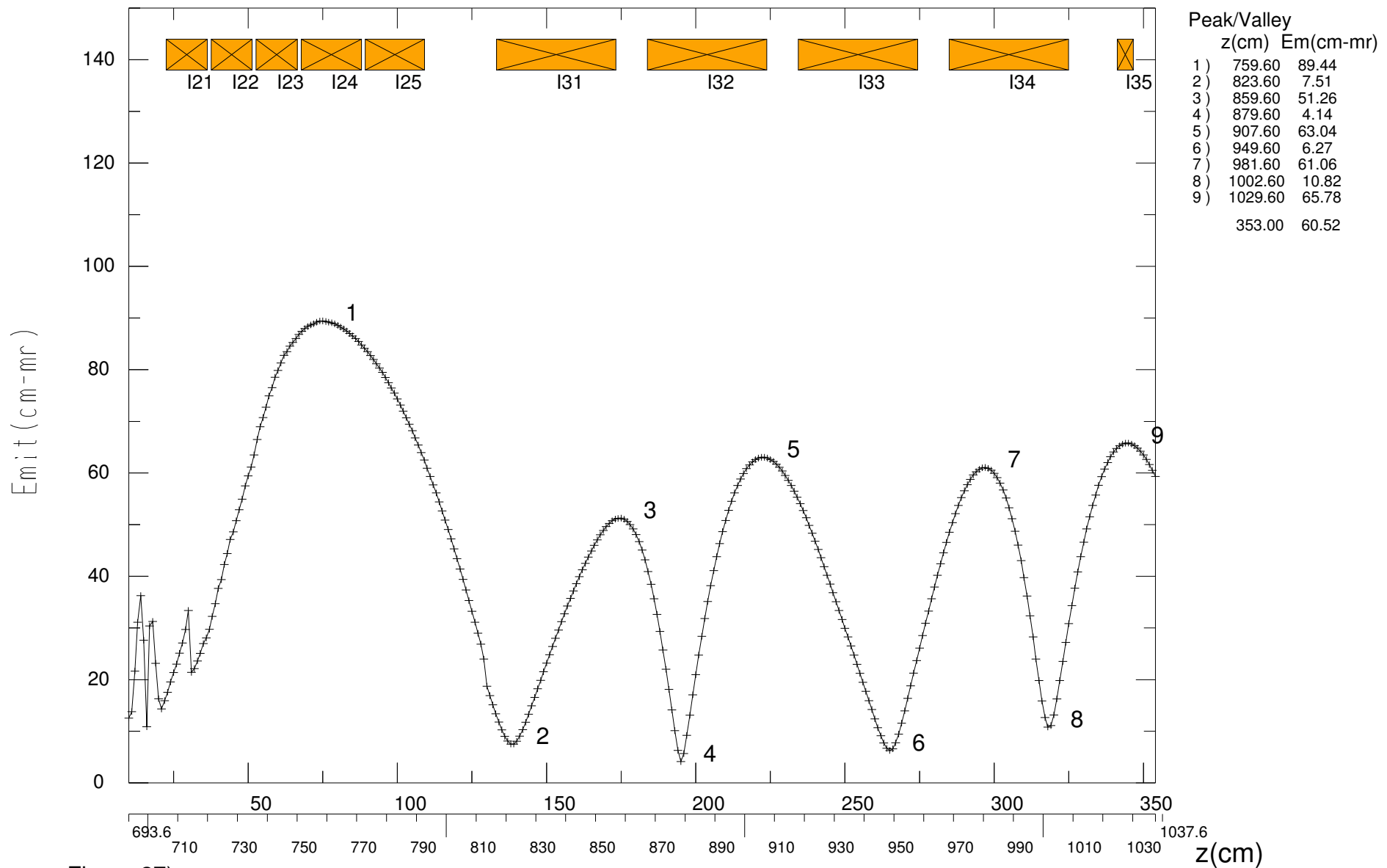


Figure 27) FXR Injector study 2 mm EGUN grid, 12cm AK gap. LIN33 Magnetic field profile. Anode potential 2.10 MV. Cathode 3624.5 Amperes beam current. Emittance range: minimum 4.14, maximum 89.44, average 39.92 $\text{cm} \cdot \text{mr}$.

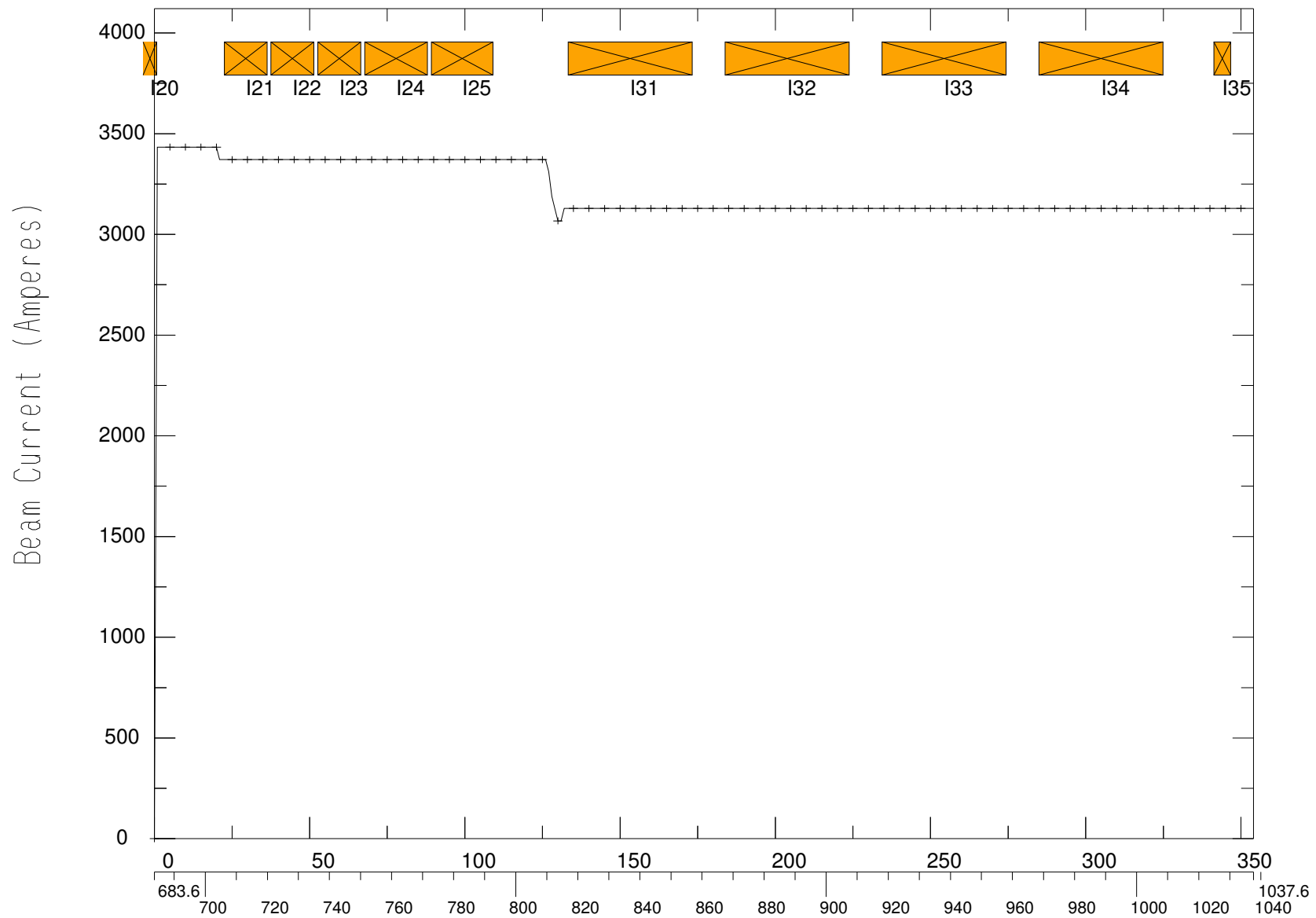


Figure 28) FXR Injector Current LIN33 Magnetic field profile 2 mm grid 12cm AK gap Anode 2.100 MV.
3624.5 Amperes beam current Ending current 3129.1 Ampere

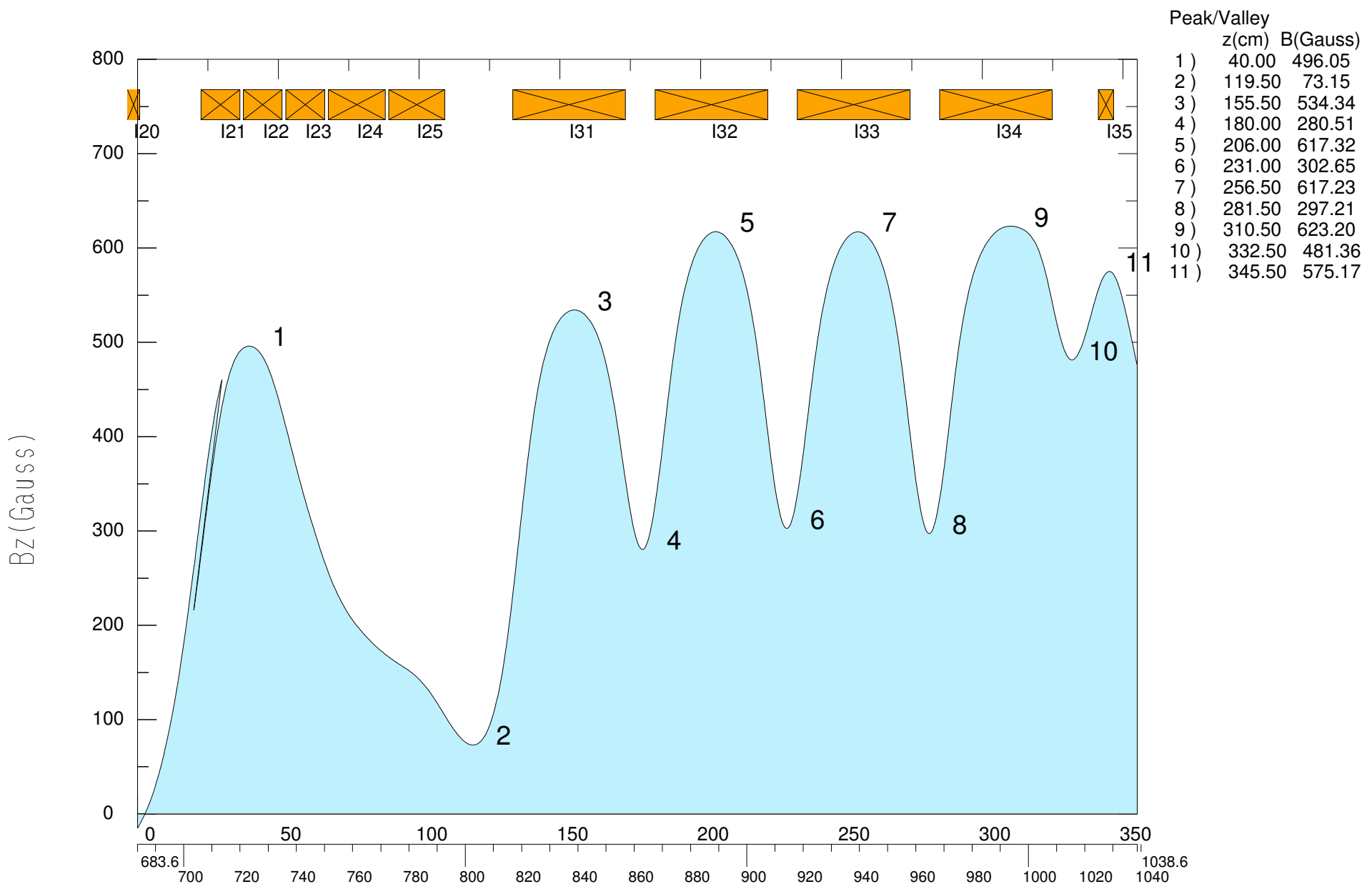


Figure 29) FXR Injector Lin33 Magnetic Field tune. Injector magnets current are:
 I20 -141.0 I21 295.0 I22 483.0 I23 109.0 I24 63.0 I25 63.0 I31 170.0 I32 196.0 I33 196.0 I34 94.0 I35 425.0 Amperes.

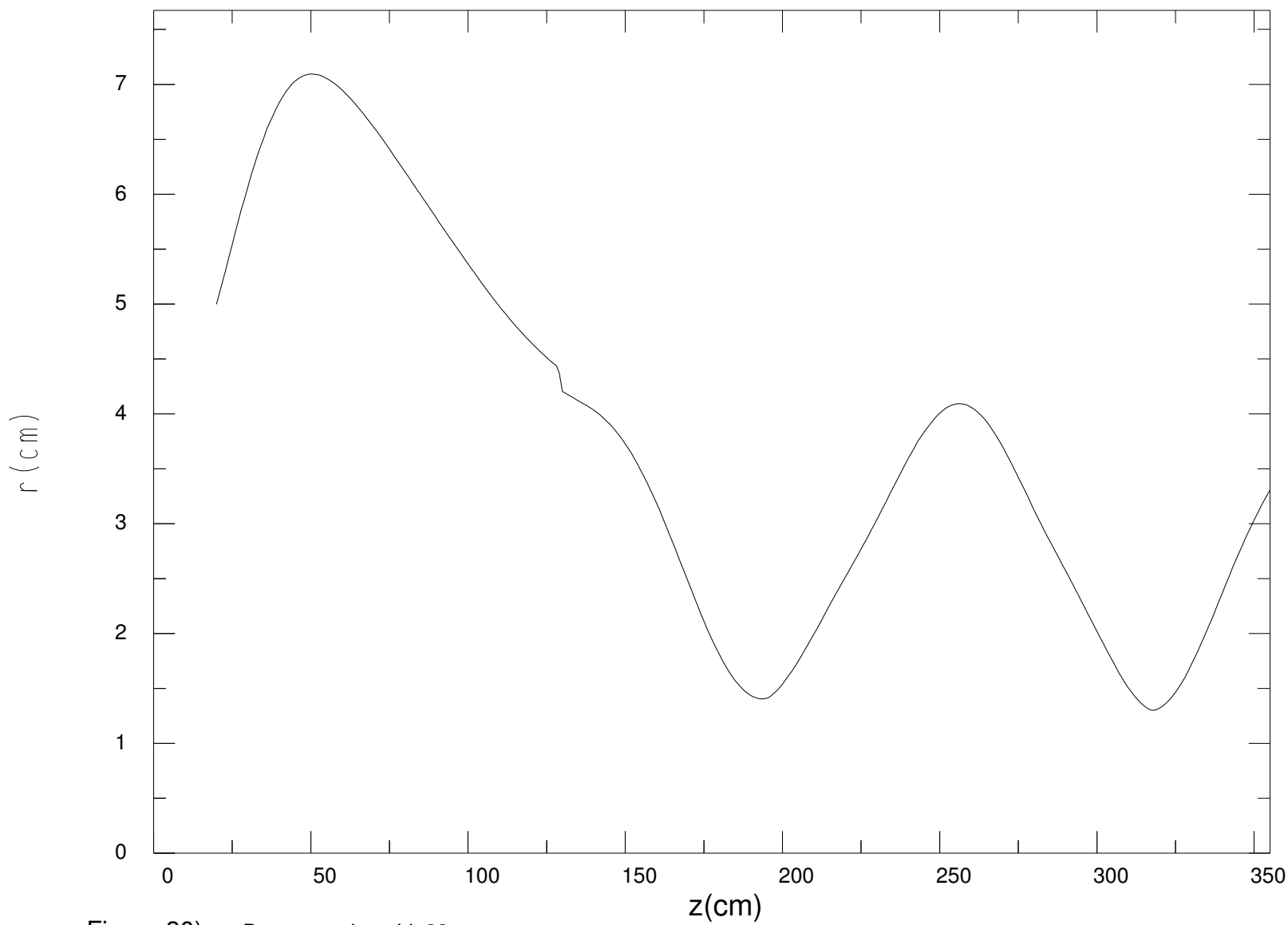


Figure 30) Beam envelope Lin33 tune.

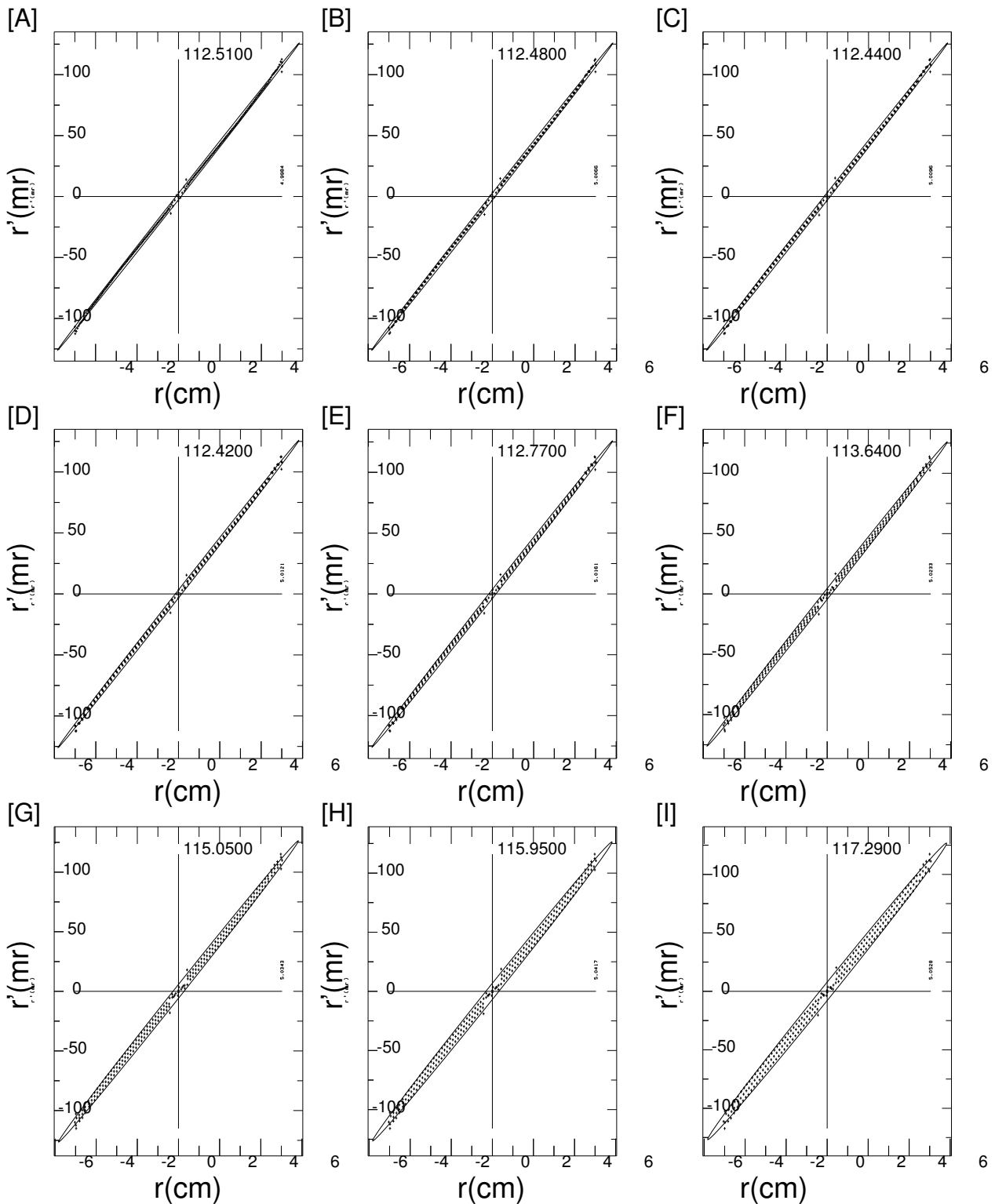


FIGURE 31

Phase space at 20 cm vs cathode temperature. A cathode temperature of 20,000 K corresponds to a beam energy of 1.7 eV. This produces an emittance of 33.9 cm-mr at 20 cm from the cathode.

(A) zero Kelvin, Emittance = 15.46 cm-mr, $r(\text{cm}), r'(\text{mr}) = 5.8259, 0.9998, 125.88$

(B) 1000 K, 16.91 cm-mr, 5.8260, 0.9997, 125.91 (C) 2000 K, 18.24 cm-mr, 5.8260, 0.9997, 125.91

(D) 3000 K, 19.47 cm-mr, 5.8260, 0.9996, 125.92 (E) 5,000 K, 21.72 cm-mr, 5.8261, 0.9996, 125.94

(F) 10,000 K, 26.41 cm-mr, 5.8264, 0.9994, 126.01 (G) 20,000 K, 33.90 cm-mr, 5.8284, 0.9989, 126.36

(H) 30,000 K, 39.81 cm-mr, 5.8286, 0.9985, 126.44 (I) 50,000 K, 46.09 cm-mr, 5.8305, 0.9981, 126.84

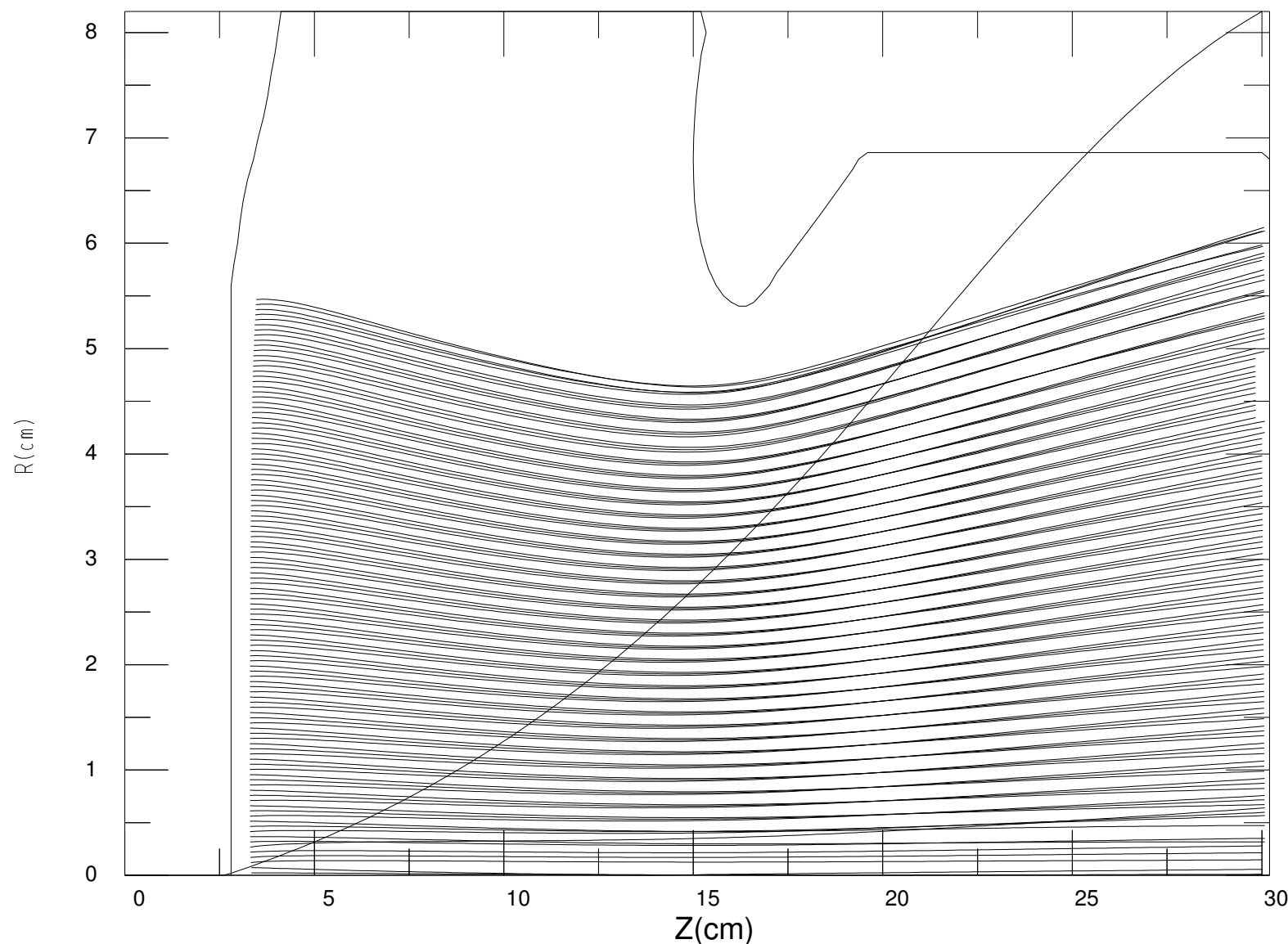


Figure 32) Lin33 Tune Plot:3 Iteration: 19 2.00E-03 meters/Mesh_Unit emitted beam current 3624. Amperes
Anode potential 2.1 MV, Cathode temperature 20,000 Kelvin

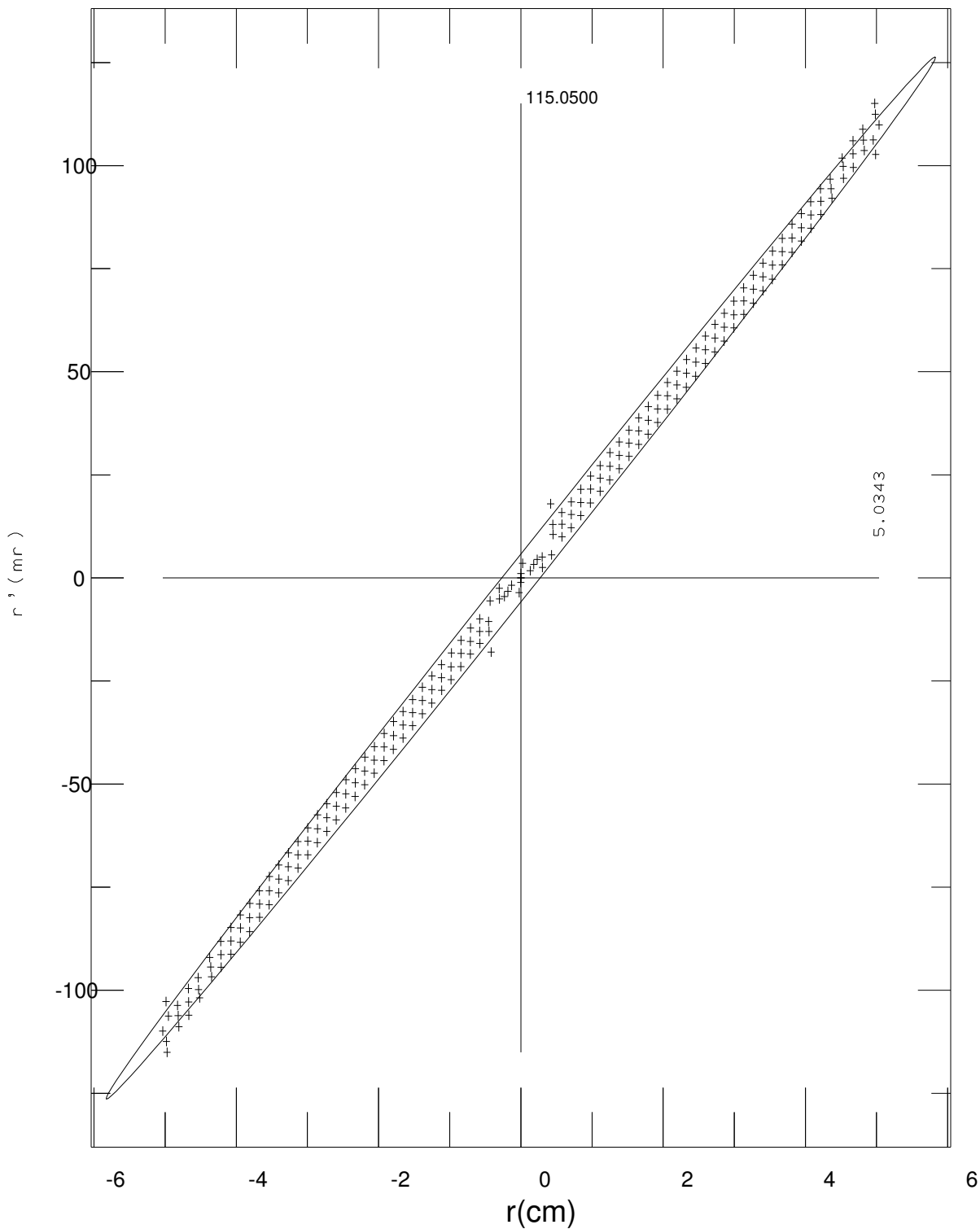


Figure 33) Phase plot Emittance: 33.904 cm-mr $r(\text{cm}), r'(\text{mr})$: 5.8284 0.9989 126.3630
 Lin33 tuen, Current 3624. Amperes Energy 1.944 MeV Z Location 100 Mesh Units 20 cm Anode potential 2.1 MV, Cathode temperature 20,000 Kelvin

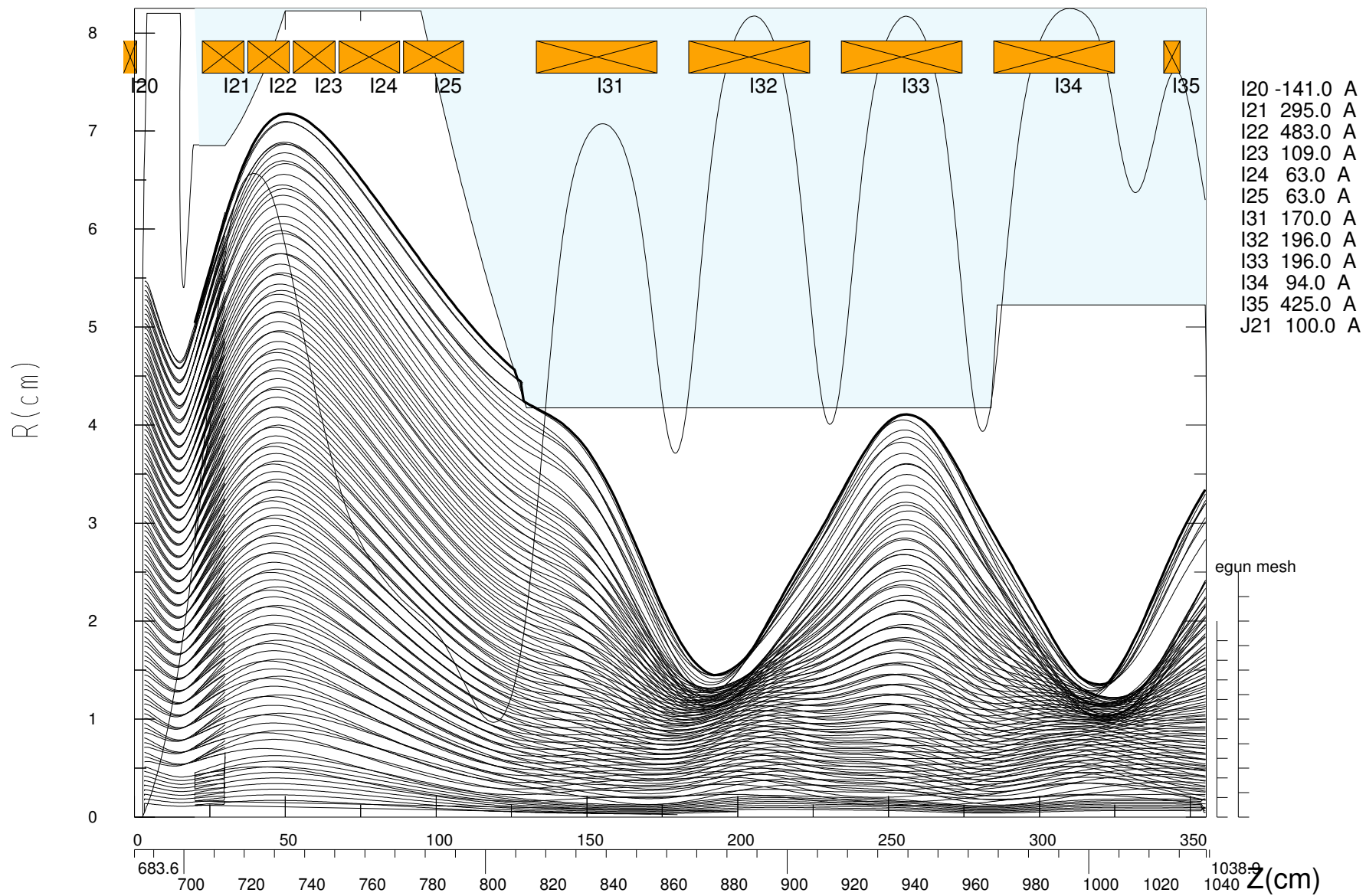


Figure 34) FXR Injector study Lin33 tune, 12cm AK gap EGUN Unit 0.002 and 0.0025 meters/mesh Anode 2.100 MV. Cathode temperature 20,000 Kelvin. cathode 386.80, anode 698.80 cm, 3624.4 Amperes beam current Beam current reaching en

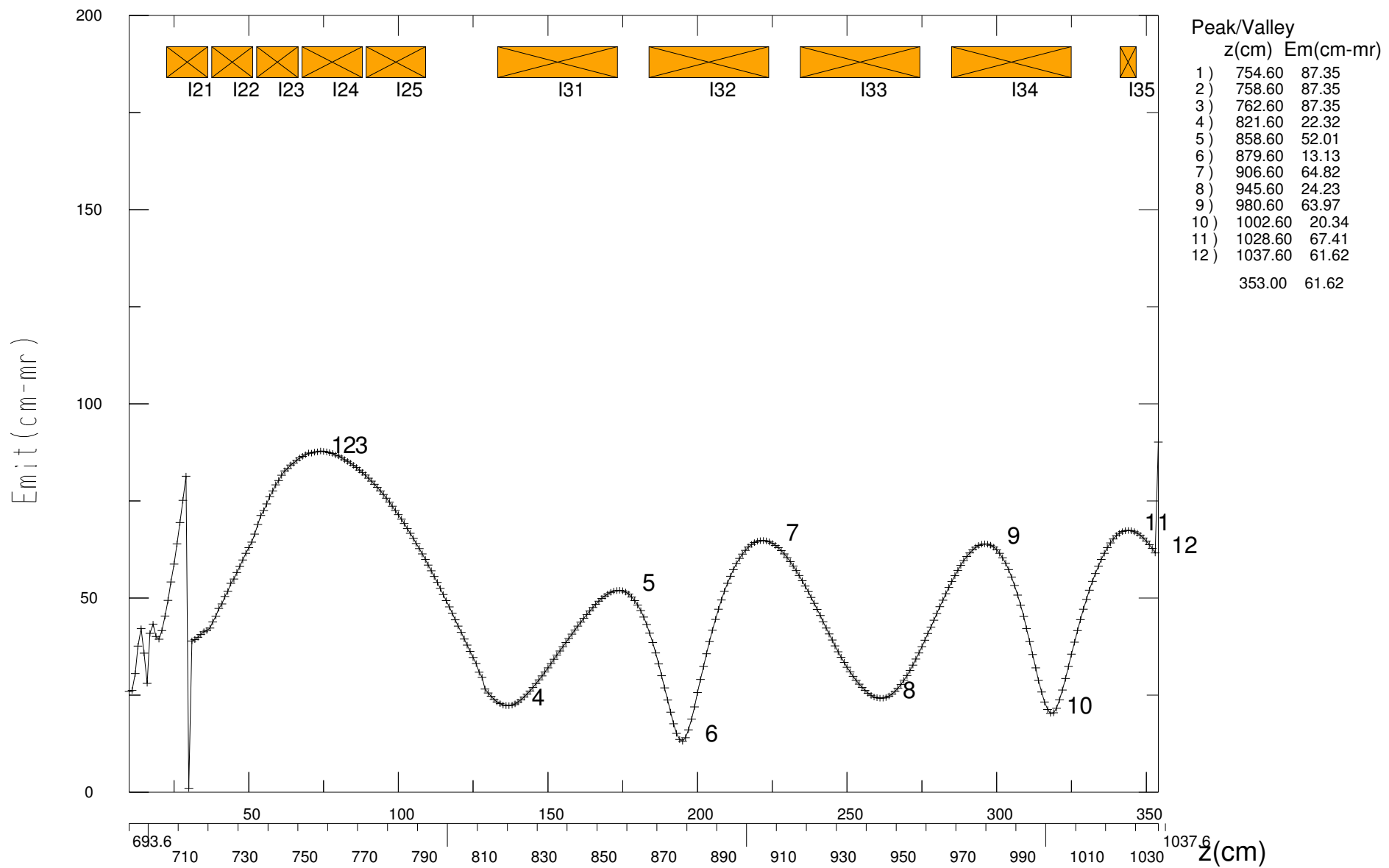
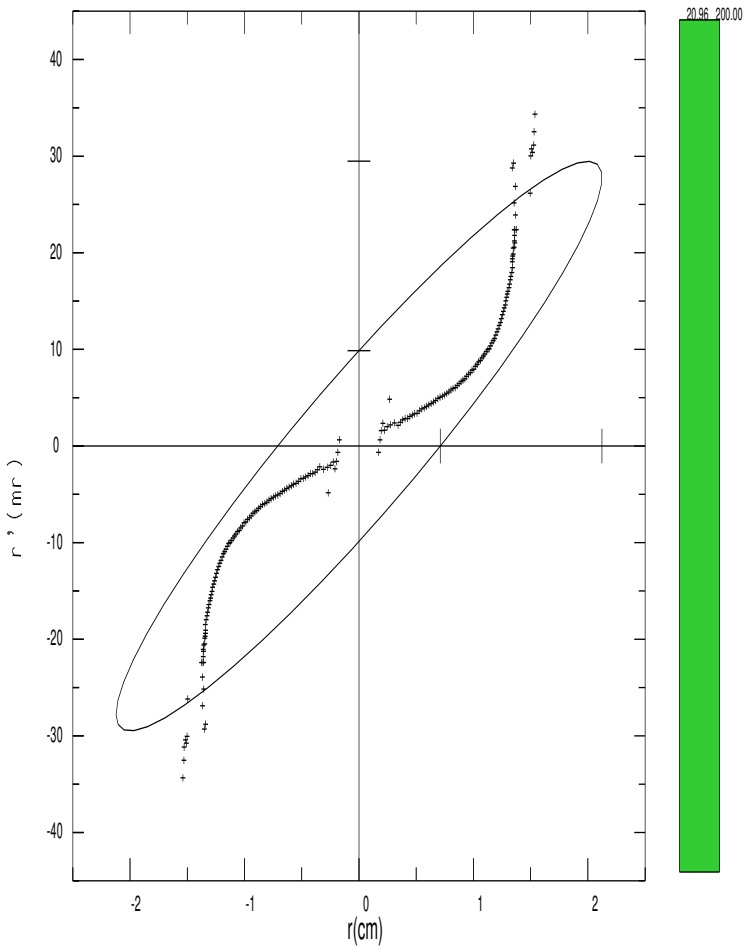
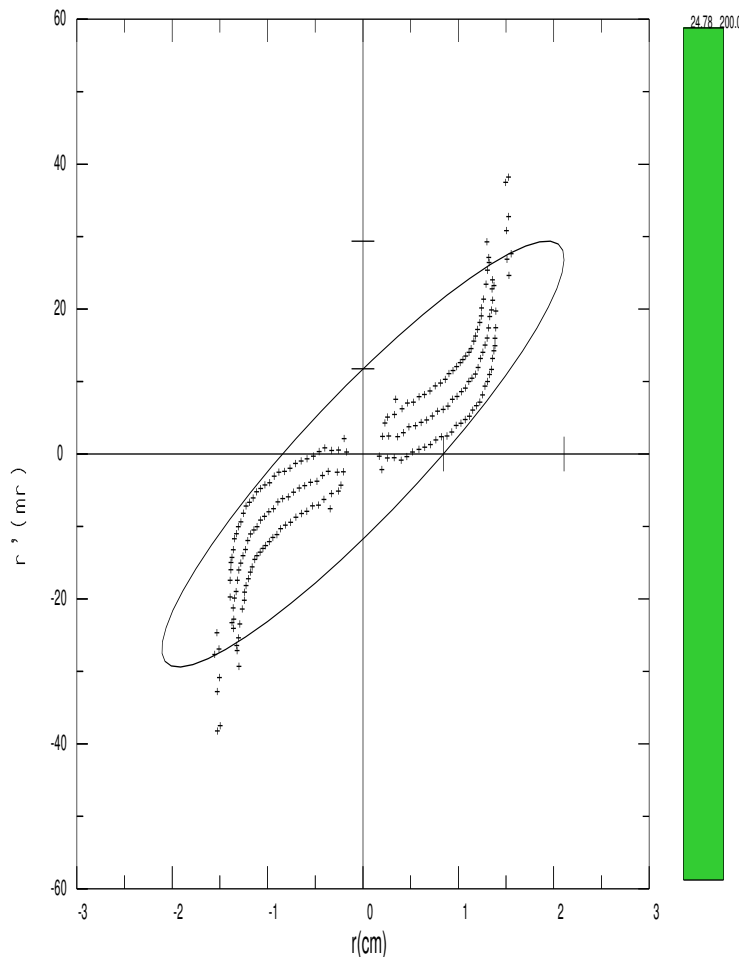


Figure 36) Phase Space at z=200 cm

36



A) Phase Space cathode temperature zero Kelvin



B) Phase Space cathode temperature 1e4 Kelvin

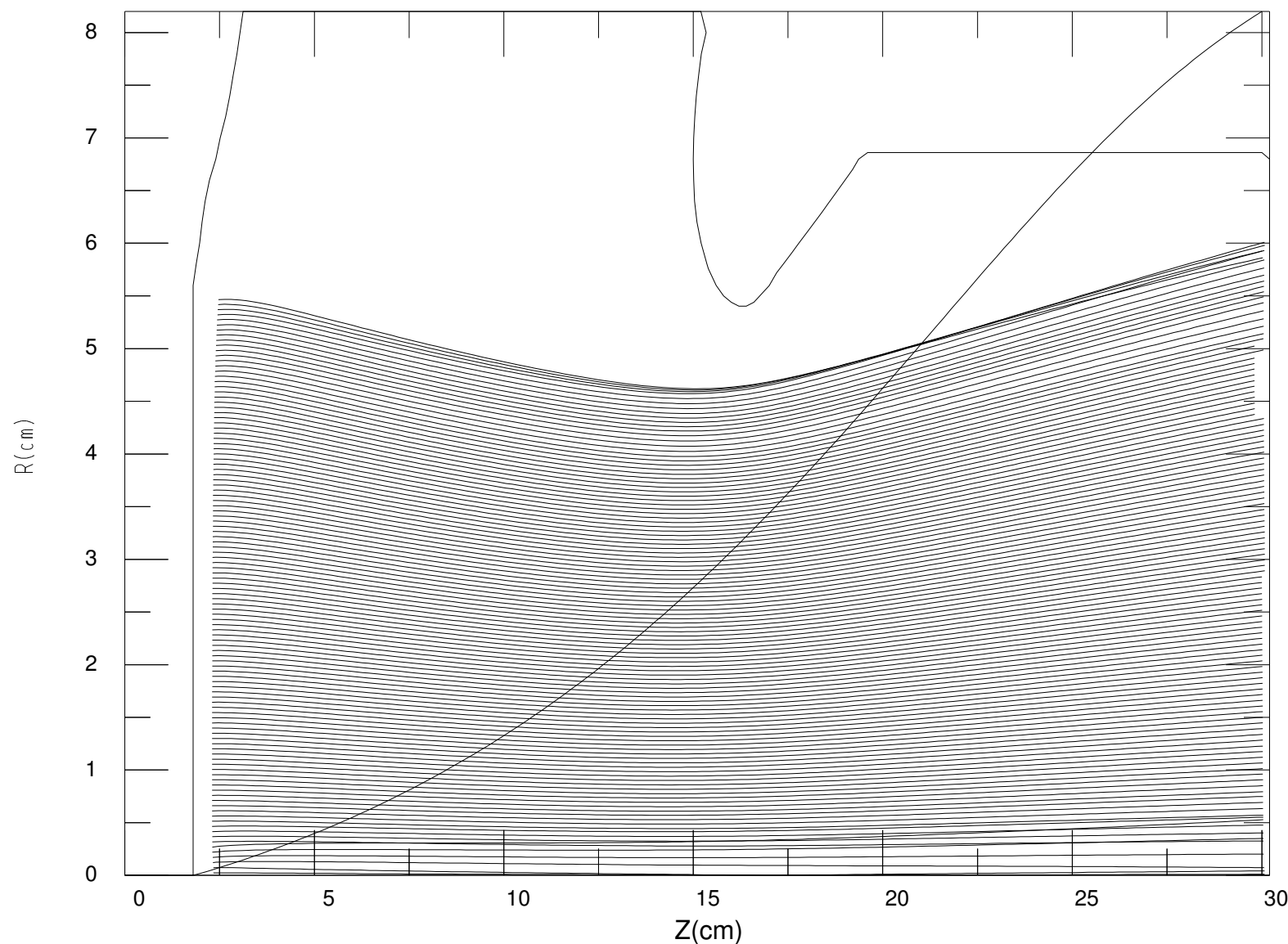


Figure 37) FXR SPU28 magnetic field tune.
EGUN iteration 19, 2.0E-03 meters/Mesh_Unit, converged beam current 3184 Amperes

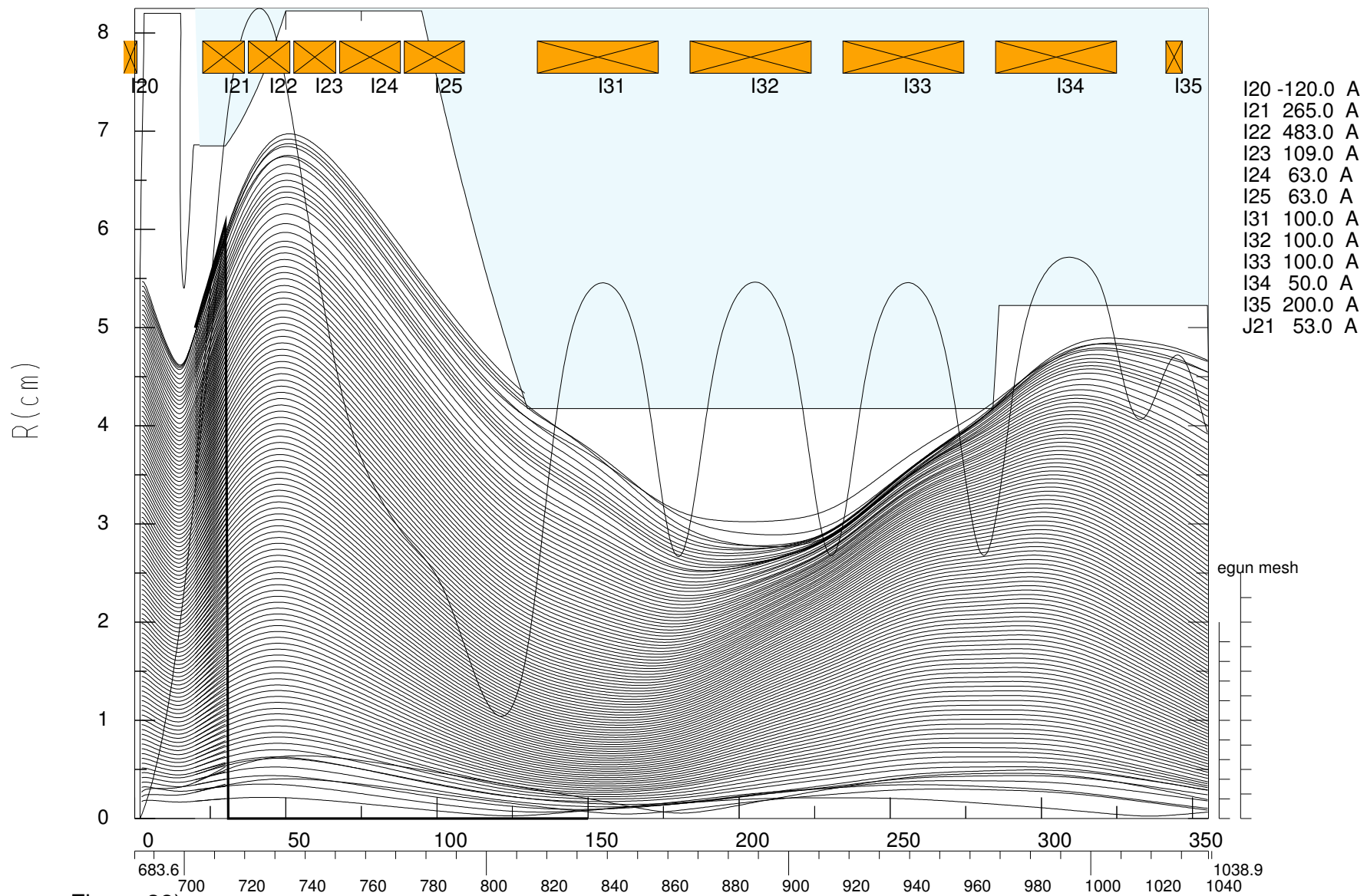


Figure 38) FXR_Injector_Study_2mm_grid_SPU28_13cm_AK_gap Unit 0.00200 0.00250 meters/mesh unit
 Anode 2.100 MV. 84 trajectories. cathode 386.80, anode 698.80 cm. 3183.8 Amperes beam current. Beam ending energy 1.
 SPU28_Magnetic_Field_Profile Beam current reaching end of injector 3069.31 Amperes
 /wrk/acpaul/fxr/spu28 EGUN data input file name: data.egunT Plot 1

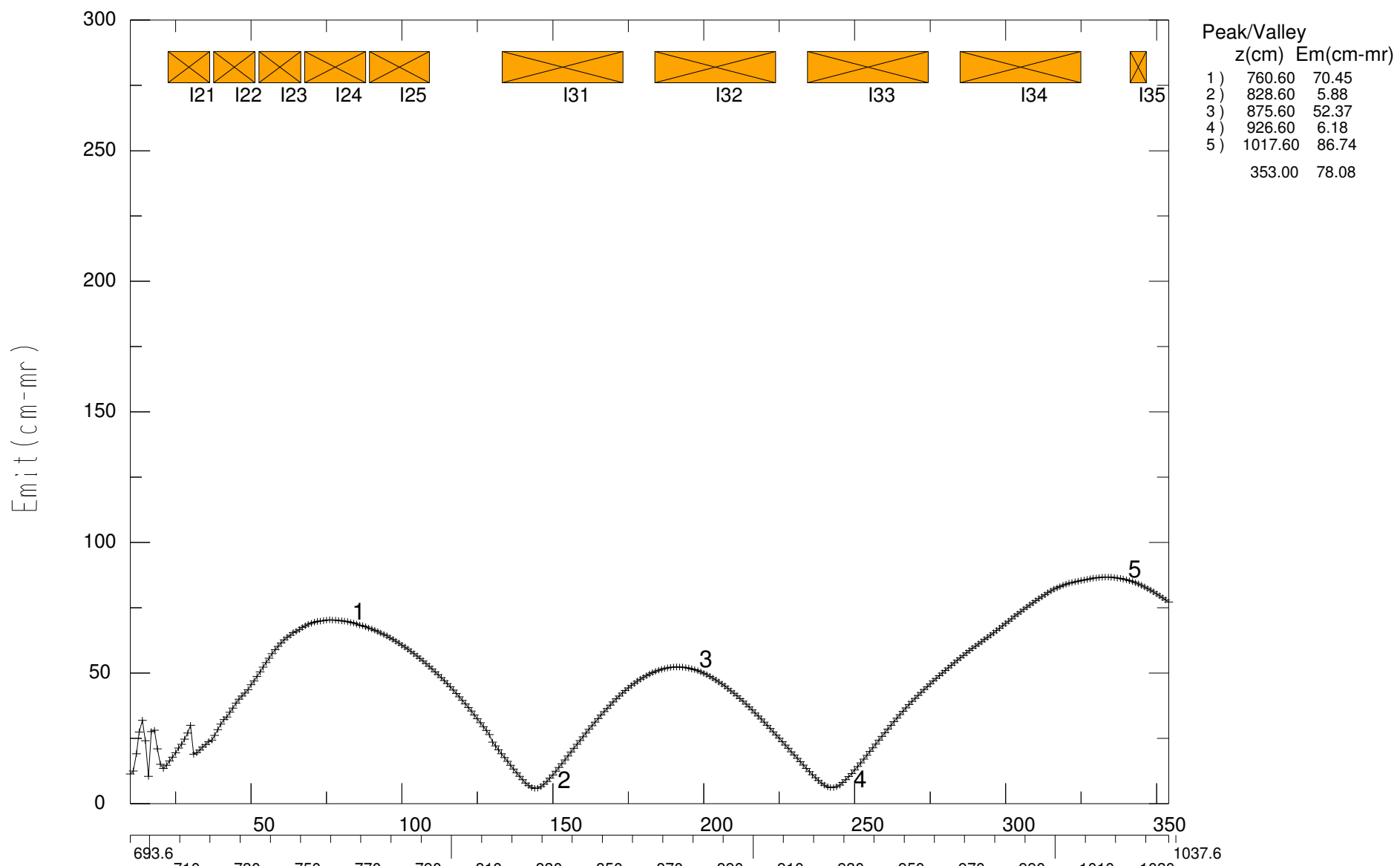


Figure 39) FXR Injector Emittance. Minimum emittance 5.88, maximum emittance 86.74, average emittance 44.32 cm-mr.
 Egun grid 2 mm, SPU28 Magnetic field tune with 13 cm AK gap and anode potential of 2.1 MV.
 Emitted cathode current 3183.8 Amperes. Current reaching end of injector 2963 Amperes.

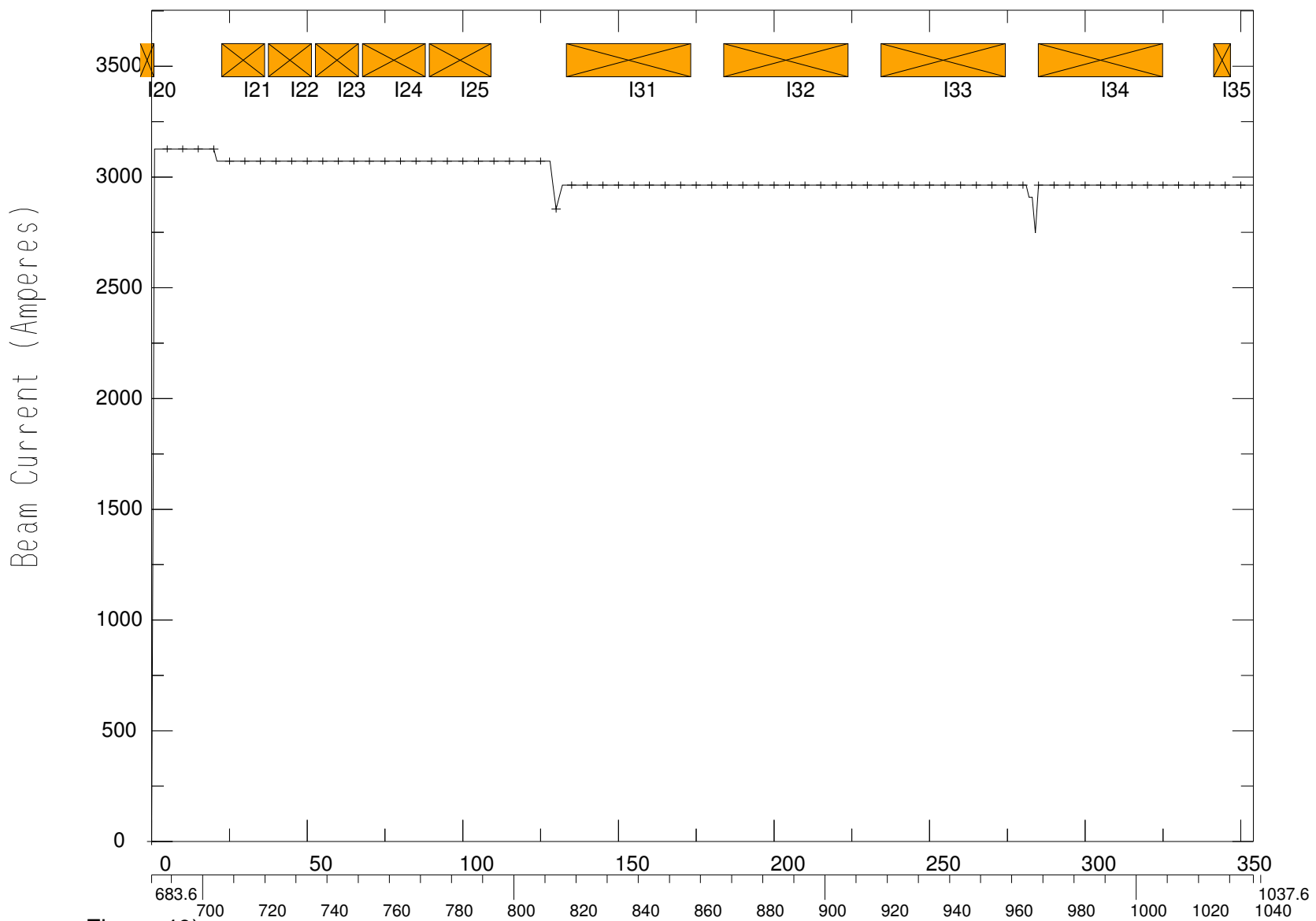
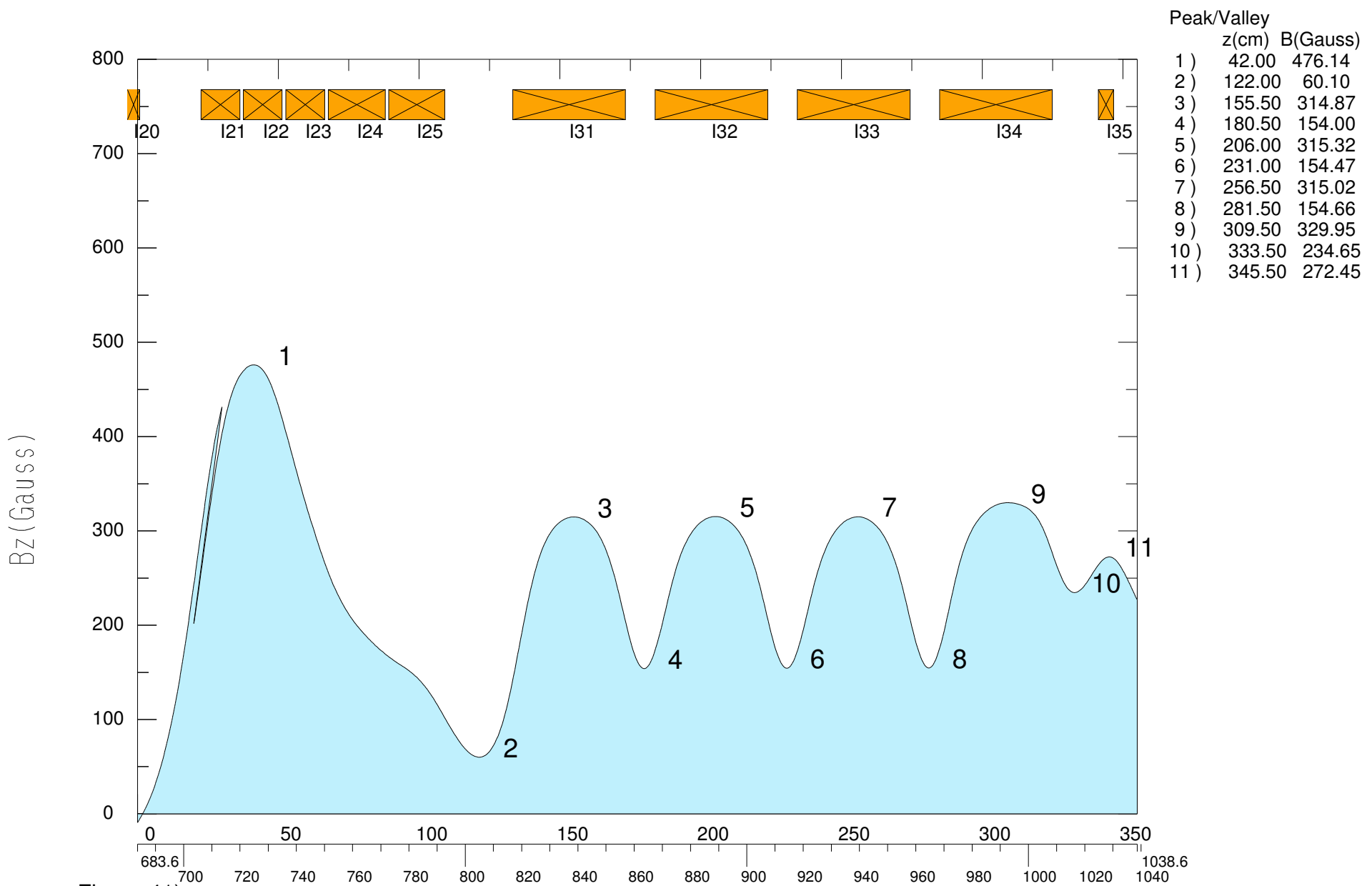


Figure 40) FXR Injector Current profile for the SPU28 magnetic field tune.

EGUN 2 mm grid with a 13 cm AK gap and anode potential of 2.1 MV.

The cathode emitted current is 3183.8 Amperes with 2980 beam current reaching the end of the injector.



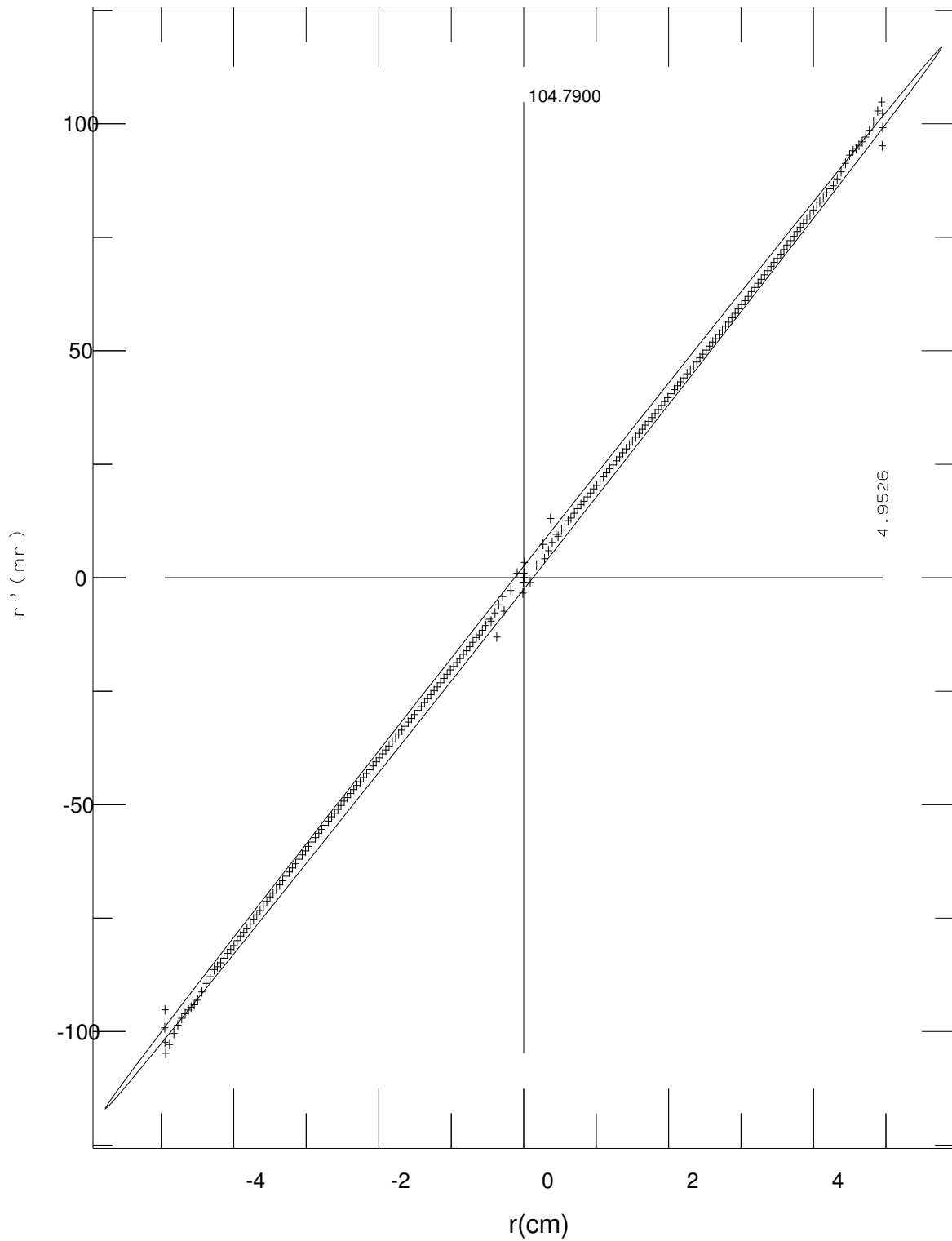


Figure 42) SPU28 tune, EGUN Iteration: 20, 2.0E-03 meters/Mesh_Unit Current 3184. Amperes Phase space at the 20 cm transfer position, energy 1.959 MeV, Anode potential 2.1 MV. Emittance 14.733 cm-mr bounding ellipse r (cm), r 21, r' (mr): 5.7717, 0.9998, 117.0021

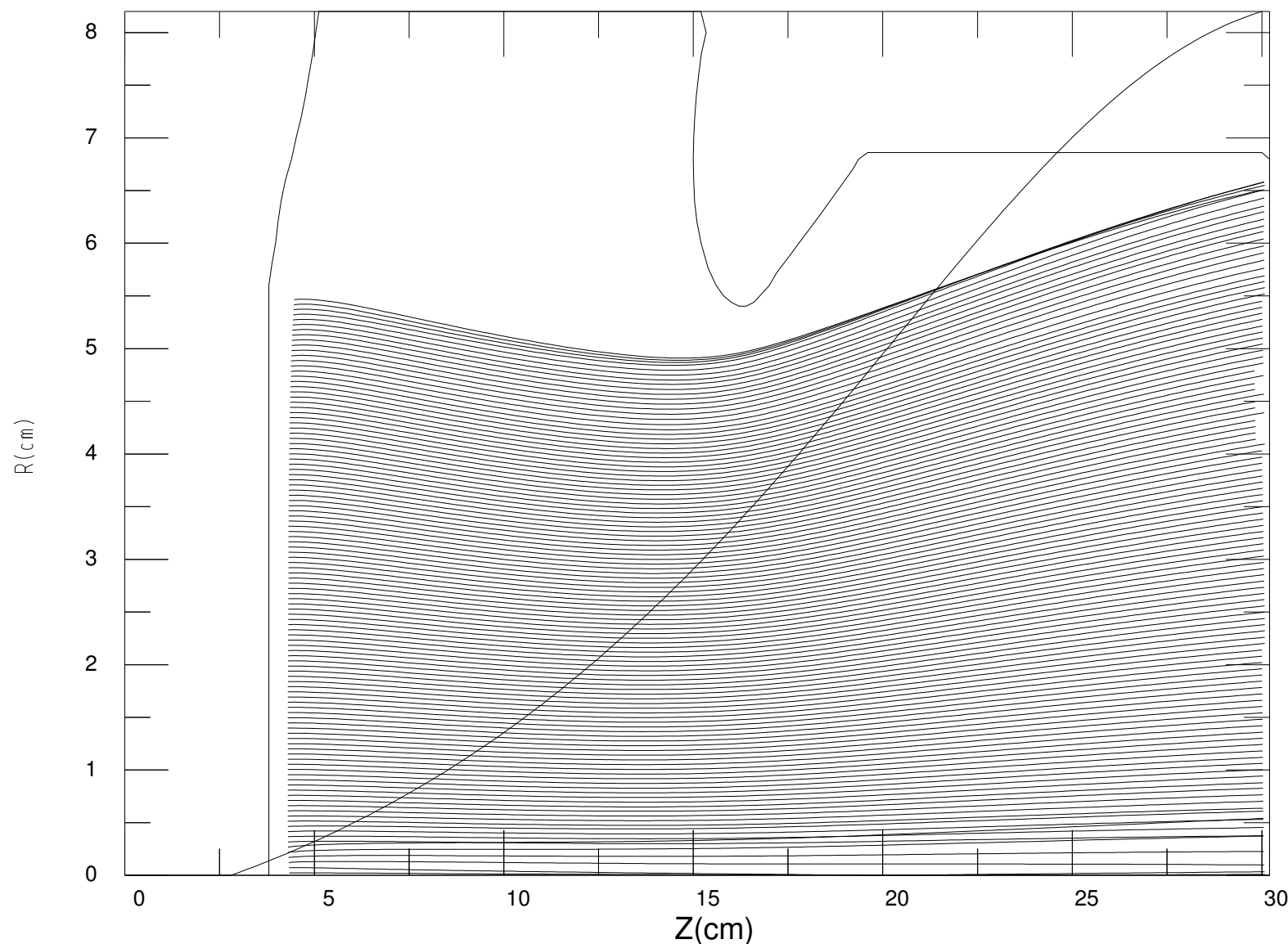


Figure 43) EGUN 2.0E-03 meters/Mesh Unit, Double pulse magnetic field tune, emitted cathode current 2523. Amperes

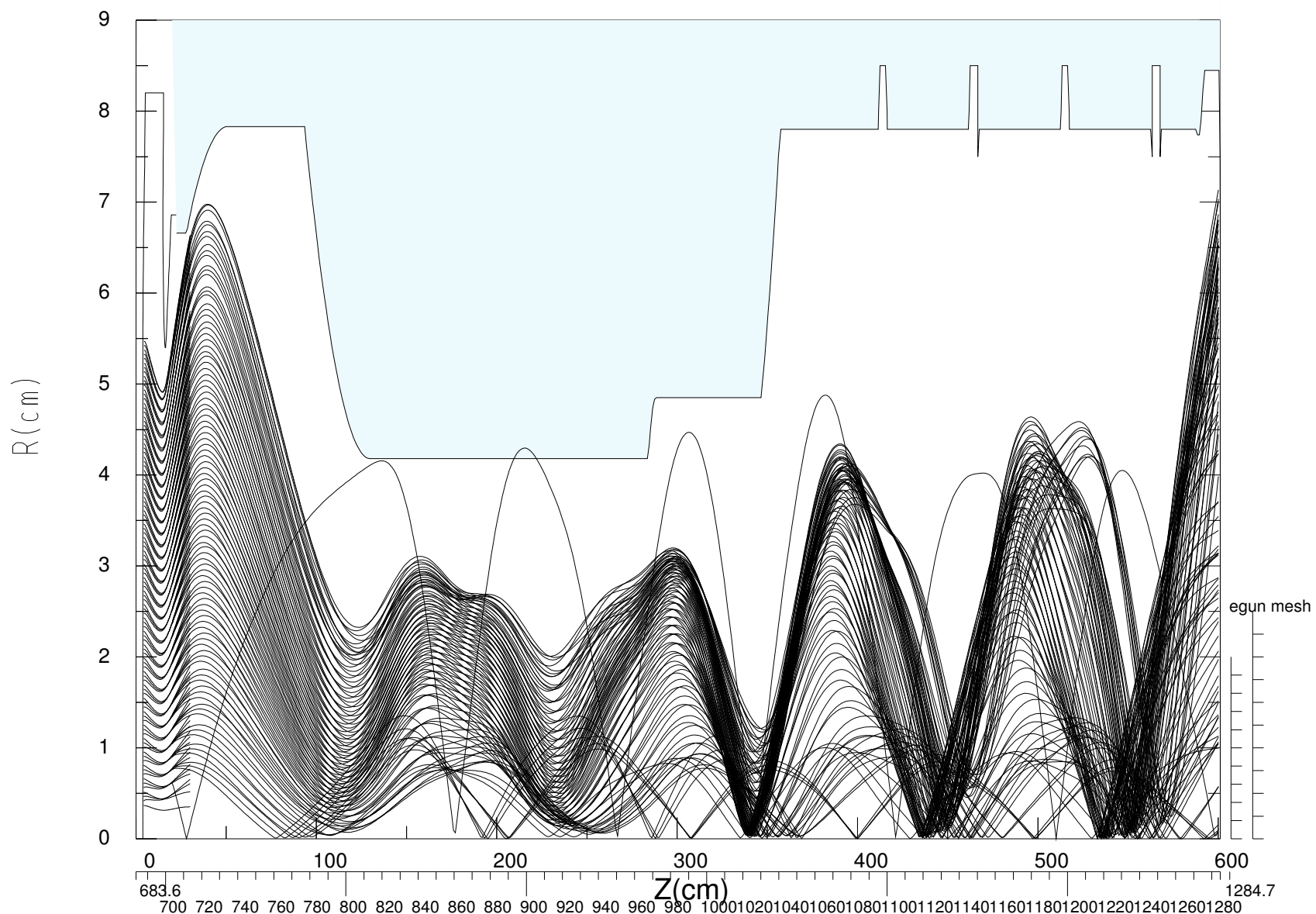


Figure 44) DP1170 Magnetic field profile 2 mm egun grid Double Pulse 11 cm AK gap 0.002 and 0.005 meters/mesh unit
Anode potential 1.450 MV, cathode 386.80 cm anode 698.8 cm, beam current 2523.0 Amperes

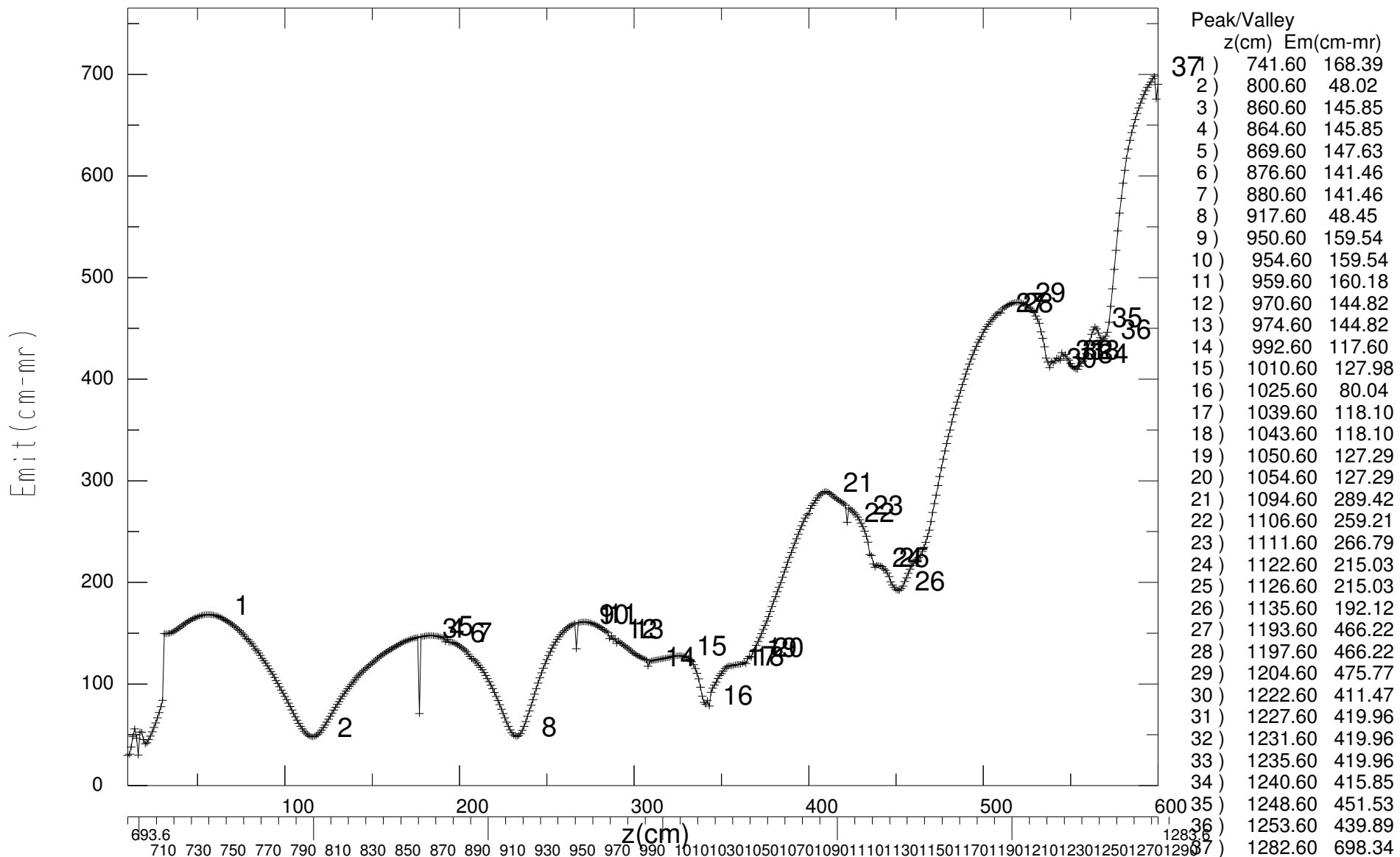


Figure 45) DP1170 Magnetic field profile. Emittance range: min,ave,max 48.02, 245.82, 698.34 cm-mr
Anode potential 1.450 MV, beam current 2523.0 Amperes 2 mm EGUN grid Double Pulse 11cm AK gap

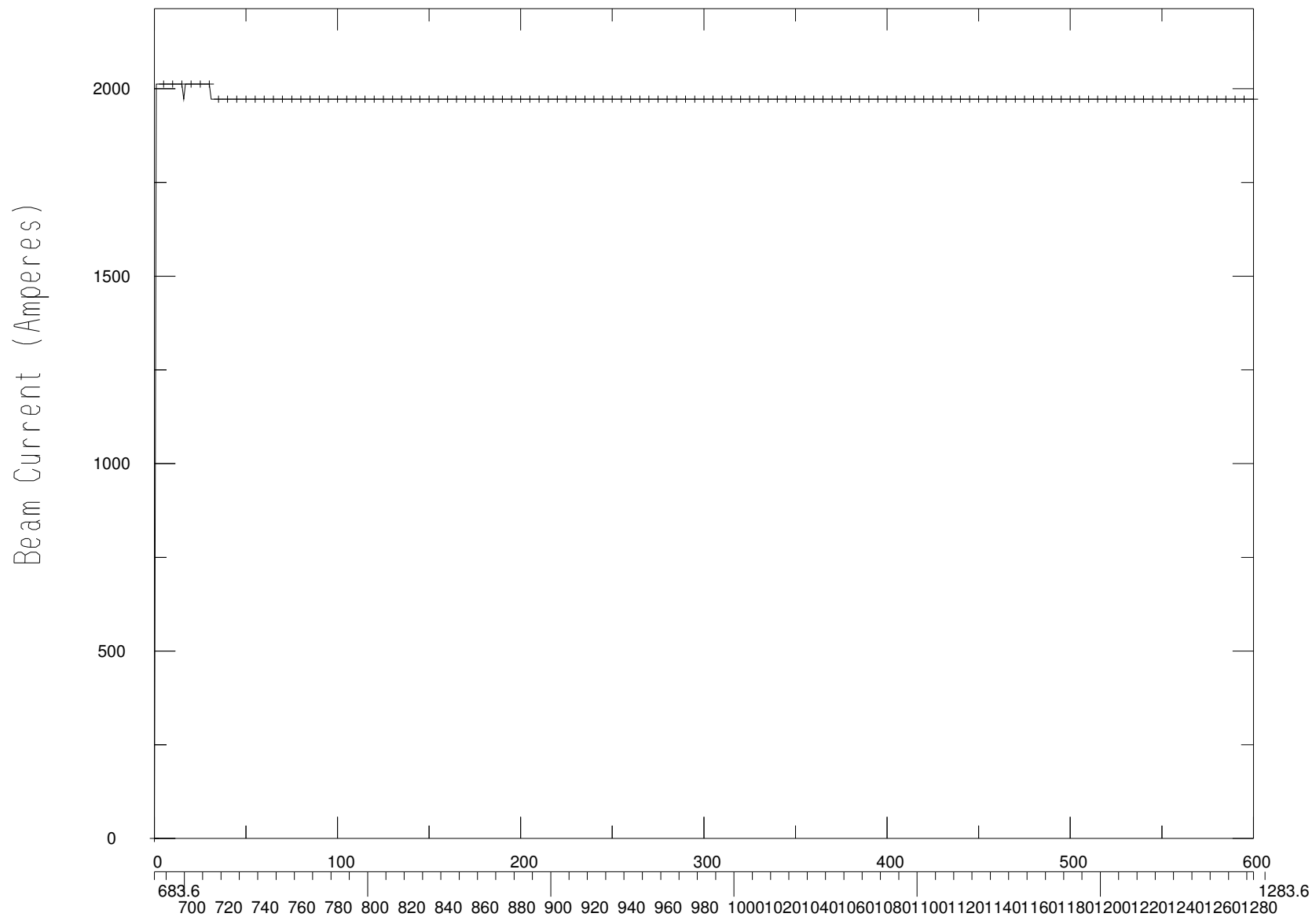


Figure 46) FXR Injector Current DP1170 Magnetic field profile. FXR Injector study 2 mm grid Double Pulse 11cm AK gap
Anode potential 1.450 MV. 2523.0 Amperes beam current Ending current 1972.2 Ampere

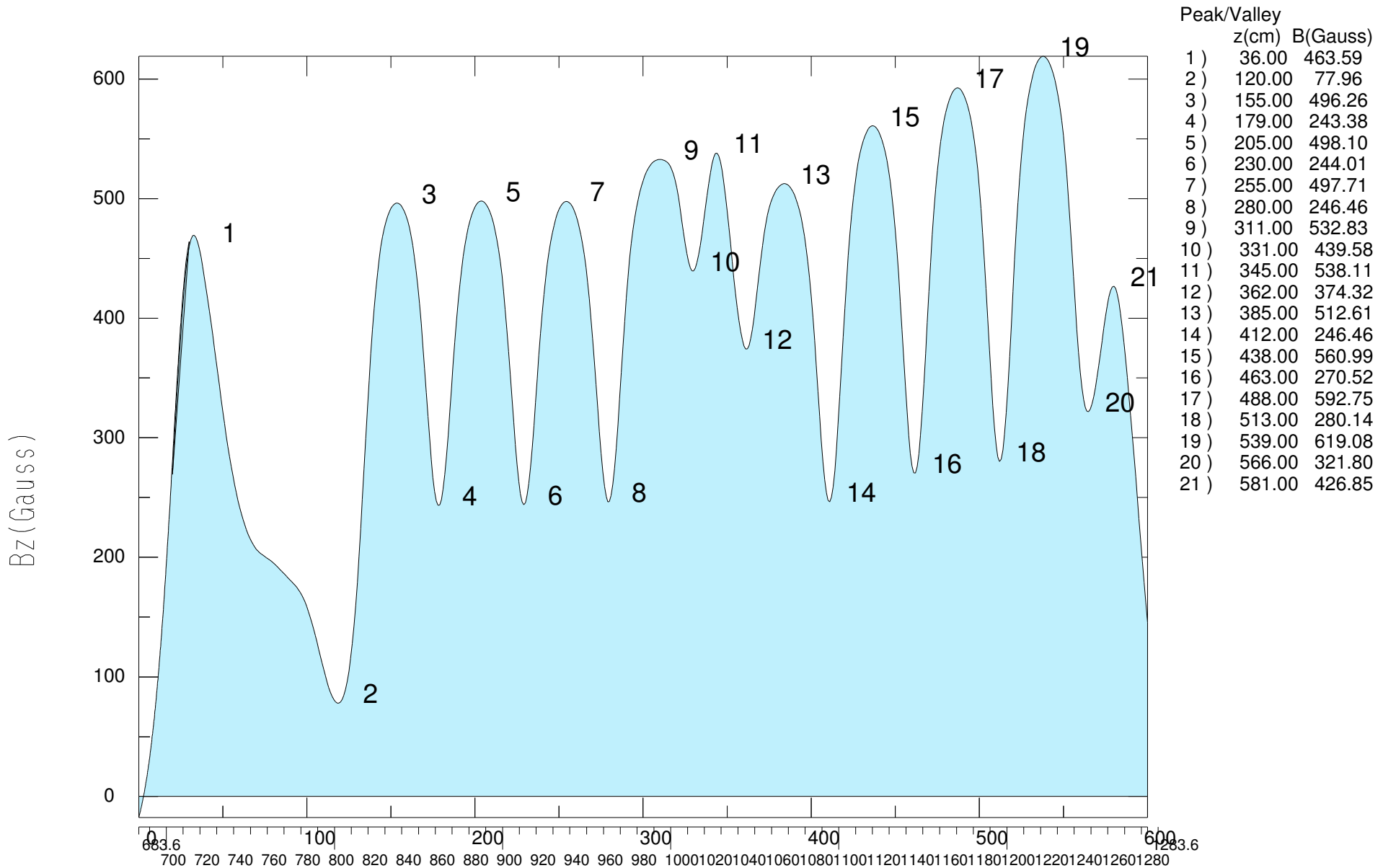


Figure 47) FXR Injector Double Pulse Magnetic Field profile.
asdf

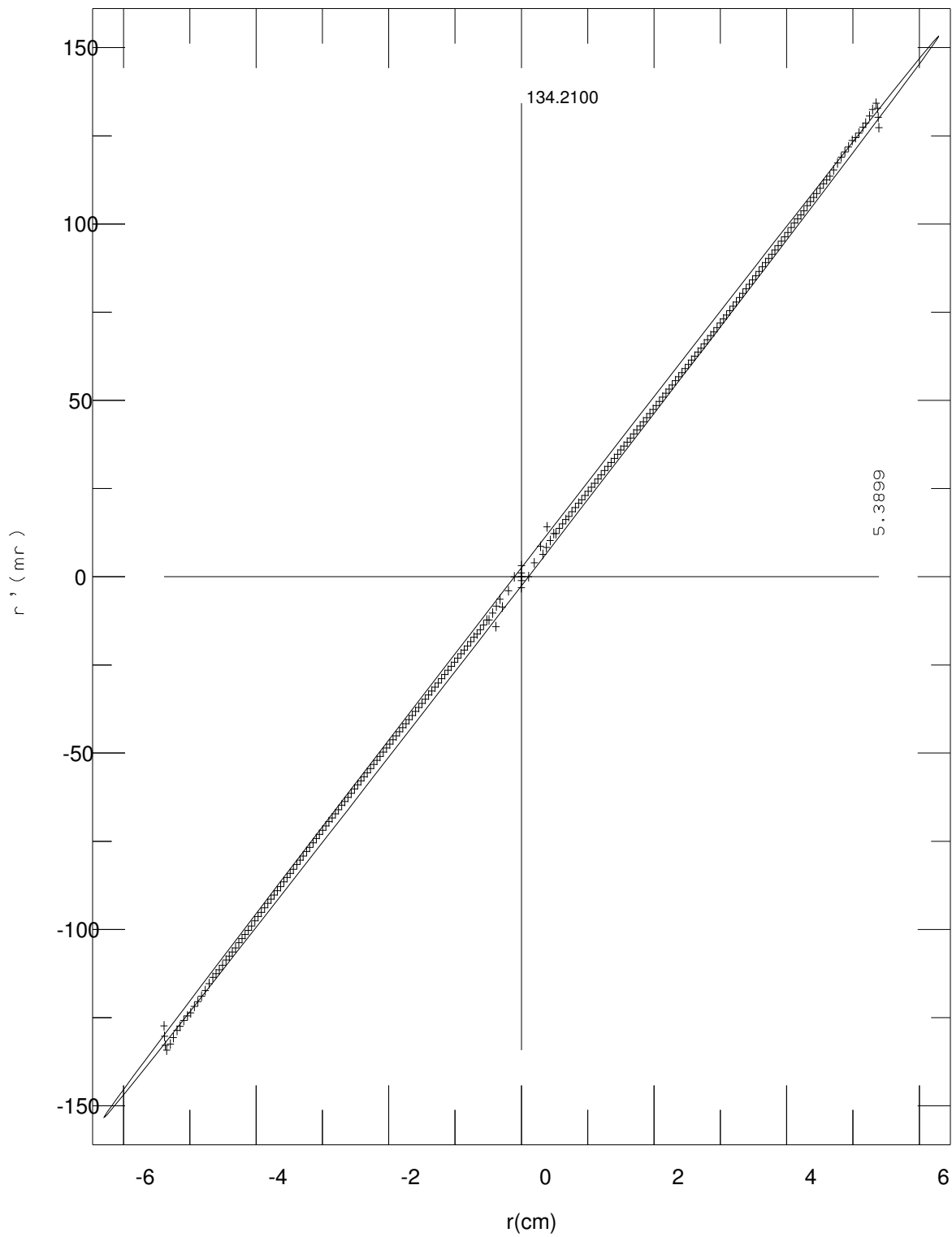


Figure 48) Phase plot

Double pulse magnetic field tune. Beam emittance 15.965 cm-mr, r (cm), r_{21} , r' (mr): 6.2936, 0.9999, 153.2873
Current 2523. Amperes Energy 1.35 MeV at Z Location of 100 Mesh Units, 20 cm.

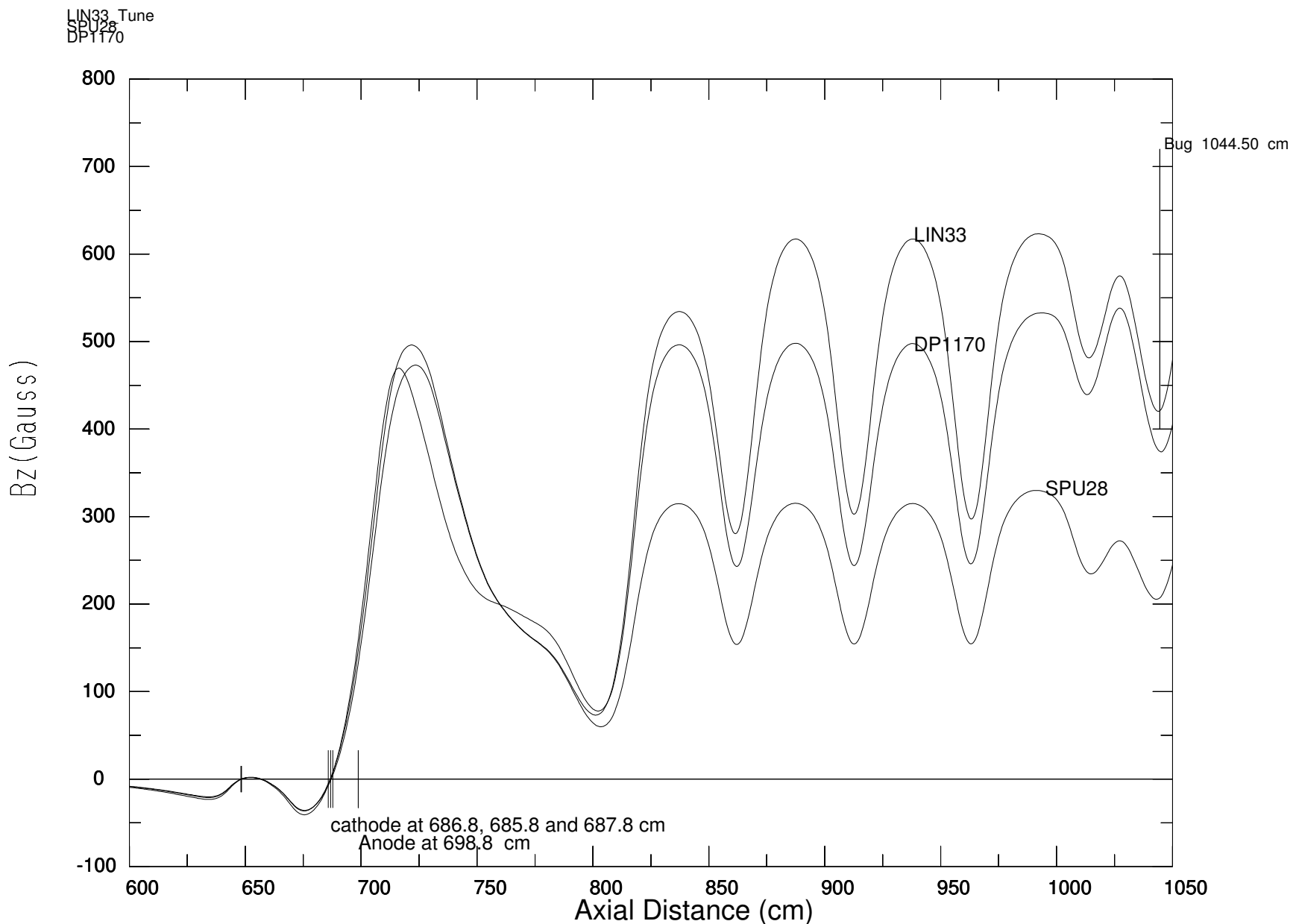


Figure 49) Overplot of magnetic fields for the three FXR tunes LIN33, SPU28 and DP1170. The field for the injector bucking coil I20, and anode coils I21,I22,...,I34 were generated from the fitting functions and summed over all axial positions.

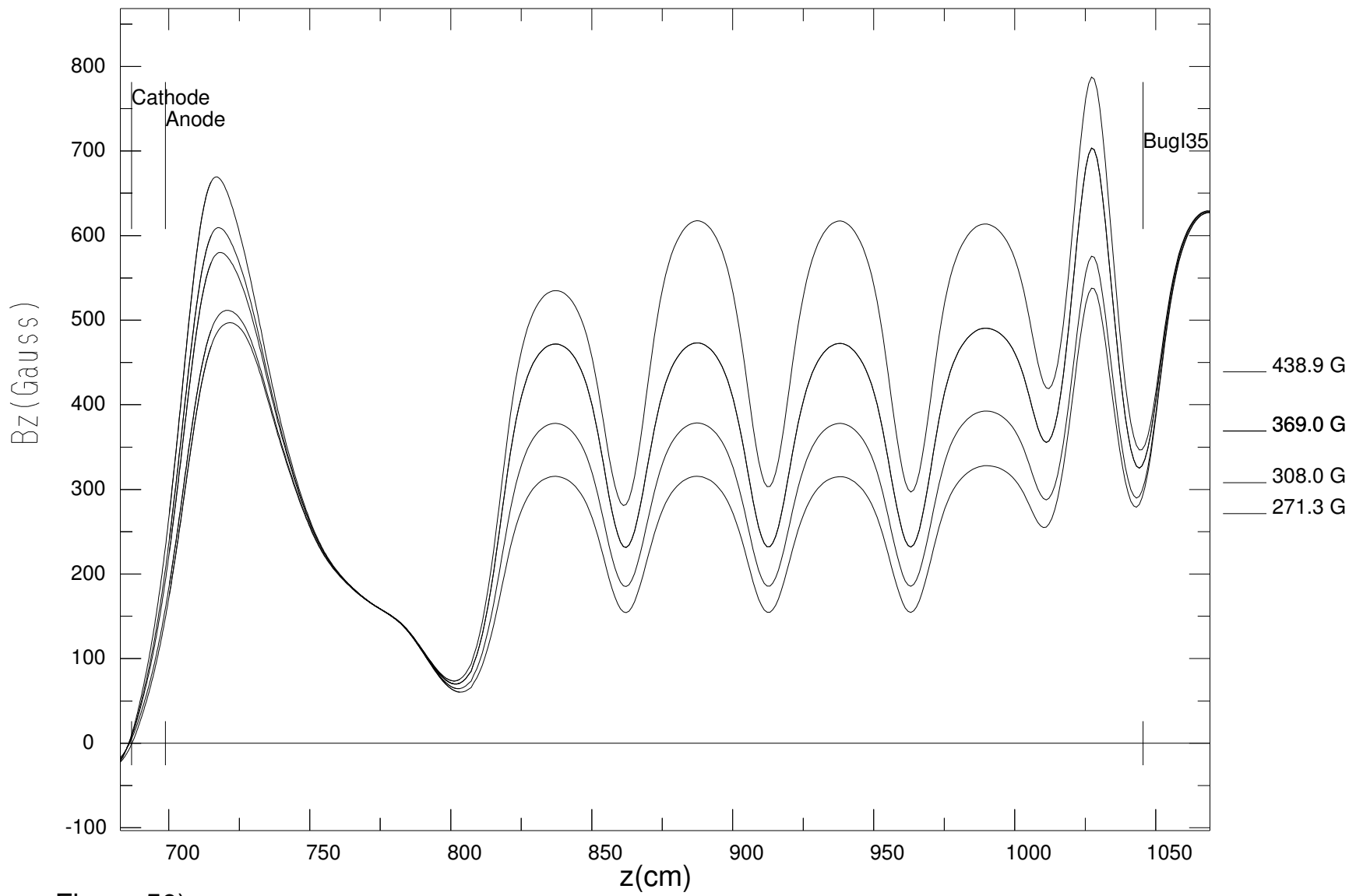


Figure 50 X Injector Field Sweeps, Zentler scan series 1, 2, 3, and Lin33. 1) data_bzaL -141 295 483 109 63 63 170 196 196 94 4
2) data_bzaUP -185 475 483 109 63 63 150 150 150 75 380 100 Amperes, 3) data_bzaU -166 415 483 109 63 63 150 150 150 75
4) data_bzaV -157 385 483 109 63 63 120 120 120 60 310 100 Amperes, 5) data_bzaW -134 310 483 109 63 63 100 100 100 50 2

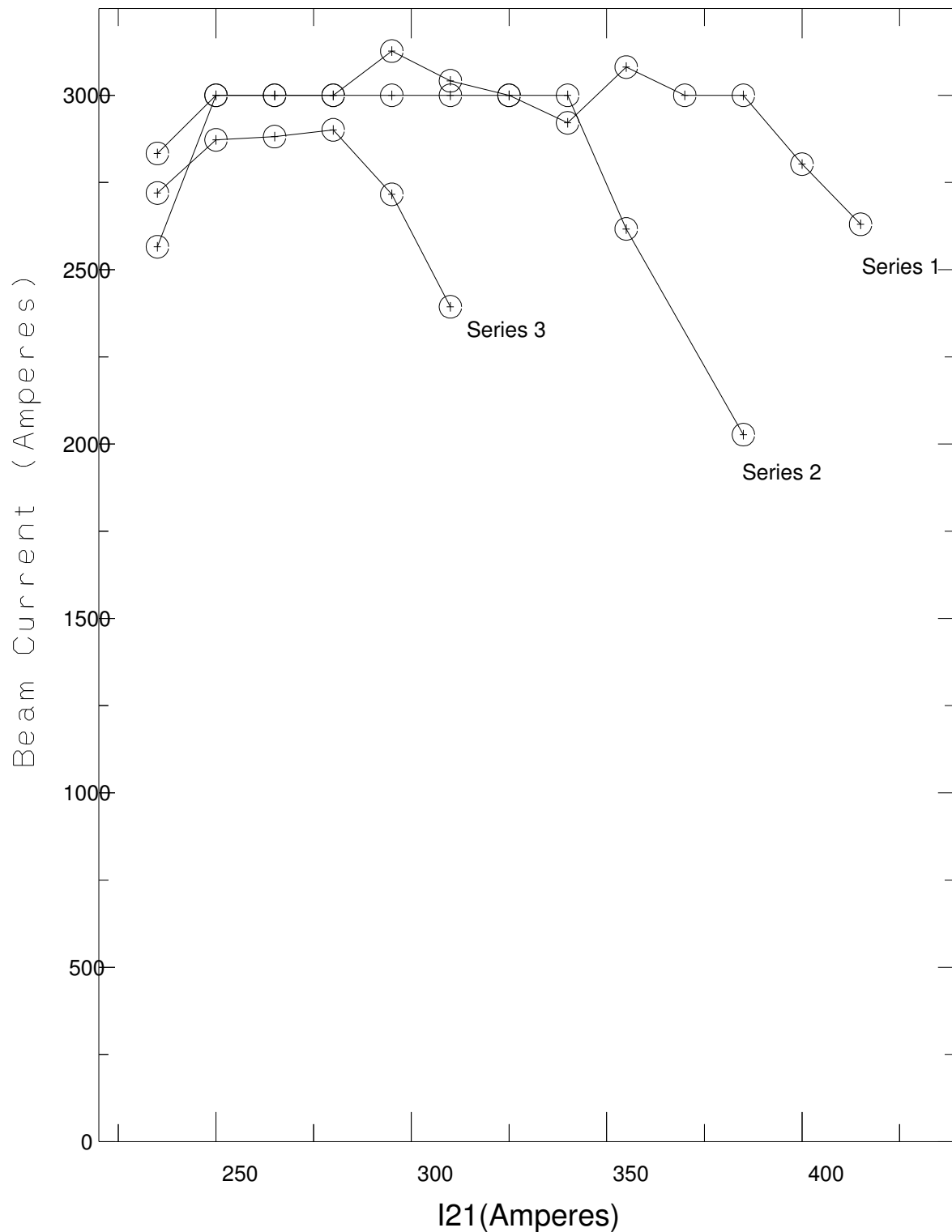


Figure 51) FXR Zentler Scans Series 1, 2, and 3. Beam current measured on the bug at the exit of the FXR injector.

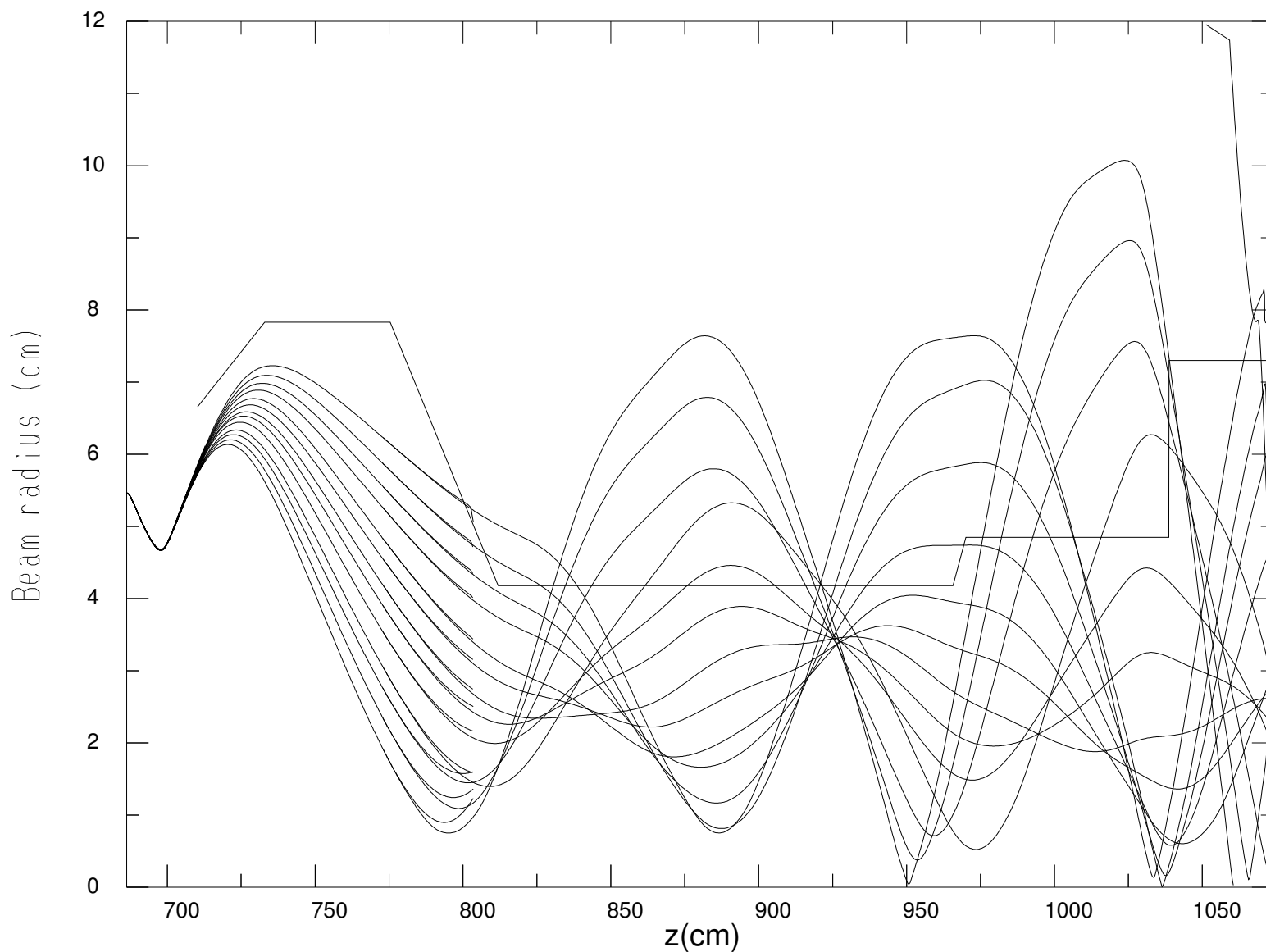


Figure 52) FXR Zentler scans showing beam envelopes for the EGUN runs, series 1.
Only the first anode magnet, I21 is scanned over 13 values.

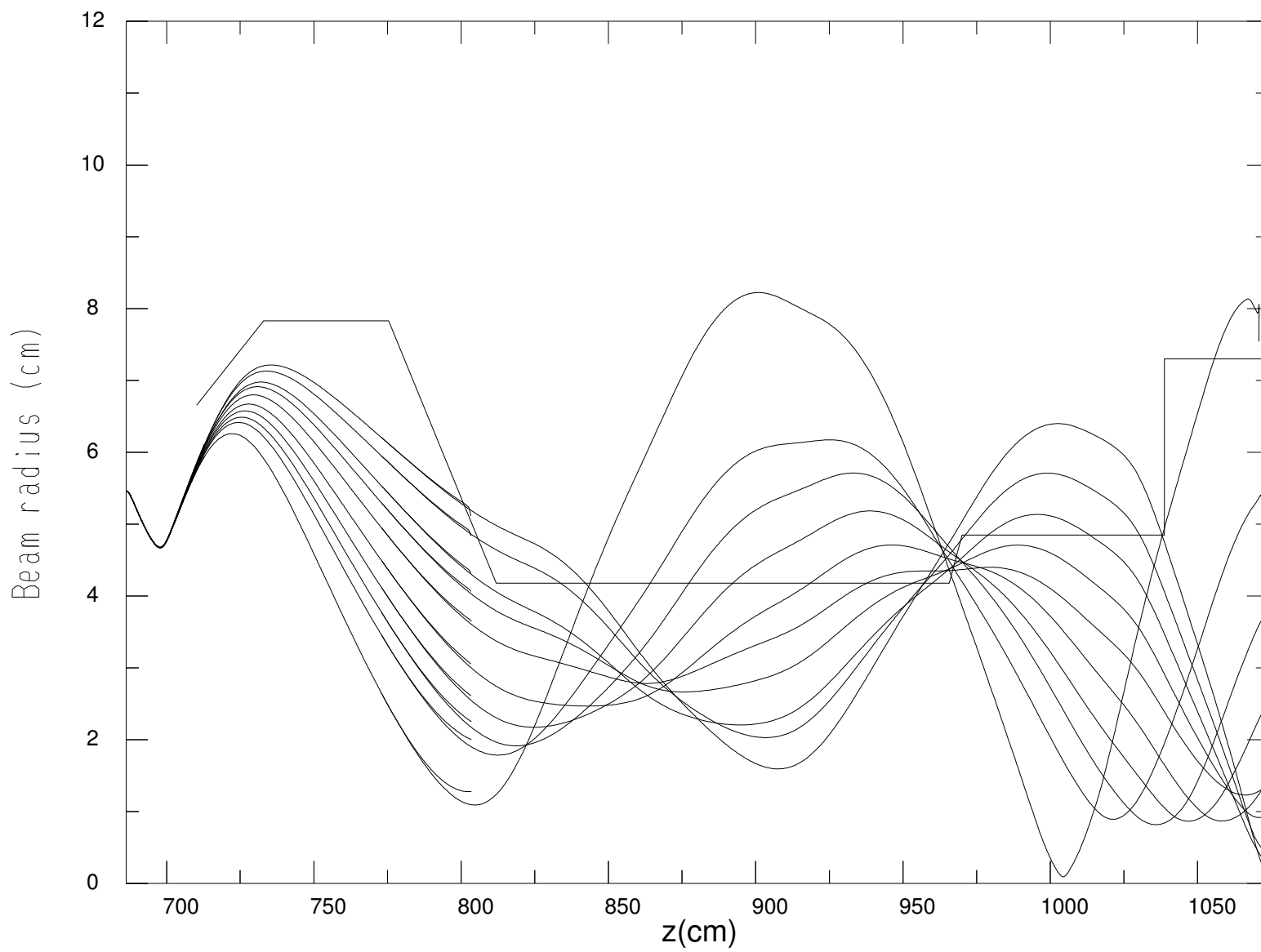


Figure 53) FXR Zentler scan, EGUN Beam envelopes - Series 2

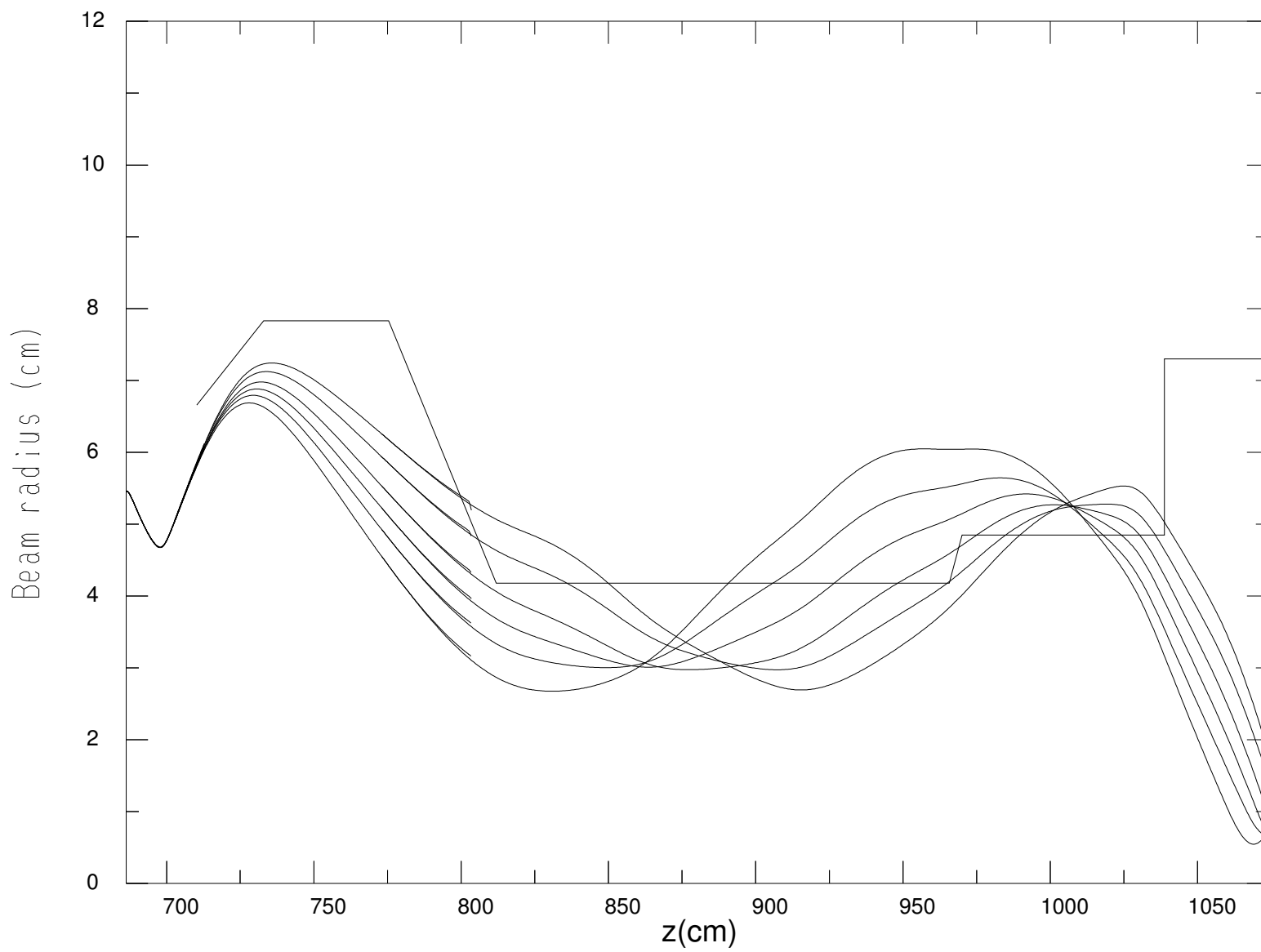


Figure 54) FXR Injector Scans EGUN Beam envelopes - Series 3

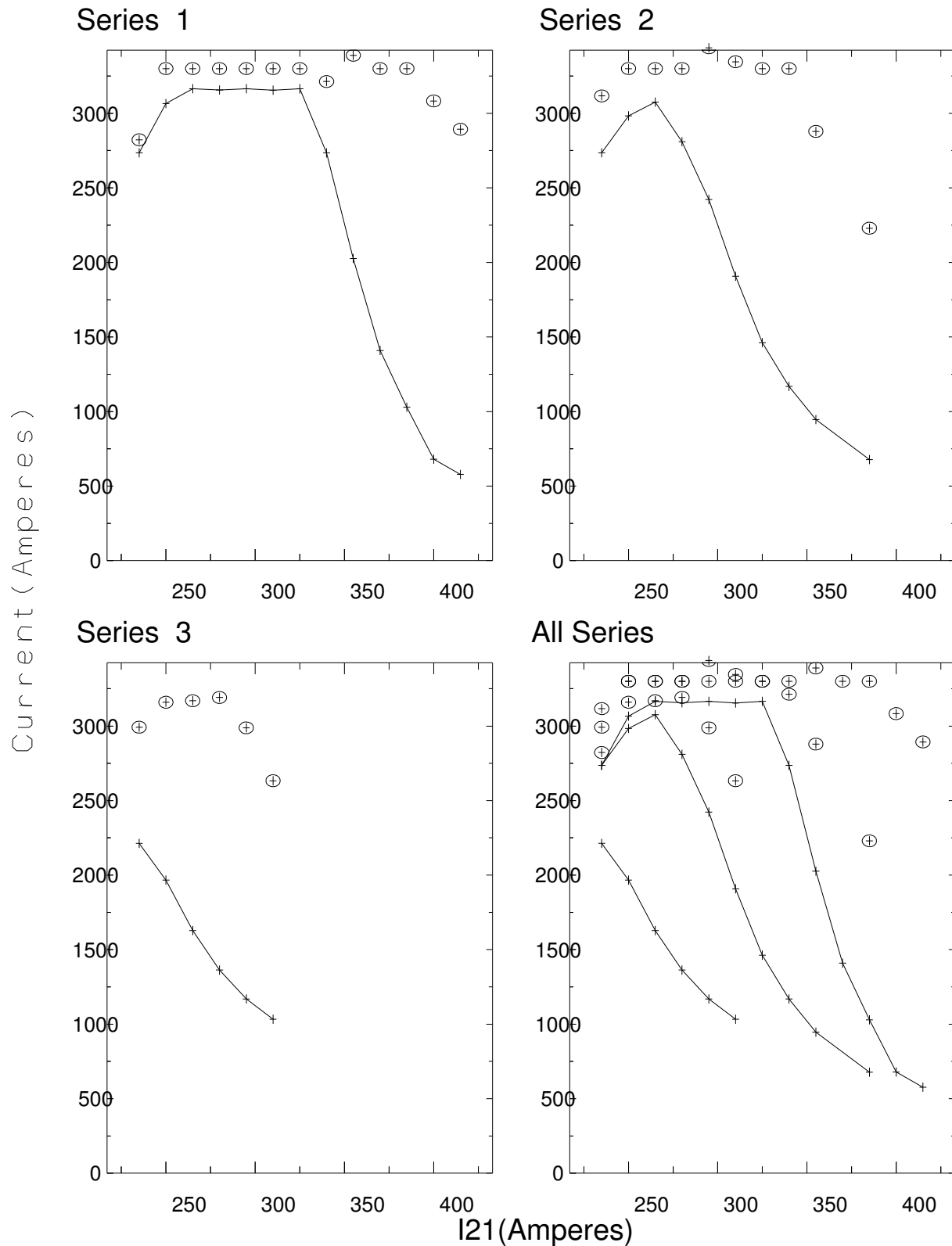


Figure 55) FXR Zentler Scans EGUN runs at 1.900 MV Anode voltage. The anode cathode gap 12.cm Uniform Current Density profile

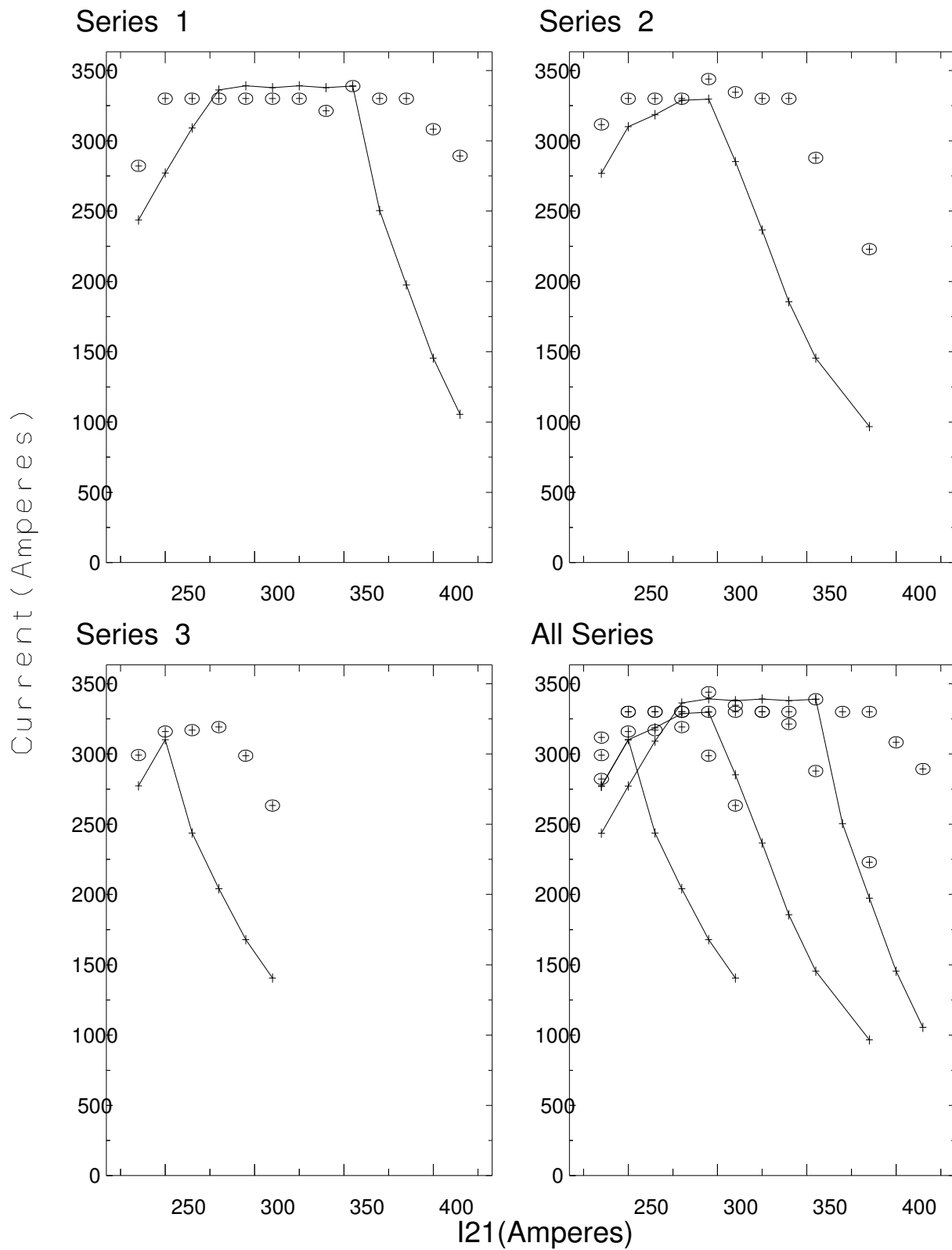


Figure 56) FXR Zentler scans, EGUN runs at 2.000 MV Anode cathode gap 12.0 cm
Uniform Current Density profile

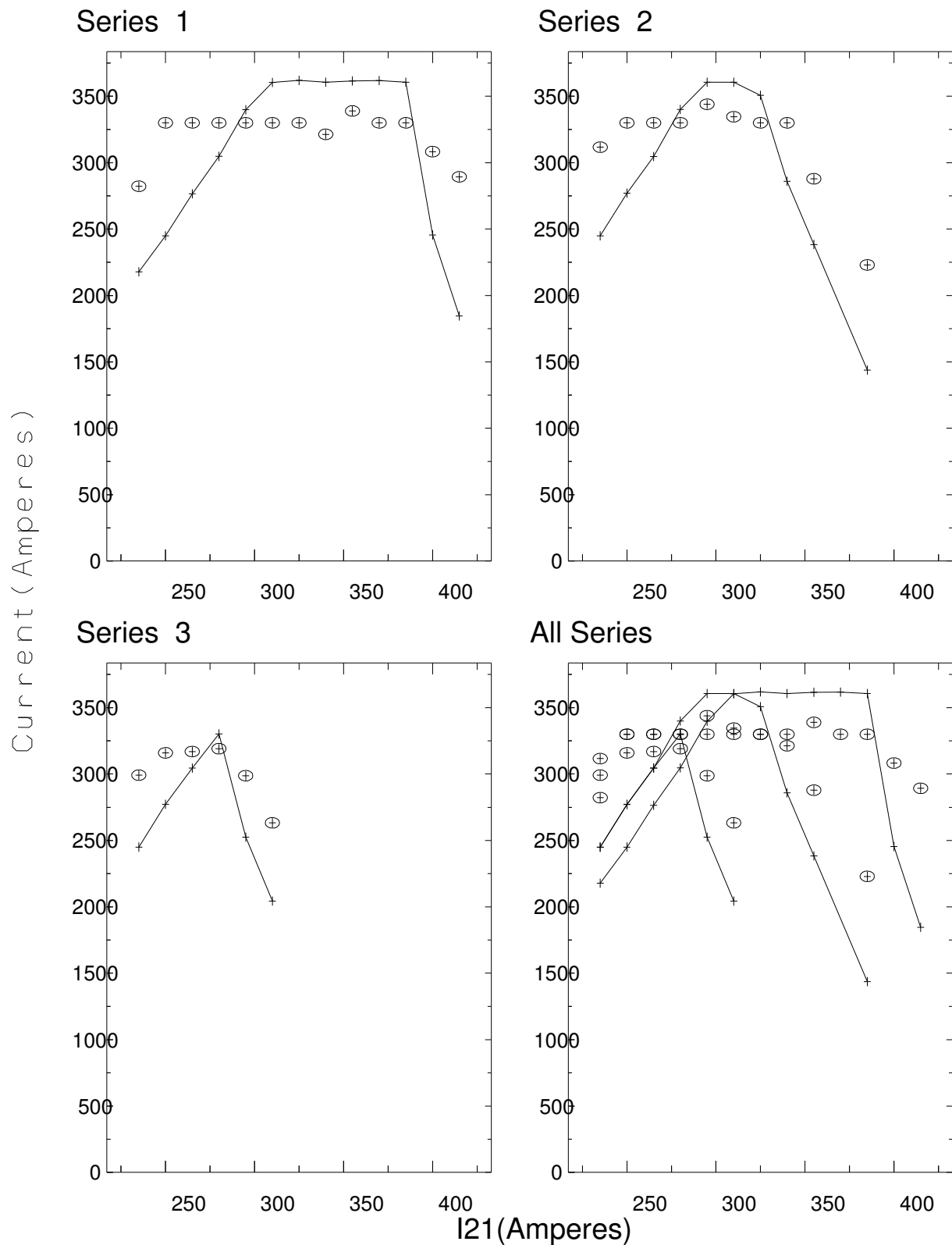


Figure 57) EGUN runs at 2.100 MV Anode cathode gap 12.0 cm
Uniform Current Density profile

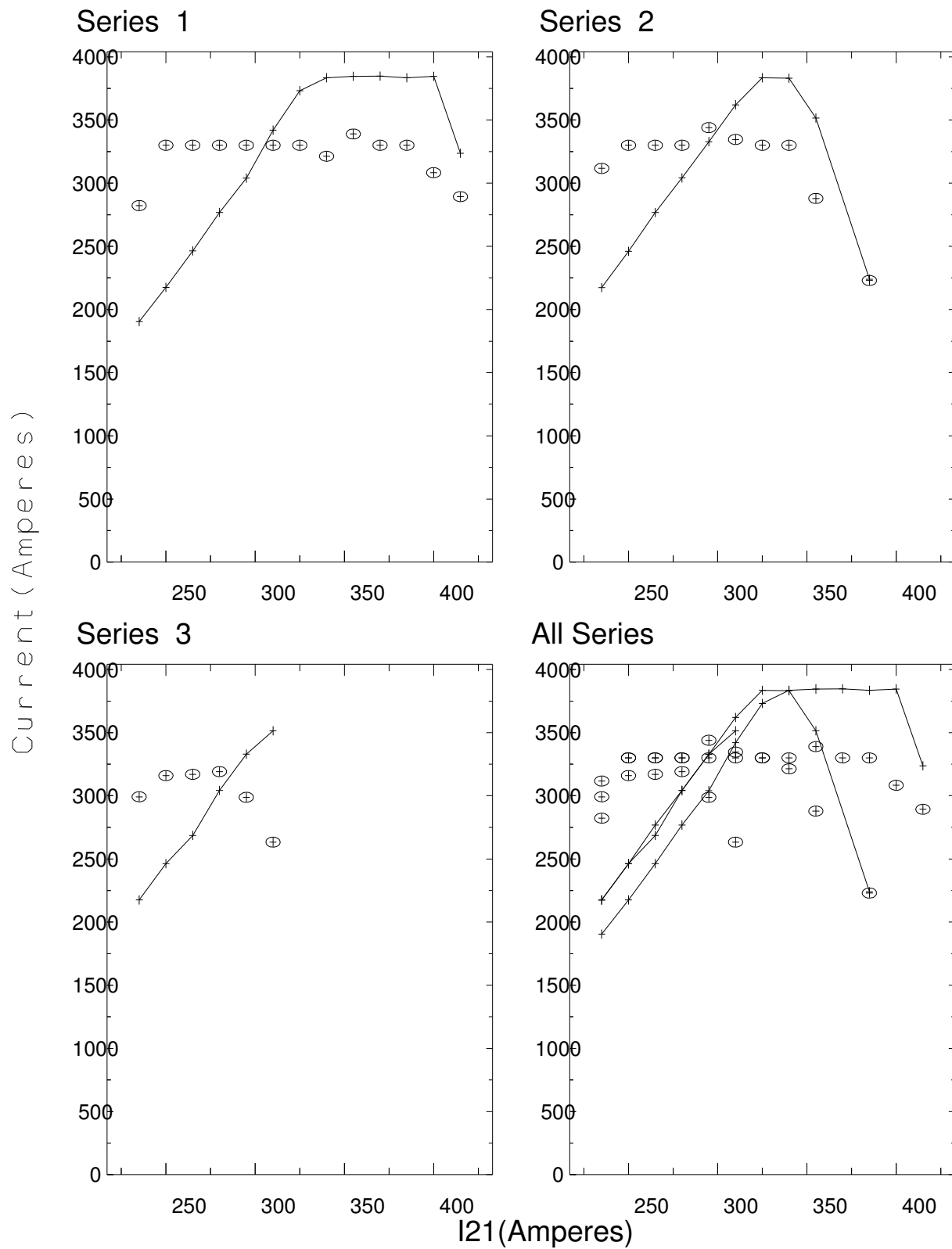


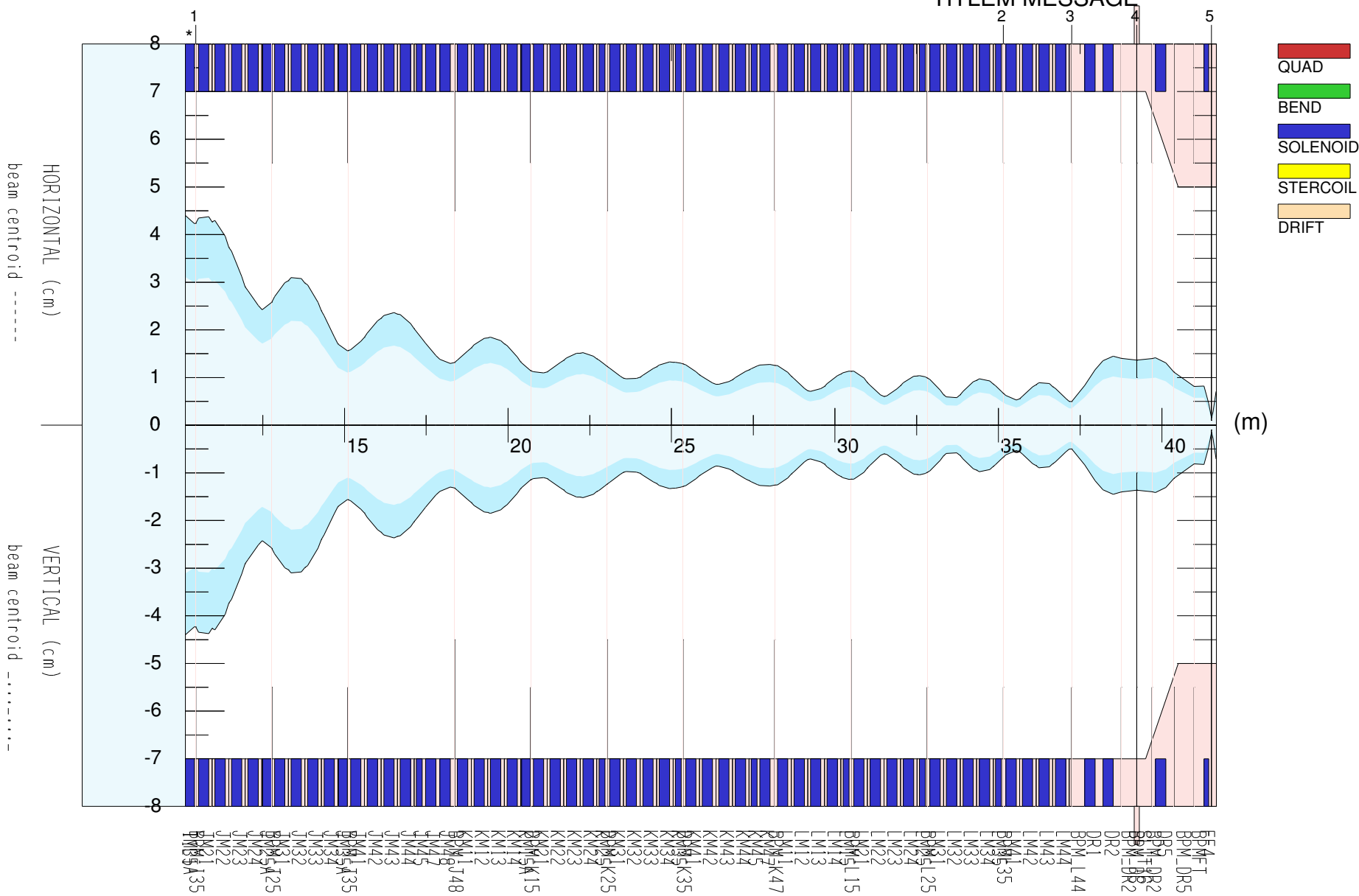
Figure 58) EGUN runs at 2.200 MV Anode cathode gap 12.0 cm
Uniform Current Density profile

03Jan15 14:08:06 14:08:06
FXR Transport line 6/18/01

P = 16.4220 MeV/C
SPC: 3300.0000 Amperes
Emit 7.718 7.718 cm-mr

zrange: 10.1320 41.6616 m

TITLEM MESSAGE



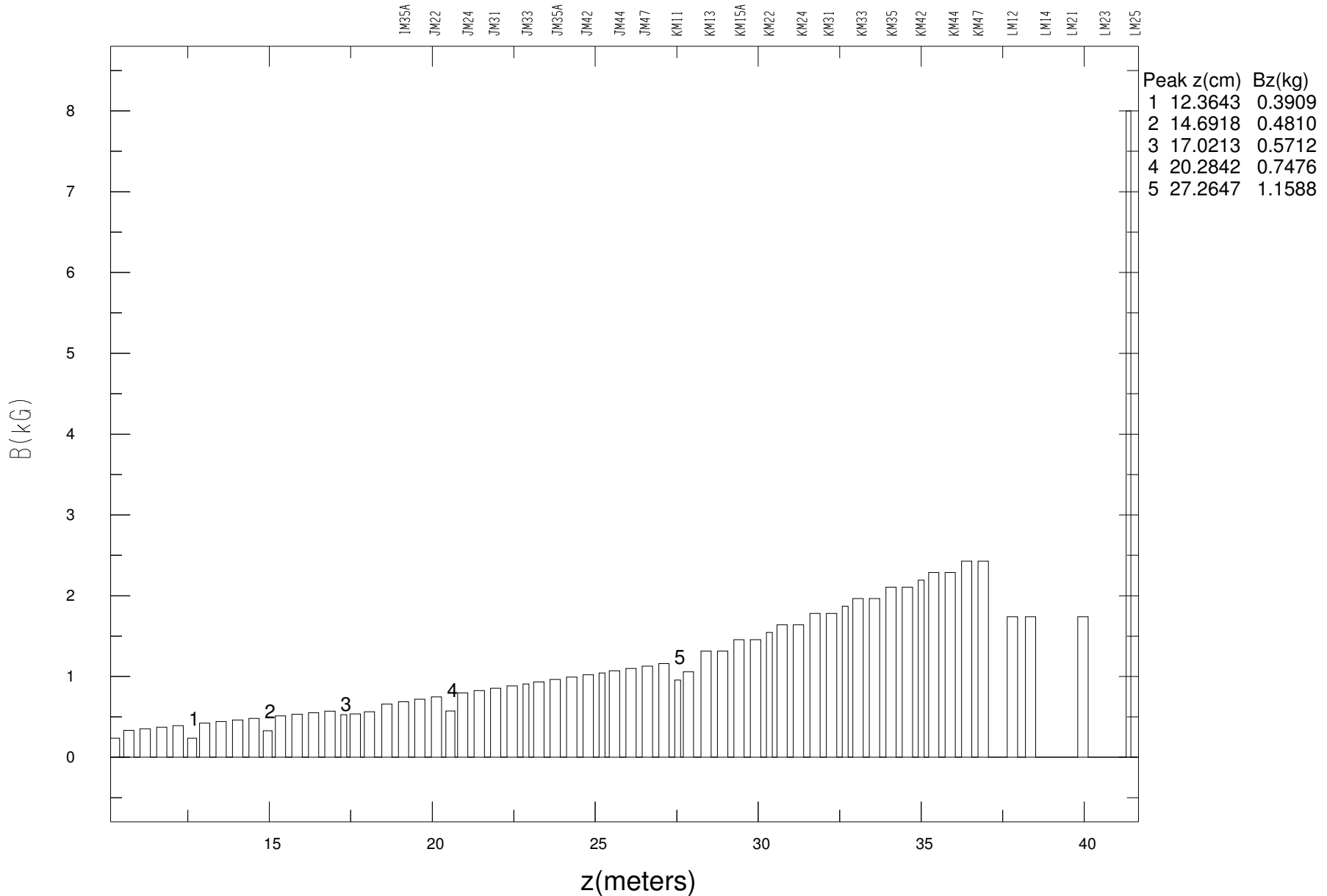
REG#: 9
RUN#: 16
PLOT: 18

/wrk/acpaul/fxr/inj/inow/case

data: data.fxr

RUN: 03Jan15 at 14:12:46

Magnetic Field Along the Beamline



Plot of the Beam Sigma Matrix

FXR Transport line 6/18/01

1: IO3 (80)

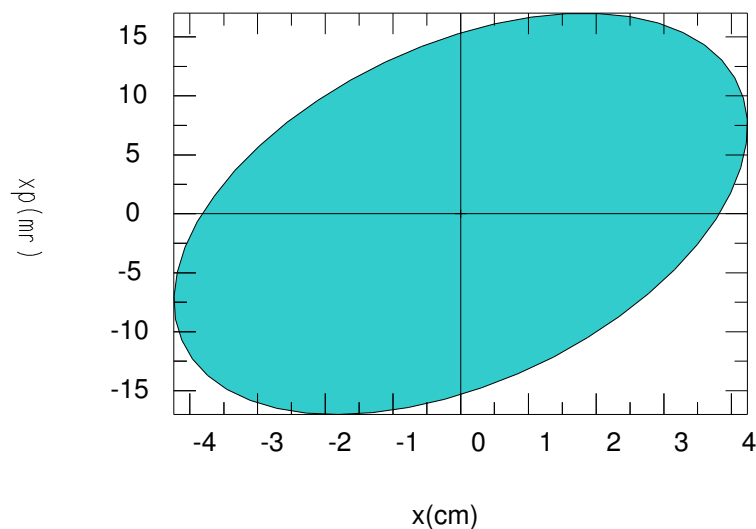
LC= 10.4498 m

P = 1.9500 MeV/C

SPC: 3300.0000 Amperes

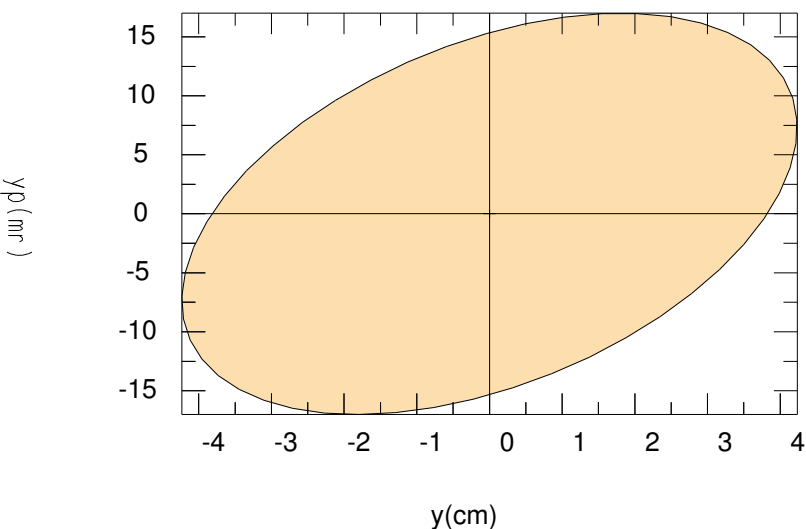
X-XP Phase Plot (0,0)

Intersection: 7.35757 -1.99844 0. 15.34621

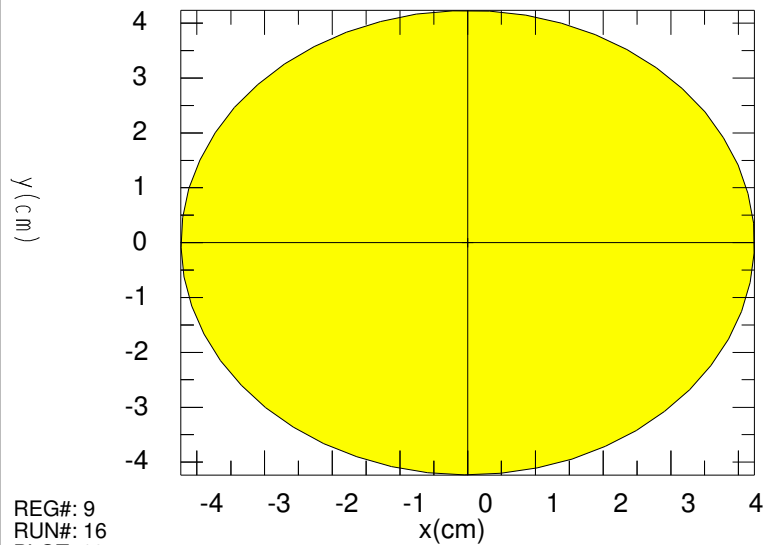


Y-YP Phase Plot (0,0)

Intersection: 7.31565 -1.99844 0. 15.35126



X-Y Beam Spot (0,0) r= 0.



REG#: 9
RUN#: 16
PLOT: 19

SI Sigma Matrix (4.2358 4.2340 19.512 d)

0.00000	(x)	0.	4.236 cm		
0.00000	(y)	0.	17.019mr	0.432	
10.44980	(z)	0.	4.234 cm	0.000	0.001
0.00000	(yaw)	0.	17.005mr	0.001	0.001
0.00000	(pit)	0.	0. cm	0.	0.
0.00000	(rol)	0.	0. pc	0.	0.

RC Transformation Matrix

0.8927	0.02816	0.491	0.01548	0	0
2.96	0.9535	1.632	0.5243	0	0
-0.4907	-0.01548	0.8926	0.02816	0	0
-1.621	-0.5243	2.955	0.9535	0	0
0	0	0	0	1	0.02041
0	0	0	0	0	1

Emittance: x= 6.500e+01 y= 6.500e+01 cm mr
Area(xy)= 5.634e+01 cm cm r= 0.

Plot of the Beam Sigma Matrix

FXR Transport line 6/18/01

5: IO7 (807)

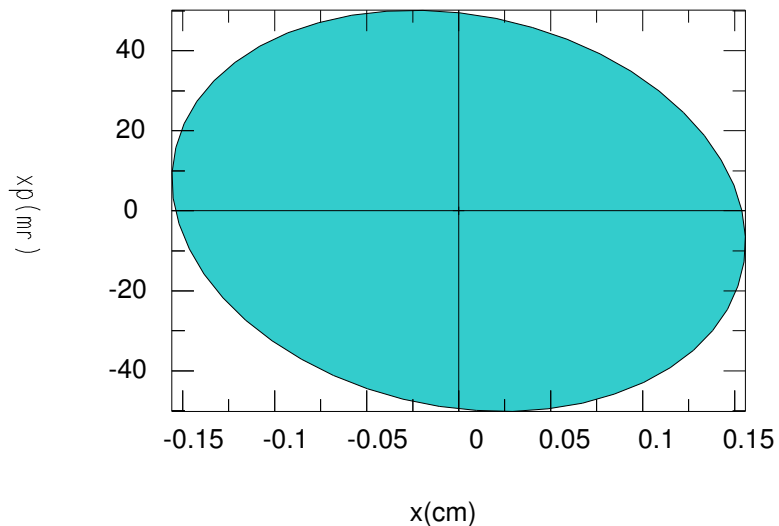
LC= 41.5116 m

P = 16.4220 MeV/C

SPC: 3300.0000 Amperes

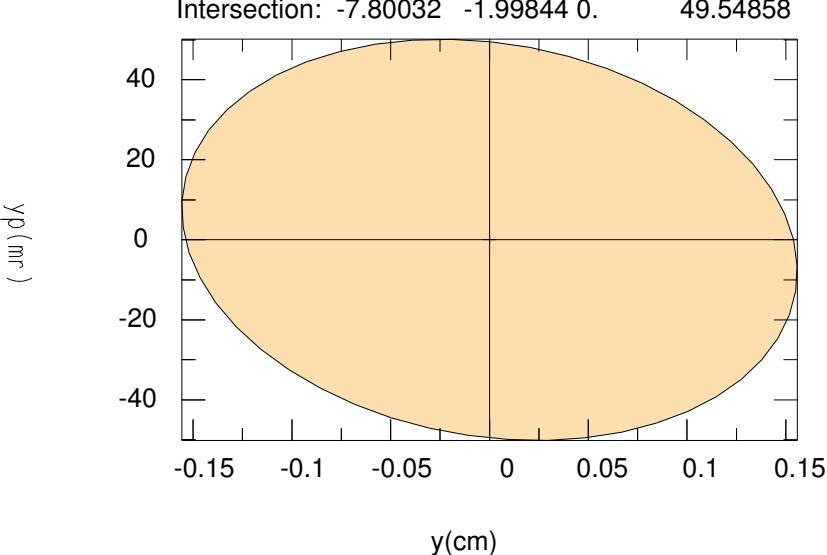
X-XP Phase Plot (0,0)

Intersection: -7.84632 -1.99844 0. 49.54287

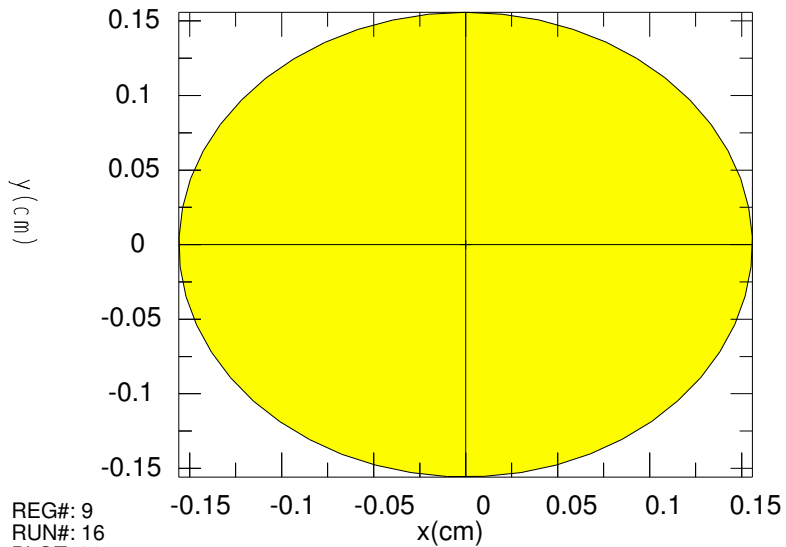


Y-YP Phase Plot (0,0)

Intersection: -7.80032 -1.99844 0. 49.54858



X-Y Beam Spot (0,0) r= 0.



REG#: 9
RUN#: 16
PLOT: 20

SI Sigma Matrix (0.1558 0.1558 -34.860 d)

0.00000	(x)	0.	0.156 cm
0.00000	(y)	0.	50.160mr -0.156
41.51040	(z)	0.	0.156 cm -0.000 0.001
0.00000	(yaw)	0.	50.159mr 0.001 0.000 -0.156
0.00000	(pit)	0.	0. cm 0. 0. 0. 0.
0.00000	(rol)	0.	0. pc 0. 0. 0. 0. 0.

RC Transformation Matrix

0.007499	0.001868	0.03514	0.008794	0	0
-1.667	0.2706	-7.836	1.271	0	0
-0.03512	-0.008799	0.007451	0.001875	0	0
7.839	-1.27	-1.669	0.2702	0	0
0	0	0	0	1	0.1429
0	0	0	0	0	0.1187

Emittance: x= 7.718e+00 y= 7.718e+00 cm mr

Area(xy)= 7.624e-02 cm cm r= 0.